DIELECTRIC MEASUREMENT OF ALGAL LIPID CONTENT FOR BIODIESEL PRODUCTION

A Dissertation

Presented to the Faculty of the Graduate School

of Cornell University

in Partial Fulfillment of the Requirements for the Degree of

Doctor of Philosophy

by

Michael S. Bono Jr.

January 2015

DIELECTRIC MEASUREMENT OF ALGAL LIPID CONTENT FOR BIODIESEL PRODUCTION

Michael S. Bono Jr., Ph.D.

Cornell University 2015

Algae are a promising feedstock for biodiesel production. Real-time monitoring of algal lipid content will enable increased productivity of algal biofuel feedstocks. Dielectric spectroscopy is well-suited to automated industrial monitoring and is sensitive to cellular properties, making it a promising method for algal lipid monitoring. In the first portion of this dissertation, I developed a method to measure the dielectric properties of algae cell suspensions and verified dielectric sensitivity to lipid accumulation via calibration with Nile red fluorometry. In order to develop an improved calibration method for my dielectric characterization, I then characterized intact algae cells via flow cytometry and quantitative ^{1}H NMR for development of an NMR-traceable flow cytometry protocol for algal lipid measurement. Flow cytometry provides information on the distribution of lipid content within algae populations, whereas ^{1}H NMR provides direct, rapid quantification of lipids in living cell suspensions without the need for cellular disruption and lipid extraction. In the final part of this dissertation, I used microfluidic single-cell impedance cytometry to simultaneously measure the impedance and fluorescence of individual algae cells with a range of lipid contents for development of an industrial algal lipid measurement system. This work has demonstrated the potential of dielectric spectroscopy for automated algal lipid monitoring, which will facilitate reliable harvest of algal biofuel feedstocks with high lipid content.

BIOGRAPHICAL SKETCH

Michael S. Bono Jr. was born in Bangor, Maine in 1987 and moved shortly after to Marietta, Georgia, where he lived until the age of 15 and began to explore science and engineering though programs such as Invention Convention, Science Olympiad, and the BEST robotics competition. In 2002 he moved to Clifton Park, New York, where he joined FIRST robotics which inspired him to decide to become an engineer. In 2005 he enrolled in Union College in Schenectady, New York as a Mechanical Engineering major. At Union he developed course materials for Prof. Ashraf Ghaly before beginning his research career by joining Union's aerogel lab led by Profs. Ann Anderson and Mary Carroll.

During his two years in the aerogel lab, Michael developed a recipe to fabricate alumina aerogels via supercritical extraction and investigated the effects of recipe formulation on aerogel properties, resulting in a publication in *Journal of Sol-Gel Science and Technology* (Bono Jr. et al., 2010). He also developed a protocol to characterize aerogels via scanning electron microscopy, and used this protocol to characterize the effects of recipe parameters on the structural morphology of alumina aerogels and superhydrophobic silica aerogels, with the latter characterization included in another publication in *Journal of Sol-Gel Science and Technology* (Anderson et al., 2010). For his senior design project, Michael built a gas-phase catalytic testing system in order to investigate aerogel-based replacements for existing automotive catalytic converters. He also minored in visual arts and mathematics and participated in indoor and outdoor track and field, which he had no natural talent at but taught him the benefits of perseverence and being surrounded by a good team of people.

In 2009 Michael enrolled in the PhD program at the Sibley School of Mechanical and Aerospace Engineering and joined Prof. Brian Kirby's lab. He

received an National Defense Science and Engineering Graduate (NDSEG) fellowship in 2010 and an honorable mention in the National Science Foundation Graduate Research Fellowship Program (NSF GRFP) the same year. In 2014, Michael traveled to the United Kingdom to work as a visiting researcher with Hywel Morgan and Daniel Spencer at the University of Southampton. Outside of the lab, he enjoys running, lifting, reading, making art, sleeping, puns, furry quadrupeds, and Gimme coffee.

For Anna Rothkranz (1914-2007), who always knew that I could do it.

ACKNOWLEDGEMENTS

First of all, I would like to thank my committee, Profs. Brian Kirby, Beth Ahner, and Jefferson Tester, for being a committee that I could brag to all of my grad-student friends about for the past few years. I'd like to thank Prof. Brian Kirby for being an excellent mentor over the years and giving me the right combination of guidance and freedom to become a better researcher. I'd like to thank Prof. Beth Ahner for the use of her lab for my algae culture, for answering my algae questions no matter how trivial, and for her many helpful comments on my journal article drafts. I'd like to thank Prof. Jefferson Tester for his insightful questions and advice during our meetings which helped me to connect my research to its intended application in sustainable energy.

Next, I'd like to thank all of the people who I've had the pleasure to do research with. I'd like to thank my colleagues in Kirby Lab for all their help over the years. In particular, I'd like to thank Jason Gleghorn for helping me to learn how to work with cells; Ben Hawkins, Charlie (Chao) Huang, and Vishal Tanson for helping me get started in electrokinetic characterization; Alex Barbati and Erica Pratt for being excellent role models as researchers; Steven Santana, Srinitya Arasanipalai, and Marie Godla for comradery during years of classes and lab work; Jim Smith for help with MATLAB licenses, international shipping, general life advice, and the LaTeX code for this document; and Tim Lannin, Fredrik Thege, Shalu Suri, and John (Jack) Hartman for giving me optimism about the future of Kirby Lab. I'd also like to thank the two undergraduate (now masters) researchers that I've had the honor of mentoring, Ravi Garcia and Dylan Sri-Jayantha. I didn't consider myself much of a leader before mentoring them, and it's been good to have motivated mentees to learn leadership from. In Ahner lab, I'd like to thank Kurt Rhoads for helping me get stared with algae

culture, Michael Walsh for the crucial suggestion to switch from NAPK to TAP medium, and Lubna Richter for helping me with my algae culture questions. I'd also like to thank Ivan Keresztes, Anthony Condo, and Christina Cowman-Eggert for helping me with my NMR measurements; Joe Sullivan for helping me fabricate the transmission line sample cell used for my initial dielectric characterization of algae cultures; and Polly Marion and Allison Pelletier for helping to coordinate meetings, signatures, and room reservations. Moreover, I'd like to thank Marcia Sawyer for her invaluable help and guidance throughout my PhD experience.

At the University of Southampton, I'd like to thank Prof. Hywel Morgan for allowing me to work in his lab and giving me expert advice on electrokinetic characterization. I'd also like to thank Dan Spencer for all of his helpful guidance, Alessandra La Gioia for teaching me how to set up the impedance cytometry experiments and unclog the microfluidic device, Jane Cooke for coordinating my arrival in the United Kingdom, Katie Chamberlain for fabricating the impedance cytometry microfluidic devices, Maria-Nefeli Tsaloglou for helping me get my algae culture set up, Isaac Jones for help with autoclaving my media, and Riccardo Reale, Josip Ivica, Elisa Battistelli, Sumit Kalsi, Faith Bateman, Prameen Kalikavunkal, Hend Alkhammash, Shimul Saha, Chang Kai Ming, Marie Held, Aaron Yu Wu, Jonathan West, Martin Fischlechner, Nima Pour, James Fraser, and Sarah Fraser for technical assistance, useful discussions, and helping me to feel at home in the United Kingdom. At Union College, I'd like to thank Profs. Ann Anderson, Mary Carroll, and Ashraf Ghaly for mentoring me in research and helping me to discover the joy of discovery.

Perhaps most importantly, I'd like to thank my parents, Michael and Margaret Bono, and sister Anne-Marie for encouraging my love of learning as a

child and continuing to offer advice and support through my time in grad school. I'd also like to thank Noel Pauli, Jesse Hopkins, Susanna Kahn, Veronica Pillar, Bri Pomeroy, Katherine Casey, Natasha Udpa, and Matthew Fulghum for commiserating with me about the joys and frustrations of science and Aaron Nagy, Michael Kimball, Steven Palleschi, Michael Ranalli, Patrick Lingane, Casey Wolfe, Jon Campano, Everett Schlawin, Kim Carroll, Sam Posen, Joe McKay, Ran Yan, Diwakar Gupta, Breanna Jackson, Giselle Klapper, Stephane Guerrier, Juliana Canale, Brittany Miller, Yifan Cheng, Carolina Acevedo Pardo, Jun Ma, Derek Plotkowski, Tim Putzke, Maria Putzke, Frank Havlak, Ben Hasseldine, Ben Johnson, Li Jiang, Matt Leineweber, Karen Chiang, Radhika Patel, Juan Gomez, Tauhira Hoossainy, Peter Ireland, Michelle Tong, Rodrigo Zeledon, Kirk Samaroo, Kathy Ehlert, Peter Radecki, Michael Mëllër, Alex Moore, Nicole Baran, Jared Maxson, Erin Wissink, Isaac Storch, and Natalia Storch for keeping me sane through the entire graduate school experience.

TABLE OF CONTENTS

Biographical Sketch . . . iii
Dedication . . . v
Acknowledgements . . . vi
Table of Contents . . . ix
List of Tables . . . xi
List of Figures . . . xii

1 Introduction 1

2 Detection of algal lipid accumulation due to nitrogen limitation via dielectric spectroscopy of *Chlamydomonas reinhardtii* suspensions in a coaxial transmission line sample cell 4
2.1 Abstract . . . 4
2.2 Introduction . . . 5
2.3 Methods . . . 9
2.3.1 Algae culture and reagents . . . 9
2.3.2 Nile red fluorescence . . . 11
2.3.3 Dielectric characterization . . . 12
2.3.4 Scattering parameter analysis and critical frequency selection . . . 14
2.4 Theory . . . 15
2.4.1 Suspension permittivity . . . 15
2.4.2 Transmission line model . . . 17
2.4.3 Parameter selection . . . 21
2.5 Results and Discussion . . . 23
2.5.1 Scattering parameters of algae suspensions . . . 23
2.5.2 Effects of nitrogen starvation . . . 25
2.5.3 Comparison with transmission line model . . . 25
2.5.4 Estimation of measurement precision . . . 28
2.6 Conclusions . . . 29
2.7 Acknowledgements . . . 30

3 Measurement of lipid accumulation in *Chlorella vulgaris* via flow cytometry and liquid-state ^{1}H NMR spectroscopy for development of an NMR-traceable flow cytometry protocol 31
3.1 Abstract . . . 31
3.2 Introduction . . . 32
3.3 Materials and Methods . . . 37
3.3.1 Algae culture . . . 37
3.3.2 Flow cytometry . . . 38
3.3.3 Liquid-state ^{1}H NMR . . . 40
3.3.4 Evaluation of measurement precision . . . 43

3.4 Results and Discussion . . . 44
3.5 Conclusions . . . 53
3.6 Acknowledgements . . . 54
3.7 Supplementary Information . . . 56

4 Detection of lipid accumulation in *Chlorella vulgaris* cells via single-cell impedance cytometry 62
4.1 Abstract . . . 62
4.2 Introduction . . . 62
4.3 Theory . . . 65
4.4 Materials and Methods . . . 67
4.4.1 Algae culture . . . 67
4.4.2 Sample preparation . . . 68
4.4.3 Data Acquisition . . . 69
4.4.4 Gating and processing . . . 71
4.4.5 Safety . . . 73
4.5 Results and Discussion . . . 73
4.5.1 Multishell modeling . . . 73
4.5.2 Combined impedance and fluorescence measurement . . . 77
4.5.3 Single-cell impedance spectra . . . 80
4.6 Conclusions . . . 89
4.7 Acknowledgements . . . 89

5 Conclusions 91

Bibliography 93

LIST OF TABLES

3.1 Culture conditions and measurements for each culture 45
3.2 Voltages used for flow cytometry detectors 56
3.3 Calculations for initial cell concentrations and TAG concentrations 58

4.1 Multivariable nonlinear fit coefficients for the complex impedance spectra measured for *Chlorella vulgaris* cells 79

LIST OF FIGURES

2.1 Coaxial transmission line sample cell 14
2.2 Multishell model, geometry of cell suspension within transmission line sample cell, and circuit representation of transmission line sample cell 17
2.3 Measured and theoretical transmission coefficient spectra for algae cell suspensions 24
2.4 Measured OD_{600} (top), normalized cellular lipid content NCLC (middle), and critical frequency f_c (bottom) for *Chlamydomonas reinhardtii* cultures over time 26
2.5 Measured critical frequencies for *Chlamydomonas reinhardtii* cells with different concentrations and lipid contents 28

3.1 Flow cytometry measurements for *Chlorella vulgaris* cells labeled with BODIPY 505/515 46
3.2 Representative measured NMR spectra for suspensions of *Chlorella vulgaris* cells 47
3.3 Background NMR spectra for TAP medium and inorganic NMR analysis solution 48
3.4 Mean BODIPY fluorescence per cell of each *Chlorella vulgaris* culture as measured via flow cytometry, plotted with respect to mean triacylglyceride (TAG) concentration per cell as measured via liquid-state ^{1}H NMR 50
3.5 Growth curves for *Chlorella vulgaris* in TAP medium for the growth conditions used in this study 56
3.6 Sample cytograms used for cell gating as described in the Materials and Methods section 57
3.7 Measured variation in BODIPY fluorescence and estimated initial cell concentration for a range of sample cell concentrations . 59
3.8 Calibration curves for the TMSP-d4 reference coaxial inserts used for the ^{1}H NMR measurements 60
3.9 Measured NMR spectra for suspensions of *Chlamydomonas reinhardtii* cells 61

4.1 Schematic of combined impedance and fluorescence cytometry setup, including microfluidic device, sensors, outputs, and triggering method. 70
4.2 Gating of impedance cytometry events based on impedance magnitude at 500 kHz ($|\mathrm{Z}(500\mathrm{kHz})|$) and chlorophyll fluorescence $(\mathrm{PMT2})_{\max}$, both measured as voltage (V). 72
4.3 Measured impedance magnitude spectra for *Chlorella vulgaris* cells and beads in PBS 77
4.4 Measured normalized complex impedance spectra for *Chlorella vulgaris* cells in PBS and fits to double-shell and triple shell models 78

4.5 Measured and complex impedance spectra for replete and nitrogen-limited *Chlorella vulgaris* cells and fits to a double-shell model 84
4.6 Measured mean single-cell impedance magnitude spectra for replete and nitrogen-limited *Chlorella vulgaris* cells 85
4.7 Measured single-cell impedance magnitude spectra for individual replete and nitrogen-limited *Chlorella vulgaris* cells 86
4.8 Measured single-cell *Chlorella vulgaris* lipid contents and estimated lipid content from a multilinear regression of single-cell impedance spectra 87
4.9 Principal component analysis of measured polar impedance components and BODIPY/Chlorophyll fluorescence ratio of replete and nitrogen-limited *Chlorella vulgaris* cells 88

CHAPTER 1

INTRODUCTION

Algae are a promising feedstock for biofuel generation due to their high growth rate and decreased land requirements relative to other biofuel feedstocks (Huang et al., 2010; Mata et al., 2010). However, the steps of the algal biofuel production process require improvement before algal biofuels can reach their full economic and energetic potential (Hannon et al., 2010). Among these challenges, cultivation is one of the most energy-demanding parts of algal biofuel production (Sills et al., 2013). As biodiesel is produced from biological lipids, reliable growth of algae with high lipid content will increase oil yield per energy input, making algae a more viable energy source (Hannon et al., 2010).

One of the most promising ways to increase algal lipid content is through environmental stesses (Huang et al., 2010). In particular, nitrogen starvation induces lipid accumulation in several algae species (Mata et al., 2010; Pruvost et al., 2009). However, these environmental stresses generally halt cell growth, resulting in an optimal harvest time (Rodolfi et al., 2008; Stephenson et al., 2010). However, algal growth is also affected by environmental factors such as light and temperature (Hoffmann et al., 2010; Hu et al., 2008), making it difficult to predict this optimal harvest time *a priori*. Use of wastewater as a growth medium can decrease production costs, but adds additional variability in growth rate and lipid accumulation (Beal et al., 2012; Sturm and Lamer, 2011). Because of these complicating factors, real-time lipid measurement is necessary in order to inform operational decisions by indicating the optimal harvest time.

However, existing lipid measurement methods are not suitable for real-time industrial monitoring, forcing industrial algae producers to cultivate and har-

vest their algae without knowledge of the lipid content over time. Traditional extraction and gravimetric determination is far too complicated for industrial monitoring, with multiple steps taking hours to days (Davey et al., 2012; Gao et al., 2008). Indirect methods such as Nile red staining (Chen et al., 2009) and Fourier-transform infrared spectroscopy (Dean et al., 2010) are faster but difficult to implement in an industrial setting due to the requirements for addition of precise amounts of dye and the need for sample drying before measurement (Mourant et al., 2003), respectively. Recently Davey et al. (2012) demonstrated a ^{1}H nuclear magnetic resonance (NMR) technique for algal lipid quantitation that is fast and accurate, but too capital-intensive for industrial lipid monitoring.

In this dissertation, I demonstrate the potential of dielectric spectroscopy as an analytical technique for algal lipid measurement in industrial settings. In Chapter 2, I show that dielectric properties of *Chlamydomonas reinhardtii* suspensions are altered by lipid content induced by nitrogen limitation. In Chapter 3, I present the use of liquid-state ^{1} NMR for calibration of flow cytometric measurement of algal lipid content. This approach enables the development of a precise NMR-traceable flow cytometry protocol that can be used for calibration of dielectric measurement techniques or investigation of algal lipid accumulation at the single cell level for development of improved strains and cultivation protocols. In Chapter 4, I measure the dielectric properties of algae cells at the single-cell level via impedance spectroscopy, fit ensemble-averaged impedance spectra to a multishell model for the dielectric properties of algae cells in suspension, and relate single-cell impedance spectra to simultaneous fluorescent measurements of algal lipid content. These accomplishments demonstrate that algal lipid accumulation results in a measurable change in dielectric properties

that could potentially be used for automated lipid monitoring of algal biofuel feedstocks.

CHAPTER 2

DETECTION OF ALGAL LIPID ACCUMULATION DUE TO NITROGEN LIMITATION VIA DIELECTRIC SPECTROSCOPY OF *CHLAMYDOMONAS REINHARDTII* SUSPENSIONS IN A COAXIAL TRANSMISSION LINE SAMPLE CELL

2.1 Abstract

In this study, dielectric characterization of algae cell suspensions was used to detect lipid accumulation due to nitrogen starvation. Wild-type *Chlamydomonas reinhardtii* (CC-125) was cultivated in replete and nitrogen-limited conditions in order to achieve a range of lipid contents, as confirmed by Nile Red fluorescence measurements. A vector network analyzer was used to measure the dielectric scattering parameters of a coaxial region of concentrated cell suspension. The critical frequency f_c of the normalized transmission coefficient $|S_{21}^*|$ decreased with increasing lipid content but did not change with cell concentration. These observations were consistent with a decrease in cytoplasmic conductivity due to lipid accumulation in the preliminary transmission line model. This dielectric sensitivity to lipid content will facilitate the development of a rapid, noninvasive method for algal lipid measurement that could be implemented in industrial settings without the need for specialized staff and analytical facilities.

The contents of this chapter were submitted to *Bioresource Technology* and accepted for publication as "Detection of algal lipid accumulation due to nitrogen limitation via dielectric spectroscopy of *Chlamydomonas reinhardtii* suspensions in a coaxial transmission line sample cell" (Bono Jr. et al., 2013)

2.2 Introduction

Algae are considered to be one of the most promising feedstocks for biodiesel production due to their high growth rate and decreased land requirements relative to other biofuel feedstocks (Mata et al., 2010). Many algae species produce significant biomass as lipids that can be converted to biodiesel, in addition to sugars that can be converted to ethanol or hydrogen without utilization of food crops or the conversion difficulties of woody or other lignocellulosic biomass (Jones and Mayfield, 2012). However, there are several aspects of the algal biodiesel production process which need to be improved before algal biofuels can become an economically feasible energy source (Hannon et al., 2010). In particular, the high lipid contents observed in laboratory cultures have been difficult to transfer to industrial production (Sturm and Lamer, 2011). Since biodiesel is produced from biological lipids, the ability to reliably grow algae with high lipid content at harvest will decrease the energy and monetary cost per unit of biodiesel produced (Hannon et al., 2010; Sturm and Lamer, 2011).

One of the most promising methods for increasing algal lipid content is to stress the cells by starving them of nutrients such as nitrogen (Pruvost et al., 2009) or sulfur (Cakmak et al., 2012). Nitrogen starvation in particular results in enhanced lipid accumulation in a wide variety of algae species (James et al., 2011; Mata et al., 2010). Because nitrogen starvation increases lipid levels at the cost of total growth, effective implementation involves a nitrogen-rich growth phase followed by a nitrogen-starved lipid conversion phase (Rodolfi et al., 2008; Stephenson et al., 2010). The average rate of lipid production then varies with time, resulting in an optimal harvest time. However, lipid production and growth rate are also affected by temperature (Hoffmann et al., 2010) and light

exposure (Pal et al., 2011). These enviromental parameters cannot be fully controlled in an industrial setting, making the optimal harvest time variable and nondeterministic. Moreover, one of the most promising ways to reduce the cost of algal biofuel production is to use wastewater as a culture medium (Sturm and Lamer, 2011); the resulting variation in the nutrient composition adds additional variability to algae cultivation process. These variations necessitate the use of real-time lipid monitoring for for optimal timing of harvesting and nutrient addition.

Industrial application of real-time monitoring requires improvements in lipid measurement techniques. Algal lipid content is traditionally measured by extraction and gravimetric determination, which is a complicated process requiring trained laboratory personnel and hours or days to complete (Gao et al., 2008; Gardner et al., 1985). Moreover, because the lipids are measured directly it is necessary to use large sample quantities — $\sim$10 g dry sample mass or $>$1 L culture volume (Gao et al., 2008) — or accurate measurement of masses on the order of μg (Gardner et al., 1985). These attributes make extraction and gravimetric determination far too slow and complicated for real-time lipid measurement.

Faster methods to quantify algal lipid content using Nile Red staining (Chen et al., 2009; Gao et al., 2008), Fourier transform infrared spectroscopy (FTIR) (Dean et al., 2010), or liquid-state ^{1}H Nuclear Magnetic Resonance (NMR) (Davey et al., 2012) are the topics of current research, and provide answers in minutes to hours. However, each of these techniques has limitations that make them difficult to translate to an industrial setting. Nile Red can be used for quantitation of neutral algal lipids (Chen et al., 2009); however, it has variable

effectiveness between algae species and organic solvents are required to penetrate the cell walls of some species (e.g. *Chlorella vulgaris*) (Chen et al., 2009; Dean et al., 2010).

FTIR of aqueous suspensions is complicated by the strong IR absorbance of water. Baseline correction is particularly difficult in cell suspensions owing to the wide variety of molecules present (Mourant et al., 2003). For these reasons, current algal lipid measurement techniques require that cells are dried before measurement (Dean et al., 2010). Liquid-state ^{1}H NMR can be used for rapid, non-invasive algal lipid measurement (Davey et al., 2012), but the high capital cost of NMR spectrometers makes this method prohibitive for industrial algal biofuel producers. All three of these methods are difficult to automate and require highly trained personnel, making them difficult to implement in industrial conditions.

Dielectric characterization methods offer a rapid (submillisecond), noninvasive, label-free method to measure cell lipid composition (Sun et al., 2007). These methods are dependent on the permittivities and conductivities of cellular components, providing insight into the composition of biological cells. Zhao et al. (2006) used dielectric spectroscopy to investigate the morphology of algae cells. Wu et al. (2005) found that *Chlorella protothecoides* cells exhibit different electrorotation spectra when grown under conditions resulting in different lipid contents, and Deng et al. (2013) used dielectrophoresis for binary separation of *Chlorella* cells with differing lipid contents. These results suggest that lipid accumulation alters the dielectric properties of algae cells. Higashiyama et al. (1999) correlated dielectric spectra with oil content in *Mortierella alpina* fungi cells, demonstrating that dielectric methods can quantitatively measure

biological lipid content.

Among these techniques, dielectric spectroscopy is most suited for online automated characterization. Electrorotation and dielectrophoretic characterization experiments both require microscopic imaging and electromechanical actuation of cells on multisecond time scales (Deng et al., 2013; Hawkins et al., 2011; Wu et al., 2005). As dielectric spectroscopy only requires measuring the electrical properties of a sample over a frequency range, it is well-suited to automated measurement. Simple one-frequency capacitance measurements have been adapted for real-time biomass monitoring (Kell et al., 1990) and are already available commercially, demonstrating that dielectric probes are capable of the simple, reliable operation that real-time lipid monitoring requires. Maskow et al. (2008) used online bulk dielectric spectroscopy for monitoring lipid accumulation in yeast, suggesting that dielectric spectroscopy can be used for algal lipid monitoring. Newly developed measurement and data processing techniques allow for automated dielectric characterization of individual cells (Sun et al., 2007), paving the way for more accurate dielectric monitoring than is possible for bulk samples and facilitating characterization of more dilute cultures without preconcentration. Dielectric lipid measurement requires calibration to a direct measure of lipid content and lacks the ability to differentiate between different lipid compositions with the same electrical properties. However, it uses relatively inexpensive instrumentation, does not require highly-trained technicians or on-site lab facilities, and is well-suited to automated measurement. These results and attributes suggest that dielectric methods will allow for reliable, automated online monitoring of algal lipid content in an industrial setting.

This work describes the dielectric characterization of wild-type *Chlamy-*

domonas reinhardtii (CC-125) cells with a range of lipid contents induced via nitrogen starvation. James et al. (2011) and Cakmak et al. (2012) observed lipid accumulation in *Chlamydomonas reinhardtii* CC-125 under nitrogen limitation, and dielectric characterization of this strain will inform the development of lipid measurement techniques for other algae species used for biodiesel production. The normalized transmission coefficient $|S_{21}^*|$ can be measured without dyeing, lysing, or drying the cells, and requires only a vector network analyzer, an affordable, commonly available electric characterization instrument. This characterization yields a critical frequency f_c that is sensitive to cellular lipid content but unaffected by changes in cell concentration. The characterization presented in this work will facilitate the development of both more accurate models of cell dielectric properties and automated single-cell dielectric characterization methods, with the end goal of an automated, online lipid measurement system that can be used for industrial monitoring of algal biofuel feedstocks.

2.3 Methods

2.3.1 Algae culture and reagents

Wild-type *Chlamydomonas reinhardtii* (CC-125, mt+) was acquired from the Stern Laboratory at the Boyce Thompson Institute of Plant Research and maintained in liquid TAP medium cultures. TAP medium for primary cultures was acquired from Invitrogen (Grand Island, NY, USA). TAP and TAP-N media for experimental cultures were prepared based on compositions from Deng et al. (2011) and Gorman and Levine (1965). Briefly,

TAP medium consisted of 10 mL 5x replete Beijerinck's solution (750 mM NH_4Cl, 35 mM $CaCl_2$, 40 mM $MgSO_4 \cdot 7H_2O$), 8.33 mL phosphate stock solution (98 mM K_2HPO_4, 54 mM KH_2PO_4), 10 mL Tris-Acetate buffer (2.00 M tris(hydroxymethyl)aminomethane, 1.75 M acetic acid), and 1 mL Hunter's trace metal solution (134 mM $Na_2EDTA \cdot 2H_2O$, 77 mM $ZnSO_4 \cdot 7H_2O$, 184 mM H_3BO_3, 26 mM $MnCl_2 \cdot 4H_2O$, 18 mM $FeSO_4 \cdot 7H_2O$, 7 mM $CoCl_2 \cdot 6H_2O$, 5 mM $CuSO_4 \cdot 5H_2O$, 8 μM $(NH_4)_6Mo_7O_24 \cdot 4H_2O$) added to milli-Q (millipore) water for each 1 L medium. TAP-N consisted of the same formulation, with the substitution of nitrogen-free 5x Beijerinck's salt solution (750 mM $NaCl$, 35 mM $CaCl_2$, 40 mM $MgSO_4 \cdot 7H_2O$) for replete Beijerinck's solution.

The effects of lipid accumulation on dielectric properties were investigated by inoculating 500 mL TAP medium in a 1000-mL Pyrex bottle with 1.4 mL liquid primary culture, then cultivating at 28 ± 1 °C and a photon flux density of 240 ± 20 μmol/m^{2}s, supplied by adjustable LED light panels (color temperature 5500 K) from Fancier Photographic Equipment (Ningbo, P.R. China). After 4 days of culturing in the initial TAP medium, cells were resuspended in either fresh TAP (replete) or TAP-N (nitrogen-limited) medium and cultured for up to 2 additional days. At resuspension, cultures were centrifuged for 14 min at 3000 g, resuspended in fresh medium at the same concentration as in the original TAP medium, and grown as 100-mL batch cultures in 250-mL Pyrex bottles. The effects of cell concentration on dielectric properties were investigated by cultivating 500-mL TAP cultures at 28 ± 1 °C and a photon flux density of 330 ± 10 μmol/m^{2}s for 4-6 days with no resuspension. In both investigations, cell concentration was quantified as the OD_{600} of the cell culture in a 1-cm-pathlength cuvette (Plastibrand 7591-65), measured using a Spectramax plus 384 spectrophotomer. The wavelength of 600 nm was selected based on mea-

sured absorption spectra of replete and nitrogen-limited cell suspensions (data not shown).

Nile red stain for fluorescence measurements was prepared by dissolving 1 mg/mL Nile red (fluorescence grade, from Sigma-Aldrich) in dimethyl sulfoxide (HPLC-grade, from Sigma-Aldrich) and storing frozen in 100-μL aliquots. Pure dimethyl sulfoxide (DMSO) was used as a negative stain control. Nile red fluorescence was measured with respect to lipid standards consisting of 2% chemically defined lipid concentrate (Gibco #11905, from Invitrogen) in deionized water, stored frozen in 1-mL aliquots.

2.3.2 Nile red fluorescence

Nile red fluorescence was used to quantify algal lipid content for calibration of the new dielectric measurement technique. Cell-free culture medium was obtained by centrifuging cell cultures for 14 min at 3000 g. The following 300-μL fluorescence samples were then prepared in a 96-well plate: 6 replicates per culture of cell suspension + 2 μL Nile red (denoted as “cells+NR"), cell suspension + 2 μL DMSO (denoted as “cells"), and cell-free medium (denoted as “med+NR"); 3 replicates per culture of suspending medium + 2 μL DMSO (denoted as “med"); and 3 replicates per experiment of lipid standard + 2 μL Nile red (denoted as “standard+NR") and deionized water + 2 μL Nile red (denoted as “DIW+NR"). The plate was then vortexed and incubated at room temperature for 30 minutes before measuring before beginning fluorescence measurements using a Synergy HT BioTek plate reader. The fluorescence was measured at 5 minute intervals for 30 minutes using an excitation filter of 530 ± 25 nm and

an emission filter of 590 ± 20 nm.

The relative Nile red fluorescence, here referred to as the relative cellular lipid content (RCLC) of each algae culture was then calculated using the following equation:

$$\mathrm{RCLC} = \frac{[\mathfrak{F}(\mathrm{cells} + \mathrm{NR}) - \mathfrak{F}(\mathrm{med} + \mathrm{NR})] - [\mathfrak{F}(\mathrm{cells}) - \mathfrak{F}(\mathrm{med})]}{\langle F(\mathrm{standard} + \mathrm{NR})\rangle - \langle F(\mathrm{DIW} + \mathrm{NR})\rangle} \tag{2.1}$$

$\mathfrak{F}(x)$ is the mean value of the maximum fluorescence for each sample of type x and $\langle F(x)\rangle$ is the mean value of all samples of type x over time. In order to account for differences in cell concentration, the RCLC for each cell culture is divided by the OD_{600} for that culture.The resulting quantity is referred to as the normalized cellular lipid content (NCLC):

$$\mathrm{NCLC} = \frac{[\mathfrak{F}(\mathrm{cells} + \mathrm{NR}) - \mathfrak{F}(\mathrm{med} + \mathrm{NR})] - [\mathfrak{F}(\mathrm{cells}) - \mathfrak{F}(\mathrm{med})]}{\mathrm{OD}_{600}\,[\langle F(\mathrm{standard} + \mathrm{NR})\rangle - \langle F(\mathrm{DIW} + \mathrm{NR})\rangle]} \tag{2.2}$$

Since the NCLC measures the Nile red fluorescence normalized by cell concentration, it provides a measure of lipid accumulation within the algae cells. The above expression for NCLC was found to be independent of cell concentration for cells diluted up to six times, with a sample coefficient of variation of 9% (data not shown). The above protocol is modeled after that of Bittar et al. (2013).

2.3.3 Dielectric characterization

Algae cell samples for dielectric characterization were prepared by centrifuging algae cultures for 14 min at 3000 g, then resuspending via aspiration in fresh TAP-N medium (conductivity $\sigma = 0.27 \pm 0.01\ \mathrm{S/m}$, measured with a Mettler-Toledo SevenMulti pH/conductivity meter). Cultures used to investigate lipid accumulation (4 days culture in initial TAP followed by 0–2 days culture in fresh

TAP or TAP-N) were concentrated by a factor of 37 ± 2. Cultures used to investigate the effects of cell concentration on dielectric properties (4-7 days culture in initial TAP, no resuspension) were concentrated by factors of 13, 20, 30, 40, and 50.

The concentrated cell suspensions were then placed in the coaxial transmission line sample cell shown in Figure 2.1. The transmission line sample cell, adapted from Maxwell (2007), consists of a semi-rigid coaxial cable (RG401/U, acquired from Pasternack Enterprises, Irvine, CA, USA) encased in two machined copper blocks. The copper outer conductor and polytetrafluoroethylene (PTFE) dielectric were removed from a 44-mm length of the coaxial cable, exposing the inner silver-plated copper conductor and creating an annular sample region with an inner diameter of 1.64 mm and an outer diameter of 6.35 mm when the sample cell was fully assembled. Aluminum machine screws were used to close the sample injection ports on top of the device, and modeling clay (Nicole Industries, Mt. Laurel, NJ, USA) was used to seal the ends of the sample cell against leakage as seen in Figure 2.1.

The dielectric scattering parameters of the algae cell suspensions in the sample cell containing were measured using a Hewlett-Packard 8753D vector network analyzer (VNA). Scattering parameters were measured at 801 frequency points log-distributed from 30 kHz to 3 GHz, with a sweep time of 3 s and 10 sweeps averaged for each scattering parameter. Scattering parameters were also measured with the same settings for the sample cell containing fresh cell-free TAP-N medium. Algae cultures were characterized using spectra of the scattering parameter S_{21}, known as the forward complex transmission coefficient.

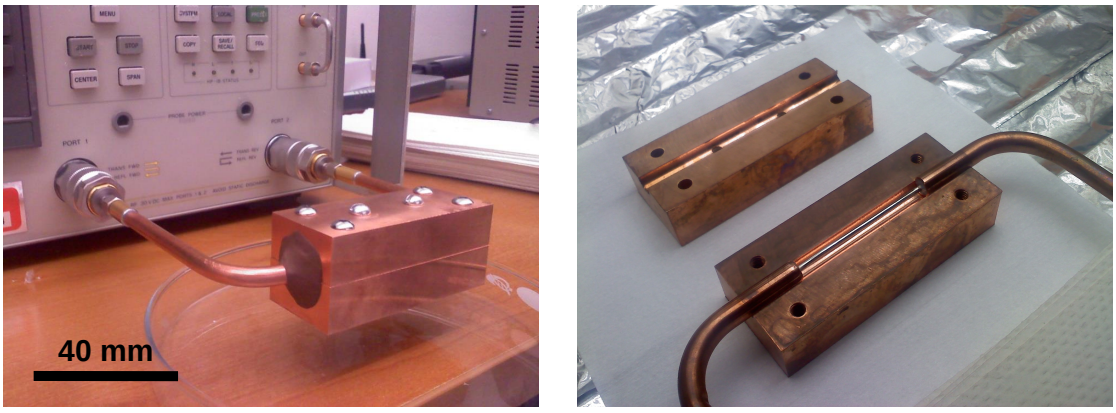

(a) (b)

Figure 2.1: Coaxial transmission line sample cell used for dielectric characterization of algae cell suspensions, shown (a) attached to the HP 8753D Vector Network Analyzer used to measure the scattering parameters of the loaded sample cell and (b) open so that the sample volume is visible. Based on a design from Maxwell (2007).

.

2.3.4 Scattering parameter analysis and critical frequency selection

The normalized transmission coefficient $|S_{21}^*|$ was calculated for each cell suspension by dividing the measured forward complex transmission coefficient S_{21} for the cell suspension by the measured S_{21} for the suspending medium with no cells present, normalizing the resulting scattering parameter by its own value at a reference frequency f_{ref} = 10 MHz, and considering the magnitudes of the resulting frequency-dependent complex quantity. The magnitude of $|S_{21}|$ is formally known as the forward gain, but $|S_{21}^*|$ is referred to as the normalized transmission coefficient for simplicity and to emphasize its physical nature of measuring the extent to which algae cell suspensions permit transmission of electromagnetic waves.

The critical frequency f_{c} of $|S_{21}^*|$ for each algae culture was determined by

smoothing $|S_{21}^*|$ using a 2^{nd}-degree Savitzky-Golay filter with a 30–point span, then numerically differentiating the smoothed spectrum and selecting the frequency with the minimal first derivative between 100 kHz and 1.25 MHz, corresponding to an inflection point in $|S_{21}^*|$ in that frequency range. MATLAB R2012a was used for all data analysis.

2.4 Theory

2.4.1 Suspension permittivity

Dielectric characterization of biological cells measures the interfacial polarization that occurs when an electric field is applied to a heterogeneous suspension. In a cell suspension, the cell components and suspending medium are lossy dielectrics: they attenuate electric fields via both polarization of the individual molecules and conduction of ions or electrons within each material. Hence, each component of the suspension is characterized by both an electrical permittivity ε, the degree to which it attenuates an electric field via polarization, and an electrical conductivity σ, the degree to which it allows passage of ions or electrons under application of an electric field. The pres-ense of both polarization and conduction results in a frequency-dependent dielectric response which can be evaluated by combining the permittivity and conductivity into a frequency-dependent complex permittivity $\varepsilon^* = \varepsilon + \sigma/j\omega$, where $j = \sqrt{-1}$ and $\omega = 2\pi f$ is the angular frequency of the applied electric field.

When an electric field is applied to a particle suspension, interfacial polarization at the particles' surfaces will result in an effective solution permittivity

$\varepsilon^*_{\text{eff}}$ that is a function of the complex permittivities of the particles (ε^*_p) and the suspending medium (ε^*_m). This change in permittivity occurs owing to the modification of the electric field near the particles, which will resemble that formed by the presence of electric dipoles. If the suspension is sufficiently dilute that these induced dipoles do not interact, then the effective suspension permittivity can be described by Maxwell's mixture equation (Kirby, 2010):

$$\varepsilon^*_{\text{susp}} = \varepsilon^*_m \left[\frac{1 + 2\varphi f^*_{\text{CM}}}{1 - \varphi f^*_{\text{CM}}} \right], \qquad f^*_{\text{CM}} = \frac{\varepsilon^*_p - \varepsilon^*_m}{\varepsilon^*_p + 2\varepsilon^*_m} \tag{2.3}$$

where φ is the volume fraction of the particles and f^*_{CM} is the complex Clausius-Mossotti factor, which describes the difference in dielectric properties between particles with complex permittivity ε^*_p and a suspending medium with complex permittivity ε^*_m.

Heterogeneous particles such as biological cells do not have a single ε^*_p; however, their behavior can be described by an effective ε^*_p that accounts for the morphology and electrical properties of the different cellular components. One simple but effective method to model the interfacial polarization within the cell is to treat it as a spherically symmetrical particle, with a cytoplasm surrounded by a discrete number of shells corresponding to different components of the cell membrane and wall. For a spherical particle consisting of a core with radius $\mathrm{R_core}$ and complex permittivity $\varepsilon^*_{\text{core}}$ surrounded by a shell with radius $\mathrm{R_shell}$ and complex permittivity $\varepsilon^*_{\text{shell}}$, the effective permittivity $\varepsilon^*_{\text{eff}}$ of the particle is (Kirby, 2010)

$$\varepsilon^*_{\text{p,eff}} = \varepsilon^*_{\text{shell}} \left[\frac{\frac{R^3_{\text{shell}}}{R^3_{\text{core}}} + 2f^*_{\text{CM}}}{\frac{R^3_{\text{shell}}}{R^3_{\text{core}}} - f^*_{\text{CM}}} \right], \qquad f^*_{\text{CM}} = \frac{\varepsilon^*_{\text{core}} - \varepsilon^*_{\text{shell}}}{\varepsilon^*_{\text{core}} + 2\varepsilon^*_{\text{shell}}} \tag{2.4}$$

This relationship can be applied iteratively to model particles with multiple shells, with the effective permittivity $\varepsilon^*_{\text{p,eff}}$ up to a given shell used as $\varepsilon^*_{\text{core}}$ for

the next core-shell interface. In the initial model, each *Chlamydomonas reinhardtii* cell is described as a spherical cytoplasm with complex permittivity ε^*_{cyt} surrounded by shells corresponding to the plasma membrane (with complex permittivity ε^*_{mem}) and the cell wall (with complex permittivity ε^*_{wall}), as shown in Figure 2.2a. More accurate modeling could be achieved by including the ellisoidal shape of the cell and the multiple components of the cell wall and cytoplasm (Goodenough and Heuser, 1985; Hawkins et al., 2011).

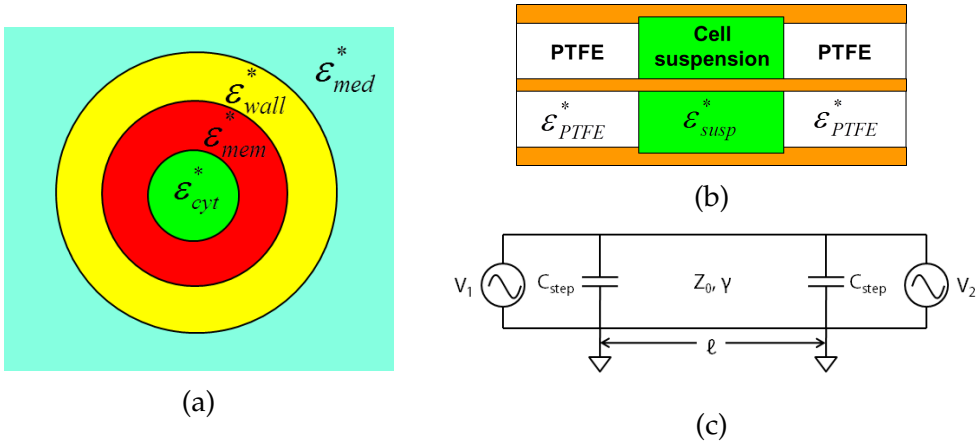

Figure 2.2: (a) Multishell model of cell morphology. ε^*_{cyt}, ε^*_{mem}, ε^*_{wall}, and ε^*_{med} are the complex permittivities of the cytoplasm, plasma membrane, cell wall, and suspending medium, respectively, as defined in section 2.4.1. (b) Geometry of algae cell suspension within coaxial transmission line sample cell used for dielectric characterization (shown in Figure 2.1). (c) Circuit representation of the coaxial transmission line sample cell. Variables defined in section 2.4.2.

2.4.2 Transmission line model

In this study, the dielectric properties of each algae cell suspension are characterized by measuring the transmission coefficient S_{21} of a transmission line containing the cell suspension. Transmission line characterization enables measurement of dielectric properties over a wide frequency range, since transmission line analysis accounts for changes in the phase of the applied electric field over

the sample geometry. This allows for characterization even when the wavelength of the applied signal approaches the sample size.

A transmission line can be characterized by measuring its scattering parameter matrix S, a complex matrix representation of the portions of an incoming electromagnetic wave that are reflected and transmitted by the transmission line. Geometric differences in the electrical properties of the transmission line materials result in partial reflection of incident electromagnetic waves, making scattering parameters an indirect measurement of the complex permittivity $\varepsilon^*_{\text{susp}}$ of a volume of cell suspension contained within the sample cell as shown in Figure 2.2b.

A uniform two-conductor transmission line is a distributed circuit characterized by its characteristic impedance Z_0, complex propagation constant γ, and length ℓ. Z_0 and γ are determined by the electrical properties of the transmission line components as encapsulated in four differential circuit parameters: the series resistance R per unit length, the series inductance L per unit length, the shunt conductance G per unit length, and the shunt capacitance C per unit length (Pozar, 2012):

$$Z_0 = \sqrt{\frac{R + j\omega L}{G + j\omega C}}, \qquad \gamma = \sqrt{(R + j\omega L)(G + j\omega C)} \tag{2.5}$$

In a coaxial transmission line sample cell like the one shown in Figure 2.1, R corresponds to the surface resistance of the electrodes and L, G, and C correspond to sample volume magnetization, conduction, and polarization, respectively. For a uniform coaxial transmission line with inner radius a, outer radius b, and electrode surface conductance R_s containing a general lossy material with complex permittivity ε^* and magnetic permeability μ, the values of R, L, G, and

C are (Pozar, 2012)

$$R = \frac{R_s}{2\pi}\left(\frac{1}{a}+\frac{1}{b}\right) \qquad L = \frac{\mu}{2\pi}\ln\frac{b}{a} \tag{2.6}$$

$$G = -\frac{2\pi\omega\,\mathfrak{Im}[\varepsilon^*]}{\ln b/a} \qquad C = \frac{2\pi\,\mathfrak{Re}[\varepsilon^*]}{\ln b/a} \tag{2.7}$$

Transmission lines may contain a combination of discrete and distributed elements. In the coaxial transmission line sample cell used in this study, the transition from the PTFE dielectric to the cell suspension is accompanied by a change in outer conductor diameter, as seen in Figure 2.1. This change in diameter results in a shunt step capacitance C_{step} before and after the coaxial transmission line, as shown in the circuit diagram in Figure 2.2c. This step capacitance is a function of the geometry of the transition and the permittivities of the two dielectrics. Numerical analysis of the electromagnetic propogation modes at the transition yields the formula (Maxwell, 2007):

$$\begin{aligned} C_{\text{step}} = \pi a \varepsilon_{r,1}\Bigg[&\frac{\varepsilon_2^*}{\pi}\left(\frac{\alpha^2+1}{\alpha}\ln\frac{1+\alpha}{1-\alpha} - 2\ln\frac{4\alpha}{1-\alpha^2}\right) \\ &+ \left(4.12\times10^{-13}\right)(0.8-\alpha)(\tau-1.4)\Bigg]\ \text{F}, \\ \text{where}\quad &\alpha = \frac{b_1-a}{b_2-a}, \quad \tau = \frac{b_2}{a}, \end{aligned} \tag{2.8}$$

a is the inner conductor radius, b_1 and b_2 are the outer conductor radius before and after the transition, $\varepsilon_{r,1}$ is the relative permittivity of the dielectric before the transition, and ε_2^* is the complex permittivity of the dielectric after the transition. Thus, the full circuit for the transmission line sample cell (Figure 2.2c) consists of two shunt capacitances C_{step} on either end of a uniform coaxial transmission line with length ℓ, characteristic impedance Z_0, and complex propagation constant γ as defined above.

Transmission lines are characterized by measuring the scattering parameters of the transmission line. The scattering parameter matrix describes the portions of an incoming electromagnetic wave that are reflected and transmitted by a network. For a two-port network such as a single transmission line, the scattering parameter matrix is defined as (Pozar, 2012)

$$\begin{bmatrix} V_1^- \\ V_2^- \end{bmatrix} = \begin{bmatrix} S_{11} & S_{12} \\ S_{21} & S_{22} \end{bmatrix} \begin{bmatrix} V_1^+ \\ V_2^+ \end{bmatrix} \tag{2.9}$$

where V_i^- denotes the amplitude of a voltage wave exiting port i and V_j^+ denotes the amplitude of a voltage wave incident on port j. The diagonal components S_{11} and S_{22} of the scattering parameter matrix correspond to the forward and reverse reflection coefficents, respectively, and the off-diagonal components correspond to transmission coefficients. The dielectric characterization method described here utilizes the forward transmission coefficent S_{21}, which is the portion of an electromagnetic wave incident at port 1 which is transmitted to port 2. Because reflection of incident electromagnetic waves arises from differences in electrical properties between the cell suspension and the rest of the coaxial cable, S_{21} is a measure of the similarity in electical properties between the cell suspension and the PTFE dielectric in the remainder of the coaxial cable.

Measured scattering parameters can be related to sample material properties through the use of the transmission matrix, also known as the ABCD matrix. Whereas the scattering parameter matrix relates incident, reflected, and transmitted waves, the ABCD matrix relates the total voltage and current at ports 1 and 2 of a two-port network (Pozar, 2012):

$$\begin{bmatrix} V_1 \\ I_1 \end{bmatrix} = \begin{bmatrix} A & B \\ C & D \end{bmatrix} \begin{bmatrix} V_2 \\ I_2 \end{bmatrix} \tag{2.10}$$

For the ABCD matrix, I_1 is defined as the current flowing into port 1, whereas I_2 is defined as the current flowing out of port 2. This definition allows for analysis of a series of N network elements by defining an ABCD matrix for each element i and multiplying them together to determine the ABCD matrix for the entire network. The ABCD matrix for the sample cell circuit shown in Figure 2.2c is the product of the ABCD matrices for a shunt capacitance C_{step}; a transmission line with characteristic impedance Z_0, complex propagation constant γ, and length ℓ; and another shunt capacitance C_{step} (Pozar, 2012):

$$\begin{bmatrix} A & B \\ C & D \end{bmatrix}_{\text{sample}} = \begin{bmatrix} 1 & 0 \\ j\omega C_{\text{step}} & 1 \end{bmatrix} \begin{bmatrix} \cosh\gamma\ell & Z_0 \sinh\gamma\ell \\ Z_0^{-1}\sinh\gamma\ell & \cosh\gamma\ell \end{bmatrix} \begin{bmatrix} 1 & 0 \\ j\omega C_{\text{step}} & 1 \end{bmatrix} \tag{2.11}$$

The ABCD matrix can then be converted to a theoretical scattering parameter matrix for comparison with measured scattering parameters (Pozar, 2012).

In order to predict the measured scattering parameters for a sample with complex permittivity $\varepsilon^*_{\text{susp}}$, the complex permittivity is first used to define Z_0, γ, and C_{step}. These transmission line properties can then be used to define an ABCD matrix for the sample cell, which can be converted to the expected scattering parameters using the above equation for comparison with measurements.

2.4.3 Parameter selection

In order to anticipate expected changes in measured scattering parameters due to lipid accumulation, typical electrical properties of cellular components were used to calculate theoretical values of $|S^*_{21}|$ for different degrees of lipid accumulation. Depending on the species of algae, lipid accumulation during nitrogen

starvation may be accompanied by changes in other morphological and biochemical properties such as cell size (James et al., 2011), membrane properties (Wu et al., 2005), and starch content (Cakmak et al., 2012; Dean et al., 2010). Since this model is intended for anticipation of observed dielectric sensitivity rather than complete prediction of measured spectra, only the property changes directly due to cytoplasmic lipid accumulation were incorporated into this model, with all other cell properties held constant.

Electrical properties were selected from previously measured values for biological cells, using values for algae when possible. Geometrically, the *Chlamydomonas reinhardtii* cell were modeled as 14-μm-diameter spherical cytoplasms surrounded by a 4.5-nm-thick plasma membrane (Hawkins et al., 2011) and a 165-nm-thick cell wall (Goodenough and Heuser, 1985). Lipid accumulation was modeled as changes in the properties of the cytoplasm owing to the increased presence of lipid deposits (Higashiyama et al., 1999). The cytoplasm was modeled as having a relative permittivity of 60 (Hawkins et al., 2011; Sun et al., 2007) and a conductivity that decreased with lipid accumulation, with values of 1200, 400, and 200 mS/m selected for cells with low, intermediate, and high lipid content, respectively, based on inferred values from Higashiyama et al. (1999). This theoretical variation of cellular lipid content is shown in Figure 2.3c. For theoretical variation of cell concentration (Figure 2.3d), σ_{cyt} was held constant at 1200 S/m.

The membrane relative permittivity and conductivity were taken to be 2.3 and 10 μS/m, respectively, based on dielectric characterization of *E. coli* cells (Hawkins et al., 2011). The cell wall conductivity was modeled as 50 mS/m (measured by Wu et al. (2005) for *Chlorella protothecoides*), and the cell wall rel-

ative permittivity was taken as 60 in order to conform with measured spectra. The suspending medium relative permittivity was taken to be 80 (that of pure water), with a conductivity equal to the measured value of 0.27 S/m. Cell volume fraction φ was varied from 0.1 to 0.2 for theoretical variation of cell concentration (Figure 2.3d) and held constant at 0.1 for theoretical variation of cellular lipid content.

2.5 Results and Discussion

2.5.1 Scattering parameters of algae suspensions

As seen in typical $|S_{21}^{*}|$ spectra (Figure 2.3a), the critical frequencies f_{c} of cell suspensions with higher normalized cellular lipid contents (NCLCs) due to nitrogen starvation are lower than the critical frequency of a suspension of cells with lower lipid content. This is the expected effect according to the theoretical transmission line model, as seen in Figure 2.3c.

However, the critical frequency f_{c} remained relatively constant ($\mu \pm \sigma = 736 \pm 61$ kHz, N = 9) for cells cultivated in replete medium and concentrated to different degrees before dielectric characterization, as seen in the representative spectra in Figures 2.3b. There was some variation in f_{c} between cultures (presumably due to slight differences in lipid content and other cellular properties) but very little change for the same culture at different concentrations and no significant non-zero slope in f_{c} with respect to OD_{600} over all cultures (Figure 2.5a). This is also in agreement with the theoretical model (Figure 2.3d), which predicts that f_{c} will be independent of cell concentration. These results

indicate that dielectric characterization yields a critical frequency that is sensitive to algal lipid content and independent of cell concentration.

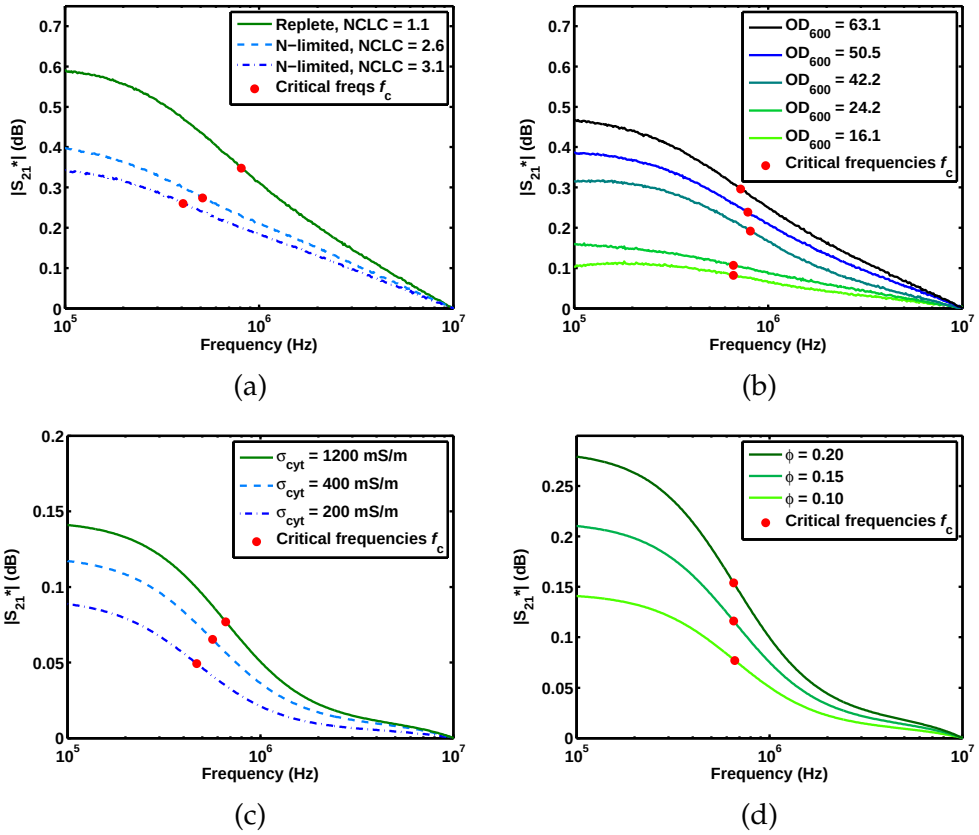

Figure 2.3: (a) Measured normalized transmission coefficients $|S_{21}^*|$ and critical frequencies f_c for *Chlamydomonas reinhardtii* cells suspended in TAP-N medium after culturing in replete or N-limited conditions for 2 days. NCLC is the normalized cellular lipid content as defined in section 2.3.2. (b) Measured normalized transmission coefficients $|S_{21}^*|$ and critical frequencies f_c for *Chlamydomonas reinhardtii* cells suspended in TAP-N medium at different concentrations after culturing in TAP medium for 4-6 days. Extrapolated OD_{600} is equal to the measured OD_{600} of the cell suspension multiplied by the factor of concentration. (c) Theoretical normalized transmission coefficients $|S_{21}^*|$ and critical frequencies f_c for cells modeled as described in section 2.4.1 with a constant volume fraction $\varphi = 0.10$, cytoplasmic conductivities from 200 - 1200 mS/m, and other properties as defined in section 2.4.3. (d) Theoretical normalized transmission coefficients $|S_{21}^*|$ and critical frequencies f_c for cells modeled as described in section 2.4.1 with volume fractions φ from 0.10 to 0.20, a constant cytoplasmic conductivity $\sigma_{cyt} = 1200$ mS/m, and other properties as defined in section 2.4.3.

2.5.2 Effects of nitrogen starvation

As seen in Figure 2.4, cells resuspended in nitrogen-limited medium exhibit greater normalized lipid content but decreased growth relative to cells resuspended in fresh replete medium, which grow significantly but actually exhibit a slight decrease in measured NCLC. This observed decrease suggests that cells grown to late-log stage in replete medium undergo a certain degree of lipid accumulation due to the reduced nutrients in the growth medium; this lipid accumulation is reversed once the cells are presented with a fresh source of nutrients. This is similar to the lipid accumulation and decreased growth observed by James et al. (2011) and Cakmak et al. (2012) for *Chlamydomonas reinhardtii* CC-125 during nitrogen starvation. The measured critical frequency f_c of the normalized transmission coefficient $|S_{21}^*|$ decreases with resuspension time in N-limited medium and increases slightly with resuspension time in replete medium, consistent with the trend of decreased f_c due to lipid accumulation shown in Figure 2.3a.

2.5.3 Comparison with transmission line model

When the measured critical frequencies f_c shown in Figure 2.4 are plotted with respect to the measured normalized lipid content (NCLC) for each algae sample, the critical frequency decreases with increasing lipid content as shown in Figure 2.5b. This is consistent with the trend predicted by the theoretical model (Figure 2.3c), in which lipid accumulation decreases the cells' cytoplasmic conductivity and thus the critical frequency f_c of $|S_{21}^*|$ for the cells in suspension.

Moreover, the measured decrease in f_c is greater than that predicted for lipid

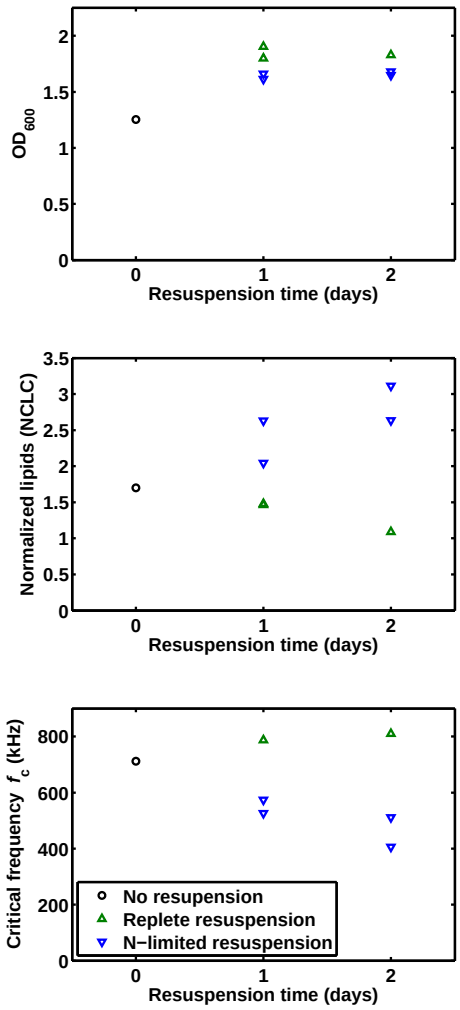

Figure 2.4: Measured OD_{600} (top), normalized cellular lipid content NCLC (middle), and critical frequency f_c (bottom) for *Chlamydomonas reinhardtii* cultures as a function of resuspension time in replete (TAP) or nitrogen-limited (TAP-N) media. Procedures for measuring OD_{600}, NCLC, and f_c are described in sections 2.3.1, 2.3.2, and 2.3.4, respectively.

accumulation alone. This is because the initial model considers only lipid accumulation and not other concurrent changes in cell morphology during nitrogen starvation. In reality, *Chlamydomonas reinhardtii* cells accumulating lipids due to nitrogen starvation also increase in size (Dean et al., 2010). Other al-

gae species have been observed to exhibit changes in the cell wall and plasma membrane (Wu et al., 2005) during lipid accumulation, suggesting the possibility of additional morphological and biochemical changes which have not yet been observed in *Chlamydomonas reinhardtii*. Further characterization of changes in microalgae cells during nitrogen starvation and other environmental stresses will enable a more detailed model which more accurately predicts changes in f_{c} during lipid accumulation.

In addition, the relaxation in $|S_{21}^{*}|$ occurs over a wider frequency range in the measured spectra than in the theoretical spectra. Cells in culture will exhibit a range of sizes and lipid contents (Berberoglu et al., 2008; Velmurugan et al., 2013). This polydispersity will result in a distribution of relaxation times τ_{cyt}, causing the measured relaxation to occur over a wider frequency range than that predicted by the current monodisperse suspension model (Asami, 2002). In addition, *Chlamydomonas reinhardtii* cells contains more components than accounted for in the initial two-shell cell model (Goodenough and Heuser, 1985). This will result in more interfaces and more relaxations, which may be sufficiently close to resemble one extended relaxation (Zhao et al., 2006). A more detailed model of *Chlamydomonas* cell morphology would result in an improved ability to estimate the electrical properties of algal cell components.

Future work will focus on investigating the distribution of lipid content and size in cells over a wide range of lipid accumulation in order to account for both morphological changes due to nutrient limitation and polydispersity within cell cultures. This will inform the development of a more accurate model for dielectric properties of algae cell suspension, facilitating more accurate lipid measurement and a better understanding of lipid accumulation due to nutrient

limitation.

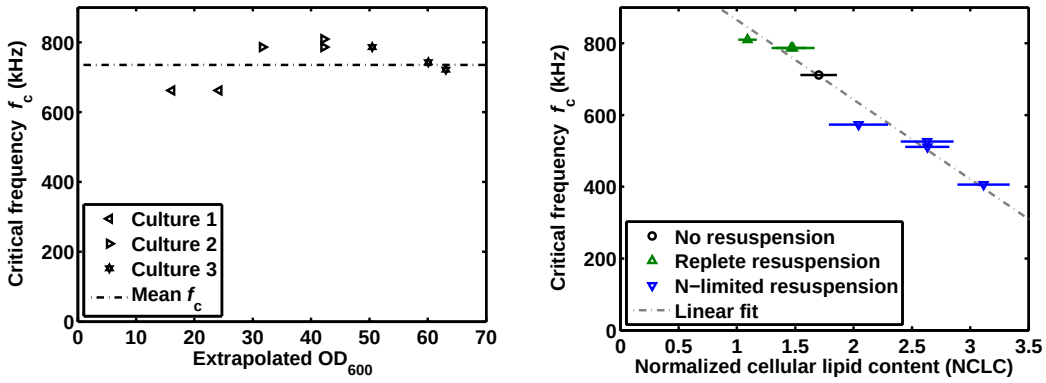

(a) (b)

Figure 2.5: (a) Measured critical frequencies f_c for *Chlamydomonas reinhardtii* cells suspended in TAP-N medium at different concentrations after culturing in TAP medium for 4-6 days, plotted as a function of extrapolated OD_{600}. (b) Critical frequencies f_c as defined in section 2.3.4 plotted with respect to normalized cellular lipid content (NCLC) as defined in section 2.3.2 for *Chlamydomonas reinhardtii* cells suspended in TAP-N medium after culturing in replete or N-limited conditions. NCLC error bars are ± 3 standard errors of the mean, calculated via propagation of error from the fluorescence replicates described in section 2.3.2. Linear fit is $\mathrm{NCLC} = 4.8970 - 0.0045 f_c$ for f_c measured in kHz.

2.5.4 Estimation of measurement precision

This study does not compare f_c to a direct measure of algal lipid content; however, the proportionality of Nile Red fluorescence to lipid content (Chen et al., 2009) allows comparison to previous direct measurements of lipid accumulation in *Chlamydomonas reinhardtii* CC-125 in order to estimate the measurement precision of the described dielectric characterization technique. James et al. (2011) measured lipid content of *Chlamydomonas reinhardtii* CC-125 as a percentage of cellular dry weight (%DW) and found that cells cultured for four days in TAP medium were 8.9%DW fatty acids, whereas cells cultured for four days in TAP-N medium were 12.9%DW fatty acids. Because their TAP culture was grown

to stagnation, it forms an analog to the cells in this study immediately before resuspension (NCLC = 1.68). Their TAP-N culture represents an upper limit of possible lipid content for CC-125, corresponding to the maximum measured NCLC of 5.35 for cells after three days of starvation (data not shown). The observed increase of 3.67 in NCLC over three days of starvation can then be said to correspond to approximately a 4%DW increase in lipids.

As described in section 2.5.3, the current model for cell permittivity does not fully describe the observed relationship between f_c and NCLC. A linear regression of NCLC as a function of f_c over the measured f_c range yields the empirical calibration curve $\mathrm{NCLC} = 4.8970 - 0.0045 f_c$ for f_c measured in kHz, with $r^2 = 0.959$ and a standard estimate error $\sigma_{\mathrm{est}} = 0.154$. If the increase in NCLC of 3.67 over three days of nitrogen starvation is taken to correspond to a lipid increase of 4%DW, then the precision of the empirical calibration curve is approximately 0.17%DW in the range of lipid contents encountered within two days of starvation. Future work will allow direct measurement of lipid content precision and deconvolution from other cellular changes in order to compliment the rough estimates presented in this study.

2.6 Conclusions

Dielectric spectroscopy is a rapid, noninvasive method for algal lipid measurement that could be implemented in industrial settings without the need for specialized staff and analytical facilities. In this study, dielectric characterization of wild-type *Chlamydomonas reinhardtii* cell suspensions was used to detect lipid accumulation due to nitrogen starvation. The critical frequency f_c of the nor-

malized transmission coefficient $|S_{21}^{*}|$ decreased with increasing cellular lipid content (as measured by Nile red fluorescence) but did not change with cell concentration, making it a promising marker for measuring algal lipid content.

2.7 Acknowledgements

This work made use of the Cornell Center for Nanoscale Systems (NSF EEC-0117770, 0646547 and NYSTAR C020071), Cornell Center for Materials Research (NSF DMR-0520404, DMR-1120296), Cornell Nanobiotechnology Center, and Emerson Manufacturing Teaching Lab. MSB was supported by the Department of Defense (DoD) through the National Defense Science and Engineering Graduate Fellowship (NDSEG) Program. The authors would like to acknowledge Lawrence Bonassar for use of the plate reader, Zackary Johnson (Duke University) for the detailed Nile red protocol, and Kurt Rhoads (Case Western Reserve University), Lubna Richter, Michael Walsh, Joseph Sullivan, Susanna Kahn, Matthew Fulghum (Pennsylvania State University), and members of the Cornell Micro/Nanofluidics Laboratory for technical assistance and helpful discussions.

CHAPTER 3

MEASUREMENT OF LIPID ACCUMULATION IN *CHLORELLA VULGARIS* VIA FLOW CYTOMETRY AND LIQUID-STATE ^{1}H NMR SPECTROSCOPY FOR DEVELOPMENT OF AN NMR-TRACEABLE FLOW CYTOMETRY PROTOCOL

3.1 Abstract

In this study, we cultured *Chlorella vulgaris* cells with a range of lipid contents, induced via nitrogen starvation, and characterized them via flow cytometry, with BODIPY 505/515 as a fluorescent lipid label, and liquid-state ^{1}H NMR spectroscopy. In doing so, we demonstrate the utility of calibrating flow cytometric measurements of algal lipid content using triacylglyceride (TAG, also known as triacylglycerol or triglyceride) content per cell as measured via quantitative ^{1}H NMR. Ensemble-averaged fluorescence of BODIPY-labeled cells was highly correlated with average TAG content per cell measured by bulk NMR, with a linear regression yielding a linear fit with $r^2 = 0.9971$. This correlation compares favorably to previous calibrations of flow cytometry protocols to lipid content measured via extraction, and calibration by NMR avoids the time and complexity that is generally required for lipid quantitation via extraction. Flow cytometry calibrated to a direct measurement of TAG content can be used to investigate the distribution of lipid contents for cells within a culture. Our flow cytometry measurements showed that *Chlorella vulgaris* cells subjected to nitrogen limitation exhibited higher mean lipid content but a wider distribution of

The contents of this chapter are in preparation for submission to *PLOS ONE* for publication as "Measurement of lipid accumulation in *Chlorella vulgaris* via flow cytometry and liquid-state ^{1}H NMR spectroscopy for development of an NMR-traceable flow cytometry protocol" (Bono Jr. et al., Manuscript in preparation)

lipid content that overlapped the relatively narrow distribution of lipid content for replete cells, suggesting that nitrogen limitation induces lipid accumulation in only a subset of cells. Calibration of flow cytometry protocols using direct *in situ* measurement of TAG content via NMR will facilitate rapid development of more precise flow cytometry protocols, enabling investigation of algal lipid accumulation for development of more productive algal biofuel feedstocks and cultivation protocols.

3.2 Introduction

The development of rapid, accurate methods to measure the lipid content of algae cells is important to the success of biodiesel production from this promising biomass resource (Lee et al., 2013b; Mata et al., 2010). Algae cells can accumulate high quantities of lipids, especially when subjected to environmental stresses such as nitrogen limitation. During environmental stress, neutral lipids in the form of triacylglycerides (TAGs) can accumulate up to 20-50% of dry cell weight (Hu et al., 2008) and are easily converted to biodiesel via transesterification (Mata et al., 2010). Because TAG biosynthesis is enhanced when algae are subjected to stresses that frequently also inhibit cell growth, algal lipid content can vary widely with growth conditions and over time (Lee et al., 2013b; Mata et al., 2010). This variability necessitates time-series measurement of lipid content for different growth conditions in order to improve cultivation protocols and monitor changes in lipid content during industrial production (Davey et al., 2012; Lee et al., 2013b). Moreover, during the screening of algae strains, investigation of lipid synthesis for genetic modification of existing strains, and development of cultivation protocols, it is particularly beneficial to characterize

algal lipid content at the single-cell level. Algae cells in culture exhibit a distribution of lipid contents for the same culture conditions (Davis et al., 2012), even for isogenic cultures (Wang et al., 2014). Single-cell lipid measurement facilitates sorting of cells with high lipid content for the development of more productive algae strains (Montero et al., 2011) and fundamental investigation of the dynamics of algal lipid accumulation (Wang et al., 2014), yielding knowledge that will enable genetic engineering of improved strains (Gimpel et al., 2013; Schmollinger et al., 2014).

Algal lipid content can be measured using a variety of methods, including direct measurement via extraction and gravimetric determination (Bligh and Dyer, 1959; Gardner et al., 1985); *in situ* spectroscopy via Fourier-transform infrared spectroscopy (FTIR) (Dean et al., 2010), Raman microspectroscopy (Wang et al., 2014), or nuclear magnetic resonance (Beal et al., 2010; Davey et al., 2012; Gao et al., 2008); electrokinetic characterization via dielectric spectroscopy (Bono Jr. et al., 2013) or dielectrophoresis (Deng et al., 2014; Hadady et al., 2014; Michael et al., 2014); and using fluorescence in bulk fluorometry (Chen et al., 2009) or flow cytometry (Cirulis et al., 2012; Hyka et al., 2013) of algae cells labeled with fluorescent lipid probes. Among these, flow cytometry is the most widely used analytical technique capable of characterizing algal lipid content with single-cell resolution. Flow cytometric instrumentation is inexpensive and widespread, and well-defined protocols exist for measuring algal lipid content simultaneously with other parameters such as cell size, internal complexity, chlorophyll autofluorescence, and enzyme activity at the single-cell level (Hyka et al., 2013). In addition, flow cytometry is capable of rapid characterization ($<$1 hr) and cell sorting in order to identify productive strains and prepare axenic cultures (Hyka et al., 2013; Montero et al., 2011) .

Algal lipid content has been measured via flow cytometry of cells labeled with Nile Red (Cirulis et al., 2012; de la Jara et al., 2003; Hyka et al., 2013). The excitation and emission maxima of Nile Red shift to lower wavelengths as the polarity of the environment surrounding the dye decreases, yielding a fluorescent probe that can be used for quantitation of neutral lipids, polar lipids, or the ratio of polar to neutral lipids in algae cells (de la Jara et al., 2003). However, as Nile Red does not specifically accumulate within lipid deposits, it can exhibit non-specific fluorescence when bound to proteins and other cellular components (Cirulis et al., 2012; O'Rourke et al., 2009). In addition, Nile Red fluorescence emission can overlap with that of chlorophyll autofluorescence (Govender et al., 2012; Hyka et al., 2013), resulting in spectral interference that complicates measurement. Nile Red uptake varies widely between cells, depending on the structure of the cell wall, and the fluorophore has limited photostability (Chen et al., 2009; Govender et al., 2012). As a result, accurate measurement often requires monitoring the Nile Red fluorescence over time in order to measure the maximum fluorescence (Bittar et al., 2013; Bono Jr. et al., 2013; Cooper et al., 2010).

Because of these limitations, the fluorophore BODIPY 505/515 (4,4-Difluoro-1,3,5,7-Tetramethyl-4-Bora-3a,4a-Diaza-s-Indacene) has been investigated as an alternative fluorescent label for algal lipid deposits (Cirulis et al., 2012; Cooper et al., 2010; Govender et al., 2012; Hyka et al., 2013). Unlike Nile Red, BODIPY exhibits uniform excitation and emission characteristics relatively independent of the pH and polarity of its surrounding environment (Cirulis et al., 2012; Govender et al., 2012). Instead of differing in emission characteristics based on the polarity of the surrounding environment, BODIPY accumulates in hydrophobic environments because of its high oil/water partition coeffi-

cient (Cooper et al., 2010), resulting in fluorescent labeling of algal lipid deposits with greater specificity than Nile Red (Govender et al., 2012). In addition, BODIPY fluorescence emission is significantly offset from chlorophyll autofluorescence, allowing for measurement without spectral interference (Hyka et al., 2013). BODIPY has good photostability and is easily transported across cell membranes because of its high oil/water partition coefficient, resulting in fluorescence that is relatively constant after cellular uptake and removing the need for time-series monitoring of cellular fluorescence (Govender et al., 2012). These characteristics make BODIPY a promising fluorophore for measuring single-cell algal lipid content.

As flow cytometry is an indirect measurement of lipid content via the fluorescence of lipid probes such as Nile Red or BODIPY, it must be calibrated to a direct measurement of lipid content. Currently, flow cytometry protocols are calibrated to lipid content measured via extraction (Cirulis et al., 2012). However, extraction of algal lipids results in fractional losses before analysis (Davey et al., 2012), and the amount of lipid extracted varies with the method of extraction (Lee et al., 2010). In addition, extraction of algal lipids using organic solvents may result in co-extraction of non-lipid components such as proteins and pigments, resulting in an overestimation of cellular lipid content when measured via simple gravimetric determination and necessitating additional steps such as transesterification and/or chromatographic separation in order to ensure that only lipids are quantitated (Lee et al., 2013b; Na et al., 2011; Weyer et al., 2010). As a result, historically algal lipid measurement via extraction has required a complicated, time-consuming process for accurate measurement (Bligh and Dyer, 1959; Gao et al., 2008; Gardner et al., 1985), although recently developed techniques for rapid extraction have somewhat decreased

the required time and complexity (Axelsson and Gentili, 2014). Because flow cytometry measures the fluorescence of lipid probes within intact algae cells, the aforementioned fractional losses and possible nonspecific extraction result in an inherent discrepancy between the quantity of lipids sampled via flow cytometry and extraction. We expect that calibration via direct *in situ* measurement of lipid deposits in intact algae cells will avoid this discrepancy, facilitating more precise calibration of flow cytometry protocols for quantification of lipid content in algae cells and other biological samples.

Nuclear magnetic resonance (NMR) spectroscopy is capable of determining the composition of complex biological mixtures with minimal sample preparation that generally avoids the complexity of chromatographic separation or chemical derivatization (Bearden, 2012). NMR spectroscopy can interrogate the interior of intact cells, enabling characterization of lipids and other metabolites within whole algae cells (Beal et al., 2010; Bondu et al., 2008; Chauton et al., 2003; Merkley and Syvitski, 2012). Of particular interest to this study, ^{1}H NMR spectroscopy has been used to quantitate intracellular TAG deposits within intact cells in biological tissues (Szczpaniak et al., 1999). Recently, Davey et al. (2012) quantitated TAGs in live microalgal cultures in their native growth media using liquid-state ^{1}H NMR spectroscopy and the quantitative NMR method developed by Henderson (2002); in this method, the reference compound is contained in coaxial inserts in order to avoid interactions between the reference and sample solutions. These results demonstrate that ^{1}H NMR spectroscopy is capable of *in situ* quantification of lipid deposits in intact cells, making it an appropriate calibration method for flow cytometry of algae cells labeled with fluorescent lipid probes. Moreover, the ease of sample preparation required for NMR spectroscopy makes it ideal for high-throughput calibration of flow cy-

tometry protocols for different algae species.

In this work, we demonstrate the utility of NMR calibration of single-cell flow cytometry measurements. We characterized algae cultures with a range of lipid contents via flow cytometric measurement of cells labeled with the fluorescent lipid probe BODIPY 505/515, and compared the resulting single-cell fluorescences with average TAG content per cell measured at the culture level via liquid-state ^{1}H NMR spectroscopy. We expect that the use of NMR spectroscopy for *in situ* direct measurement of lipid content will facilitate more accurate calibration of flow cytometry protocols based on the fluorescence of lipid probes within intact algae cells. As calibrated flow cytometry protocols can measure lipid content at the single-cell level, they provide valuable information on the distribution of lipid accumulation within a cell culture that can be used to investigate mechanisms for lipid accumulation dynamics, sort productive cells for improved strain development, or identify superior cultivation protocols for maximum biofuel production.

3.3 Materials and Methods

3.3.1 Algae culture

Chlorella vulgaris Beijerinck (UTEX 259) was acquired from the UTEX Culture Collection of Algae at The University of Texas at Austin and maintained in liquid TAP medium cultures. Media for primary and experimental cultures were acquired and prepared as described in Bono Jr. et al. (2013) based on earlier formulations for replete and nitrogen-free TAP media (Deng et al., 2011; Gorman

and Levine, 1965). Experimental cultures were prepared by inoculating 500 mL of TAP medium with 1.4 mL liquid primary culture and cultivating for 14 days at 24 ± 1 °C, a photon flux density of 150 ± 20 $\mu\mathrm{mol/m^2s}$, continuous lighting, and no stirring or shaking. These conditions were found to result in a growth rate of 0.26 ± 0.01 days^{-1} and a biomass concentration of 0.6 g/L during stationary phase (growth curves in supplementary information). We modulated the lipid accumulation by resuspending the *Chlorella vulgaris* in fresh nitrogen-replete or nitrogen-limited TAP medium and cultivating resuspended cells in 100-mL cultures for an additional 3–4 days at the culture conditions described above, resulting in the cultures described in Table 3.1. All other experimental details are as described in Bono Jr. et al. (2013).

3.3.2 Flow cytometry

We labeled *Chlorella vulgaris* cells with BODIPY 505/515 (4,4-Difluoro-1,3,5,7-Tetramethyl-4-Bora-3a,4a-Diaza-s-Indacene, Life Technologies, Grand Island, NY, USA) and measured their fluorescence with flow cytometry using a protocol adapted from Cirulis et al. (2012). Samples were prepared by first removing approximately 8 mL from the experimental culture without shaking or stirring. This ensured measurement consistency with the NMR measurement by characterizing only cells fully suspended within the medium as opposed to cells settled on the bottom of the culture vessel, as the suspended cells would be more likely to remain suspended in the reference region of the NMR sample tube during measurement.

Flow cytometry samples were then prepared by combining 930 μL sodium

phosphate buffer (40 mM, pH = 5.16), $10\ \mu$L cell culture, $1\ \mu$L BODIPY 505/515 stock solution (1 mg/mL in HPLC-grade dimethyl sulfoxide, stored frozen in 10-μL aliquots), and $50\ \mu$L CountBrite Absolute counting bead solution (Life Technologies). The BODIPY stock solution and counting bead solution were added in a darkened room to minimize photobleaching. We measured cellular fluorescence and scatter using an LSR II flow cytometer (BD Biosciences, San Jose, CA, USA) equipped with 488-nm and 355-nm lasers. For each flow cytometry event, we measured forward scatter (FSC) and fluorescence through the following fluorescence filters: FITC (530 ± 15 nm excited at 488 nm), PE-Cy7 (780 ± 30 nm excited at 488 nm), PerCP-Cy5.5 (695 ± 20 nm excited at 488 nm), Pacific Blue (450 ± 25 nm excited at 355 nm), and AmCyan (525 ± 25 nm excited at 355 nm). Voltages for each detector are listed in the supplementary information.

Cell events were gated according to their chlorophyll autofluorescence following the method developed by Cirulis et al. (2012). Briefly, chlorophyll autofluorescence was measured as infrared (PE-Cy7-A) and far red (PerCP-Cy5.5-A) fluorescence and plotted as cytograms of infrared vs. far red (sample cytograms in supplementary information). Events with insufficient infrared fluorescence (PE-Cy7-A $<$ 200 FIU) were rejected as debris. The remaining cell events exhibited a consistent ratio of infrared vs. far red fluorescence attributable to chlorophyll, resulting in a narrow linear distribution of cell events on the flow cytogram. Other events such as counting beads and BODIPY dye precipitate exhibited a lower ratio of infrared vs. far red fluorescence, resulting in linear distributions further down on the infrared vs. far red cytogram that could be easily excluded by a diagonal boundary below the cell events. Additional gating details are described in the supplementary information. The fluorescence of cells labeled with BODIPY 505/515 was measured using the FITC

filter. The voltage of the FITC detector was selected by characterizing unlabeled cells and adjusting the voltage so that between 10 and 100 out of 100,000 unlabeled cell events had FITC-A $>$ 100 FIU. The initial cell concentration of each culture was calculated from the number of counting bead events according to the instructions from the manufacturer; detailed calculations and a description of this approach are included in the supplementary information. At least 50,000 total events were measured for each flow cytometry sample, yielding at least 36,000 cell events.

3.3.3 Liquid-state ^{1}H NMR

Quantitative liquid-state ^{1}H NMR spectra were measured at 600 MHz on a Varian INOVA 600 spectrometer (Varian, Inc., Palo Alto, CA, USA), controlled using VnmrJ 1.1C software, using the method of containing the reference standard in coaxial inserts developed by Henderson (2002) and used by Davey et al. (2012) to quantify TAGs *in situ* in *Chlorella* cultures. In addition, we implemented a multipoint calibration of the reference coaxial inserts instead of the single-point calibration used by Henderson (2002) and Davey et al. (2012). NMR samples were prepared by first removing 12 mL of cell culture from the experimental culture without shaking or stirring the experimental culture. This ensured that only cells fully suspended within the medium were removed, as these suspended cells would be more likely to remain suspended in the reference region of the NMR sample tube during measurement. In order to increase cell concentration and minimize overlapping peaks from the tris(hydroxymethyl)aminomethane and acetate in the TAP medium, culture samples were centrifuged for 14 min at 3000 g and resuspended in 6 mL of an

inorganic NMR analysis solution isotonic to the TAP medium and consisting of 15 mM NaCl, 700 μM $\mathrm{CaCl_2}$, and 800 μM $\mathrm{MgSO_4 \cdot 7H_2O}$ in $\mathrm{H_2O}$.

Each final NMR sample was then prepared by pipetting $550\ \mu\mathrm{L}$ of resuspended algae culture into an NMR sample tube (Wilmad 535-PP-7, Wilmad-LabGlass, Vineland, NJ, USA) and inserting a coaxial insert (Wilmad WGS-5BL, Wilmad-LabGlass) containing $100\ \mu\mathrm{L}$ of a reference solution consisting of 2 mg/mL TMSP-d4 [3-(Trimethyl)propionic-2,2,3,3-d4 acid sodium salt, Sigma-Aldrich, St. Louis, MO, USA] and $60\ \mu\mathrm{g/mL}$ Diethylenetriaminepentaacetic acid gadolinium(III) dihydrogen salt hydrate (Sigma-Aldrich) in $\mathrm{D_2O}$ (99.9% D, Cambridge Isotope Laboratories, Tewksbury, MA, USA). Because the TMSP-d4 reference solution in the coaxial inserts occupies a different volume than the sample solution in the main NMR sample tube and is thus measured differently by the spectrometer receiver coils (Henderson, 2002), it was necessary to determine the effective concentration of TMSP-d4 in the sample solution due to the inserts by characterizing the inserts in sample solutions with known composition. To do this, we calibrated each insert by measuring ^{1}H NMR spectra for the insert placed in sample tubes containing $550\ \mu\mathrm{L}$ of sucrose ($\geq 99.5\%$, Sigma-Aldrich) in $\mathrm{D_2O}$ for sucrose concentrations from 5 to 50 mg/mL. The area of the signal for the anomeric proton of sucrose ($\delta = 5.4$ ppm) was normalized by the signal for the TMSP-d4 protons and correlated with the known sucrose concentrations — at least two concentrations for each insert, covering the range from 5 to 50 mg/mL — in order to calculate the effective TMSP-d4 proton concentration in the sample due to each insert. Sucrose calibration plots can be seen in the supplementary information.

NMR spectra for algae samples were measured after presaturation of the

water peak using the PRESAT pulse sequence provided by Varian. To determine the optimal presaturation frequency for each sample, the presaturation frequency was initially placed at the location of the water peak in a standard ^{1}H NMR spectrum and then varied to minimize the absolute value of the measured water peak in the PRESAT spectrum. Samples were characterized at $25\ ^{\circ}\mathrm{C}$ with no spinning. Spectra were measured from δ = -3.0 to 14.0 ppm with a presaturation delay of 2.0 s, a presaturation power of 160 Hz, a 90° observer pulse width of $7.25\ \mu$s, and a spectral width of 10191.1 Hz. Data sets of 16384 complex points were collected over an acquisition time of 1.608 s. To increase sensitivity, receiver gain was maximized for each sample with final values ranging from 46 to 54 dB. For final quantitative spectra, 1024 scans were averaged for each sample; however, acceptable spectra could also be acquired from as few as 64 scans.

We processed and analyzed the NMR spectra using the MestReNova software package (version 8.1.2, Mestrelab Research S.L., Santiago de Compostela, Spain). Phase correction was adjusted manually for each spectrum. Baseline correction was achieved by fitting each spectrum to a 4^{th}-order Bernstein polynomal. To determine the concentration of protons contained in algal TAG deposits, we integrated each spectrum over the TAG integral region from δ = 2.90 to 0.25 ppm, minus the region from δ = 1.92 to 1.89 ppm containing a peak from residual acetate in the suspending medium, and normalized the resulting intensity by the TMSP-d4 reference region from δ = 0.20 to -0.20 ppm. The normalized integral was then multiplied by the effective TMSP-d4 proton concentration in the sample due to the coaxial insert in order to calculate the concentration of protons in the TAG integral region. The concentration of protons in the TAG integral region was also measured for the NMR analysis solution

with no cells present, calculated to be 1.0 ± 0.3 mM, and subtracted from the concentrations of protons in the TAG integral region for each algae spectrum to determine the concentrations of protons per culture volume due to algal TAG deposits.

To convert the proton concentration to TAG concentration, we used the model TAG values developed by Davey et al. (2012) based on chromatographic analysis of isolated algae neutral lipids. Their calculated model triacylglyceride contained an average of 85 protons per molecule in the TAG integral region and a molecular weight of 850 g/mol. We divided each measured TAG proton concentration by the model number of protons per molecule, multiplied the resulting lipid concentration (in mol/L) by the model molecular weight, and divided by the factor of concentration after resuspension in the NMR analysis solution, yielding TAG concentrations as mass per volume of culture. These values were then divided by the initial cell concentration in the culture as measured via flow cytometry using absolute counting beads in order to calculate the measured concentration of TAGs per cell. Detailed calculations are shown in the supplementary information.

3.3.4 Evaluation of measurement precision

We evaluated the precision of the flow cytometric measurements for mean BODIPY fluorescence and initial cell concentration by characterizing flow cytometric samples of replete and nitrogen-limited cells over a range of concentrations. Flow cytometry samples were prepared as described above, but with added cell culture volumes of 1, 5, 10, 25, and 50 μL for each culture. We then charac-

terized each sample via flow cytometry as described above and calculated the coefficient of variation of the measured BODIPY fluorescence and cell concentration for samples from each culture. We used the highest measured coefficient of variation for each measured parameter as its relative uncertainty.

We evaluated the precision of the ^{1}H NMR measurements using the calibration for the reference coaxial inserts. As described above, each coaxial insert used for the ^{1}H NMR measurements was calibrated by measuring NMR spectra for known concentrations of sucrose containing the insert. The absolute uncertainty of this NMR measurement in terms of proton concentration was taken as the standard error of the estimate for a linear regression, with no constant term, of sucrose concentration with respect to normalized intensity of the sucrose anomeric proton. Plots of measured flow cytometric parameters with respect to sample cell concentration and the sucrose calibration plots can be seen in the supplementary information.

3.4 Results and Discussion

Flow cytometry experiments revealed that *Chlorella vulgaris* cells cultured in nitrogen-limited medium to induce lipid accumulation (Bono Jr. et al., 2013; Mata et al., 2010) exhibited greater BODIPY fluorescence per cell than cells cultured in nitrogen-replete medium (Figure 3.1). Cytograms of BODIPY fluorescence vs. forward scatter (Figure 3.1a) showed that cell events in each population with greater forward scatter (proportional to cell size) had greater BODIPY fluorescence, consistent with larger cells having higher absolute lipid content per cell. However, histograms of forward scatter (Figure 3.1b) showed that

the nitrogen-limited *C. vulgaris* cells exhibited approximately the same range of cell sizes as replete cells, whereas distributions of BODIPY fluorescence (Figures 3.1c and 3.1d) showed that nitrogen-limited cells exhibited substantially higher lipid accumulation than replete cells.

In addition, NMR spectra of nitrogen-limited cells exhibited increased intensity in a series of peaks from $\delta = 2.90$ to 0.25 ppm relative to spectra for unstressed cells cultured in replete media (Figure 3.2), indicating increased TAG deposits in the stressed nitrogen-limited cells. These TAG peaks are broader than those corresponding to the TMSP-d4 reference ($\delta = 0$ ppm) and residual growth medium components ($\delta = 1.9$ and 3.7 ppm), as seen when comparing these spectra to the background spectra for TAP medium and inorganic NMR analysis solution shown in Figure 3.3. This is because differences in magnetic susceptibility between the cellular components and the growth medium result in a heterogeneous applied magnetic field within the cells. This has previously been observed in liquid-state NMR measurement of cellular lipids by Davey et al. (2012) and Millis et al. (1997). By normalizing the integrated intensity of these peaks by the reference peak due to the calibrated coaxial insert placed in each algae NMR sample, we calculated the TAG content per culture volume which could then be converted to TAG content per cell using flow cytometric measurement of cell concentration for each culture.

Table 3.1: Culture conditions and measurements for each culture

Days after resuspension	Culture medium	Mean BODIPY fluorescence (FIU)	Cell conc. (10^6 cells/mL)	NMR TAGs (μg/mL culture)	NMR TAGs (fg/cell)
3	Replete	2500 ± 300	104 ± 6	20 ± 2	190 ± 20
3	N-limited	4300 ± 400	70 ± 4	49 ± 1	700 ± 40
4	Replete	1900 ± 200	137 ± 7	15 ± 1	110 ± 10
4	N-limited	5700 ± 600	56 ± 3	58 ± 2	1020 ± 60

Our NMR-derived values for TAG content (Table 3.1) are in agreement with

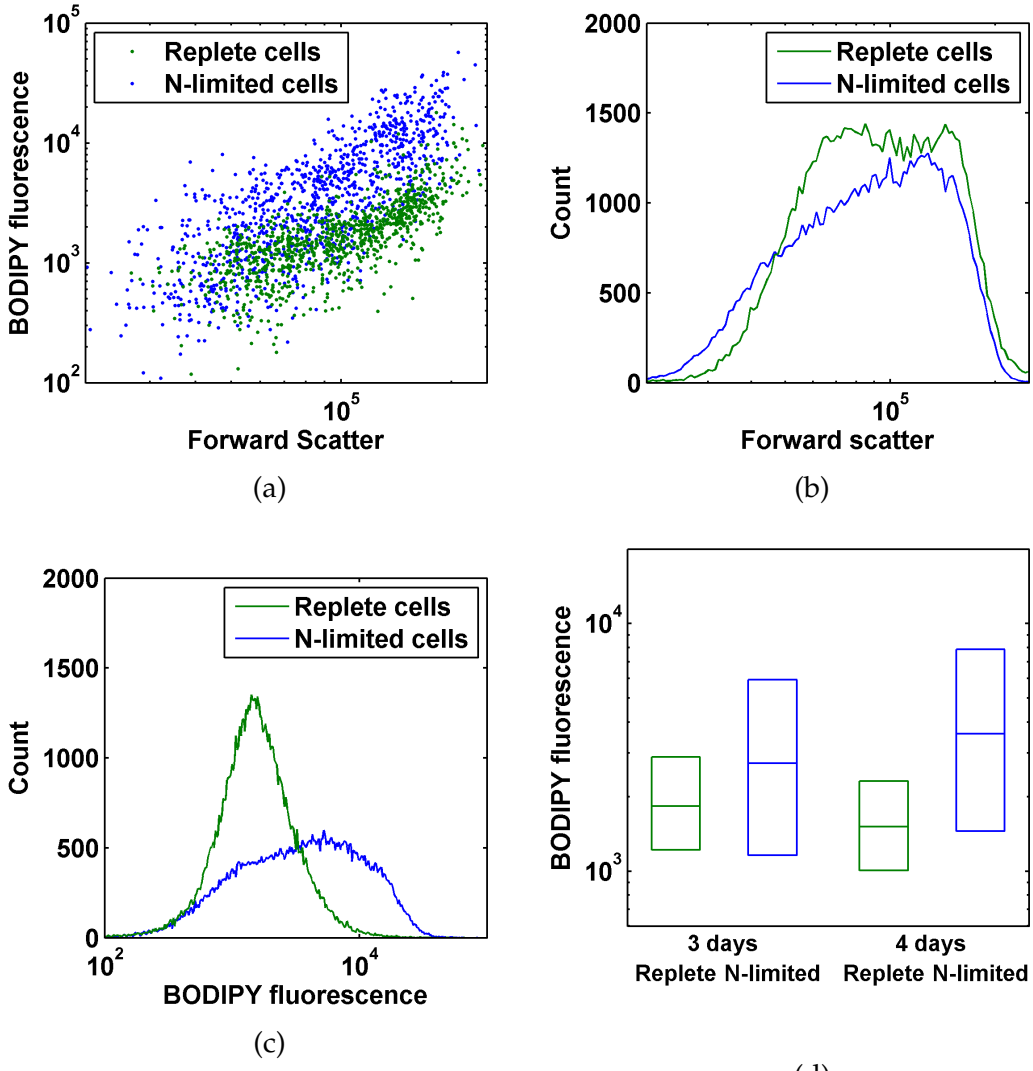

Figure 3.1: Flow cytometry measurements for *Chlorella vulgaris* cells labeled with BODIPY 505/515. All axes are logarithmic scale. (a) Flow cytogram of BODIPY fluorescence vs. forward scatter of cells after four days culturing in replete or nitrogen-limited medium. (b) Histogram of forward scatter for cells after four days culturing in replete or nitrogen-limited medium. (c) Histogram of BODIPY fluorescence for cells after four days culturing in replete or nitrogen-limited medium. (d) Box plot of medians and interquartile ranges (25th and 75th percentiles) for BODIPY fluorescence of cells after three and four days culturing in replete or nitrogen-limited medium.

previously measured values for *Chlorella* TAG content per cell and by culture volume. Vigeolas et al. (2012) measured a TAG concentration of approximately

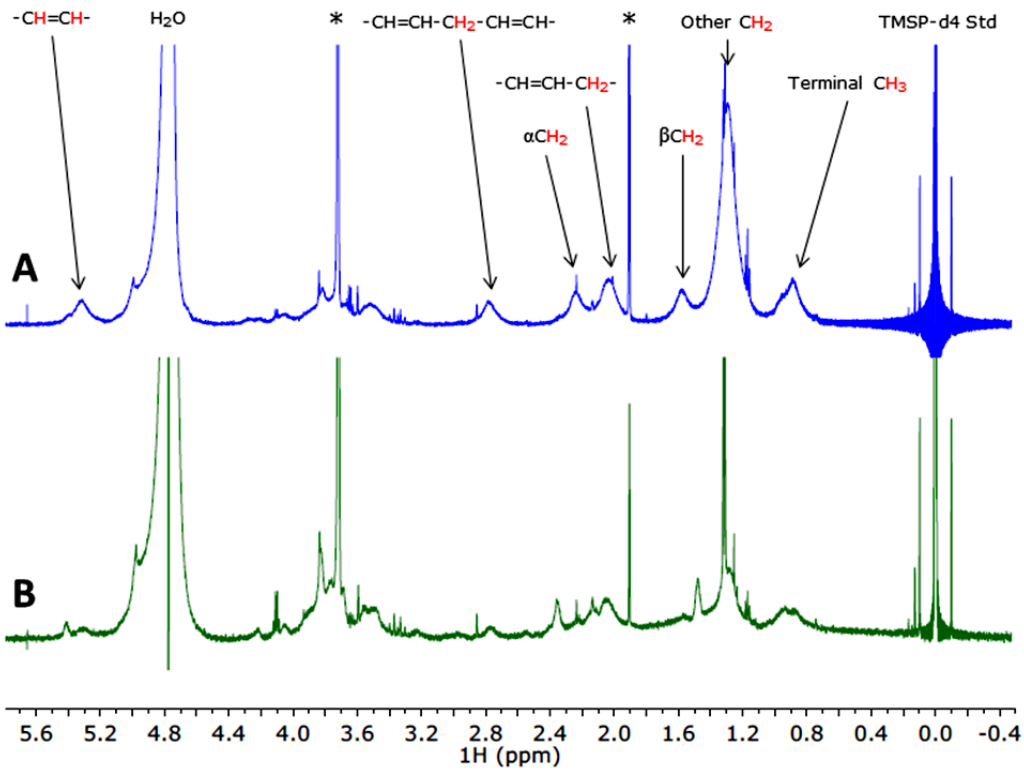

Figure 3.2: Representative measured NMR spectra for suspensions of *Chlorella vulgaris* cells cultured in (A) nitrogen-limited and (B) replete media, resuspended in an inorganic NMR analysis solution, and characterized with a coaxial insert containing a TMSP-d4 reference as described in the Materials and Methods section. Peak assigments taken from Davey et al. (2012). Asterisks indicate peaks due to residual tris(hydroxymethyl)aminomethane ($\delta = 3.7$ ppm) and acetate ($\delta = 1.9$ ppm) from the TAP medium. For scale, note that the side peaks located at $\delta = \pm 0.1$ ppm are ^{13}C satellite peaks for the TMSP-d4 reference. The combined integral intensity of these peaks is 1.1% of total TMSP-d4 intensity, corresponding to approximately 120 μM effective concentration.

110 fg/cell for *Chlorella sorokiniana* cultivated mixotrophically in TAP medium up to mid-exponential phase, similar to our measured value for *C. vulgaris* 4 days after resuspension in fresh replete TAP medium. Our measured TAG concentrations for *C. vulgaris* during nitrogen limitation are within previously measured ranges of up to 1600 fg per cell for *C. vulgaris* (Chia et al., 2013) and up to 222 μg per mL of culture volume for *Chlorella* sp. MAT-2008a (Davey et al., 2012). We also detected TAG deposits in nitrogen-limited *Chlamydomonas rein-*

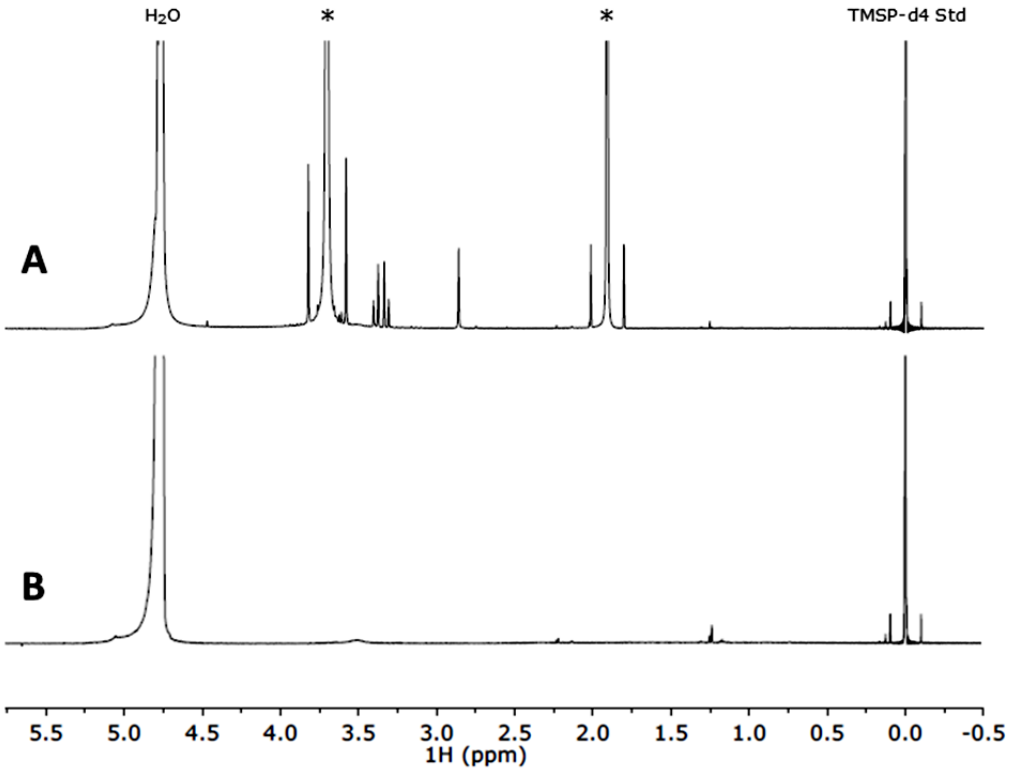

Figure 3.3: Background spectra for (A) the TAP medium that the algae were cultivated in and (B) the inorganic NMR analysis solution (15 mM NaCl, 700 μM $\mathrm{CaCl_2}$, and 800 μM $\mathrm{MgSO_4 \cdot 7H_2O}$ in $\mathrm{H_2O}$) that the algae were resuspended in for ^{1}H NMR measurements. Asterisks in the TAP medium spectrum indicate peaks from tris(hydroxymethyl)aminomethane ($\delta = 3.7$ ppm) and acetate ($\delta = 1.9$ ppm) that are also visible in our algae spectra due to residual tris(hydroxymethyl)-aminomethane and acetate, and are similarly indicated in those spectra. As in Figure 3.2, the side peaks located at $\delta = \pm 0.1$ ppm are ^{13}C satellite peaks for the TMSP-d4 reference, with a combined integral intensity of approximately 120 μM effective concentration.

hardtii CC-125 cells but not replete *C. reinhardtii* cells (spectra in supplementary information), consistent with previous measurements indicating that wild-type *C. reinhardtii* contains very low TAG concentrations under unstressed conditions but accumulates TAGs during nitrogen limitation (Siaut et al., 2011).

When we compared the mean BODIPY fluorescence and corresponding average TAG content per cell from ^{1}H NMR spectroscopy for each culture, there

was an excellent correlation between the two measurements of lipid content as shown in Figure 3.4. The observed relationship and the Gaussian shape of the BODIPY histogram for the replete cells in Figure 3.1c are consistent with a linear fluorescent response of BODIPY in algal lipid deposits as observed previously (Cirulis et al., 2012). A linear regression of mean BODIPY fluorescence $\langle \mathrm{BODIPY} \rangle$ in fluorescence intensity units (FIU) as a function of TAGs per cell by NMR [TAGs] in fg/cell yielded the linear fit $\langle \mathrm{BODIPY} \rangle = 3.911[\mathrm{TAGs}] + 1614$, with $r^2 = 0.9971$, $p = 0.0014$, and a standard error of the estimate of 112 FIU. This correlation compares favorably with the correlation measured by Cirulis et al. (2012) ($r^2 = 0.95$) between BODIPY fluorescence measured by flow cytometry and fatty acid per cell measured via extraction and titration, and is comparable to correlations between Nile Red fluorescence and lipid content via extraction achieved by Chen et al. (2009) using a plate reader assay ($r^2 = 0.998$) and Cirulis et al. (2012) using flow cytometry ($r^2 = 0.99$). However, correlations between Nile Red and lipid content are subject to the aforementioned limitations of Nile Red such as non-specific fluorescence (O'Rourke et al., 2009), spectral interference with chlorophyll autofluorescence (Govender et al., 2012; Hyka et al., 2013), and inconsistent uptake depending on cell wall structure (Chen et al., 2009), which complicate development of repeatable fluorescence protocols.

Based on our characterization of flow cytometry samples with cells from a given culture diluted to a range of sample cell concentrations, described in the section on evaluation of measurement precision, we determined that the flow cytometry protocol described here can be used for sample cell concentrations from 10^5 to 10^7 cells/mL with relative uncertainties of up to 10.3% for BODIPY fluorescence and 5.4% for estimated initial cell concentration. The standard error of the linear fit for BODIPY fluorescence as a function of TAGs by NMR

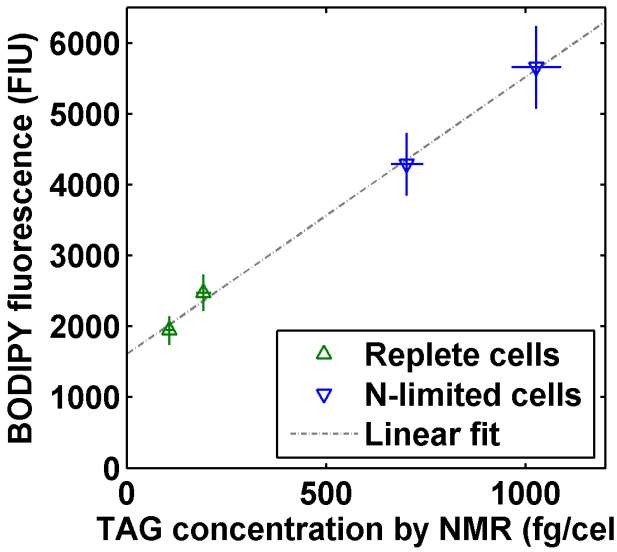

Figure 3.4: Mean BODIPY fluorescence per cell of each *Chlorella vulgaris* culture as measured via flow cytometry, plotted with respect to mean triacylglyceride (TAG) concentration per cell as measured via liquid-state ^{1}H NMR. Error bars for TAG concentration by ^{1}H NMR are calculated via propagation of uncertainty from the measured variation in estimated initial cell concentration and NMR quantification described in the evaluation of measurement precision section. Error bars for BODIPY fluorescence are taken directly from the measured variation in BODIPY fluorescence described in that section. Linear fit is $\langle \mathrm{BODIPY} \rangle = 3.911[\mathrm{TAGs}] + 1614$ ($r^2 = 0.9971$, $p = 0.0014$) for a linear regression of mean BODIPY fluorescence $\langle \mathrm{BODIPY} \rangle$ in fluorescence intensity units (FIU) as a function of mean TAGs per cell by NMR [TAGs] in fg/cell, with 95% confidence intervals of [3.268, 4.553] for the slope and [1209, 2020] for the intercept.

was only 112 FIU, considerably less than the calculated uncertainties in BODIPY fluorescence for each culture shown in Table 3.1. This is expected because the relative uncertainty of 10.3% for BODIPY fluorescence was measured over a factor of 50 in sample cell concentration and the cell concentrations used in the main study varied by less than a factor of 3. Based on the calibration of the reference coaxial inserts used for the ^{1}H NMR measurements, we estimated that the absolute uncertainties of the NMR measurements were 301 μM and 174 μM proton concentration for the inserts used, equivalent to 3.01 μg and 1.74 μg TAGs

per mL of sample culture volume. As seen in Figure 3.4, the measured BODIPY fluorescence and TAG concentration by NMR were within their combined uncertainties from the linear fit for all cultures characterized.

The calculated linear fit indicates that there is additional BODIPY fluorescence (1614 FIU) which is not accounted for by the TAGs measured via liquid-state ^{1}H NMR. We hypothesize that this is due to fluorescence from BODIPY molecules accumulated in non-TAG lipids such as phospholipids (Chandler and Volz, 2004; Govender et al., 2012). Liquid-state NMR only samples protons in molecules that can rotate freely, such as TAGs present within cytoplasmic lipid deposits (Davey et al., 2012). Protons in lipids with restrained motion, such as membrane phospholipids, are not detected because of line broadening due to chemical shift anisotropy and dipole-dipole interactions (Millis et al., 1997). Our NMR measurements are in agreement with those of Davey et al. (2012), who found that the lipid content of algae cultures measured via liquid-state NMR was less than that measured via fatty acid methyl ester derivation followed by gas chromatography (FAME-GC), which can quantitate both TAGs and ordered lipids such as membrane phospholipids. Use of semisolid NMR techniques such as high-resolution magic-angle spinning (HR-MAS) or intermolecular multiple-quantum coherence (iMQC) would facilitate quantitation of these ordered lipid molecules for improved calibration of BODIPY fluorescence (Cai et al., 2014). However, the excellent correlation that we measure between BODIPY fluorescence and TAG content by liquid-state NMR suggests that the cellular concentration of these ordered lipids is relatively unaffected by nitrogen limitation, with additional lipid accumulation mostly in the form of TAGs which can be quantitated via liquid-state NMR. This is in agreement with existing knowledge of the chemical composition of algal lipids synthesized in

response to environmental stress (Hu et al., 2008). Our current measurement approach facilitates develoment of an NMR-traceable flow cytometry protocol for quantification of cellular TAG deposits, with additional BODIPY fluorescence present which could be explained by the use of semisolid NMR techniques capable of quantifying ordered non-TAG lipids.

Our flow cytometry measurements suggest that nitrogen limitation induces lipid accumulation in only a subset of *C. vulgaris* cells. As we have shown that the mean BODIPY fluorescence of labeled cells in a culture measured via flow cytometry is strongly correlated with TAG content per cell by NMR, we can hypothesize that the distribution of measured BODIPY fluorescence for cells within a culture also indicates the distribution of lipid content for those cells. As seen in Figure 3.1c, *C. vulgaris* cells cultured in replete medium have a narrow distribution of BODIPY fluorescence, suggesting a relatively uniform lipid content. However, cells cultured in nitrogen-limited medium exhibit a wider range of BODIPY fluorescence that overlaps the range of fluorescences exhibited by replete cells. These measurements suggest that nitrogen-limited cells experience a range of lipid accumulation, with some cells accumulating no additional lipids. We observed this heterogeneity in lipid accumulation across cultures reuspended for 3 and 4 days, as seen in the box plot in Figure 3.1d. Heterogeneous lipid accumulation in algae cells during nitrogen limitation was also observed by Davis et al. (2012) in *Neochloris oleoabundans* cultures, and was even observed by Wang et al. (2014) in isogenic *Nannochloropsis oceanica* cultures, indicating that the observed heterogeneity is not entirely due to genetic differences within cultures. Lee et al. (2013a) used fluorescence microscopy to observe heterogeneous lipid accumulation in small populations (60 cells) of *Chlorella vulgaris* cells immobilized in hydrogel microcapsules and labeled with BODIPY.

However, to our knowledge no one has yet used a calibrated quantitative lipid measurement protocol and large sample populations (>36,000 cells per sample) to demonstrate increased heterogeneity in the lipid content of *Chlorella vulgaris* cells due to environmental stress.

Further study using isogenic algae cultures is necessary to determine if this observed heterogeneity is entirely due to variations in light and nutrient conditions (e.g. carbon dioxide due to diffusion from the culture air-water interface) within the unstirred cultures or is an instance of phenotypic heterogeneity as a bet-hedging survival strategy and part of the overall stress response, which has been observed in other microbial organisms (Holland et al., 2014; Levy et al., 2008) and suggested but not yet fully demonstrated in algae (Wang et al., 2014).

3.5 Conclusions

Single-cell fluorescence of *Chlorella vulgaris* cells labeled with BODIPY is strongly correlated with TAG content per cell as measured via liquid-state ^{1}H NMR, with a correlation coefficient $r^2 = 0.9971$ that compares favorably with the correlation between a similar flow cytometry protocol and lipid content measured via extraction. In their current forms, the flow cytometry and NMR protocols described here could be used to develop an NMR-traceable flow cytometry protocol for quantification of cellular TAG deposits. We expect that semisolid NMR techniques such as high-resolution magic-angle spinning (HR-MAS) or intermolecular multiple-quantum coherence (iMQC) would facilitate detection of ordered non-TAG lipids in order to account for fluorescence from BODIPY accumulated in these non-TAG lipids. The increased variability in

measured single-cell BODIPY fluorescence within each culture for nitrogen-limited cells suggests that only a subset of *C. vulgaris* cells accumulate additional lipids during nitrogen limitation. Heterogeneous lipid accumulation due to environmental stress has previously been observed in other algae species, but not *C. vulgaris*. Calibration of algal single-cell BODIPY fluorescence measured via flow cytometry and TAG content measured via liquid-state ^{1}H NMR enables more accurate calibration of single-cell fluorescence to absolute lipid content, facilitating measurement of single-cell lipid content for development of improved algal strains and cultivation protocols for biodiesel production.

3.6 Acknowledgements

This work made use of the Cornell University NMR Facility and the Cornell University Flow Cytometry Core Laboratory. The Flow Cytometry Core Laboratory acknowledges support by the ESCC Fund through NYS DOH Contract C026718. MSB was supported by the US Department of Defense (US DoD) through the National Defense Science and Engineering Graduate (NDSEG) Fellowship program and received partial support from the National Institutes of Health (NIH) via the Physical Sciences-Oncology Center at Cornell University. The authors would like to acknowledge Ivan Keresztes, Anthony Condo, and Christina Cowman-Eggert for assistance with acquiring NMR spectra, Lavanya Sayam for assistance in acquiring flow cytometry measurements, and Lubna Richter, Jefferson Tester, Jonathan West (University of Southampton), Zackary Johnson (Duke University), Frank Havlak, and members of the Cornell Micro/Nanofluidics Laboratory for technical assistance and helpful discussions. Opinions expressed here are solely those of the authors and do not necessarily

reflect those of the ESCC Board, the NYS DOH, NYS, the US DoD, or the NIH.

3.7 Supplementary Information

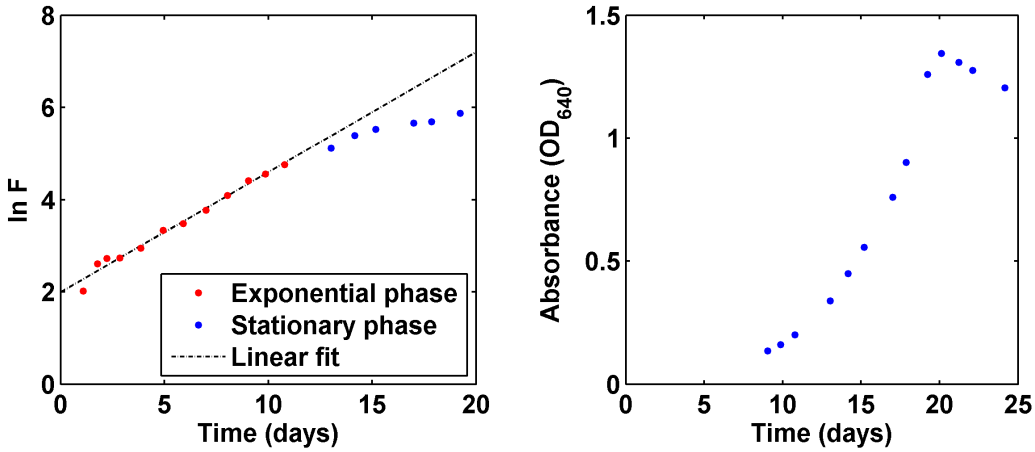

(a) (b)

Figure 3.5: Growth curves for *Chlorella vulgaris* in TAP medium for the growth conditions used in this study, plotted as (a) natural log of chlorophyll autofluorescence, excited at 440 nm and emission measured at 680 nm, and (b) absorbance at 640 nm. Chlorophyl autofluorescence was measured in order to calculate growth rate μ (in days^{-1}) by linear regression of the equation for exponential growth, $\mu = t \ln \mathrm{F} + \mathrm{C}$, to measurements for natural log of fluorescence $\ln \mathrm{F}$ during exponential growth, plotted with respect to time t measured in days. Absorbance was measured during stationary phase in order to determine the time of peak cell concentration. We measured fluorescence and absorbance using a Synergy H1 Hybrid Multi-Mode Microplate Reader (BioTek Instruments, Winooski, VT, USA). We measured the biomass at the end of stationary phase by removing 80 mL culture, concentrating it to 12 mL via centrifugation and resuspension, and lyophilizing the resuspended culture for five days in a FreeZone 4.5 Liter Benchtop Freeze Dry System (Labconco, Kansas City, MO, USA) before weighing the lyophilized biomass. From this measurement, we calculated a biomass concentration of 0.6 g/L at the end of stationary phase.

Table 3.2: Voltages used for flow cytometry detectors.

Detector	Excitation (nm)	Emission (nm)	Voltage (V)	Use in study
Forward scatter (FSC)	-	-	451	Size measurement, singlet gating
FITC	488	530 ± 15	302	BODIPY fluorescence
PE-Cy7	488	780 ± 30	429	Infrared, cell gating x-axis
PerCP-C5.5	488	695 ± 20	429	Far red, cell gating y-axis
Pacific Blue	355	450 ± 25	302	Counting bead gating
AmCyan	355	525 ± 25	302	Counting bead gating

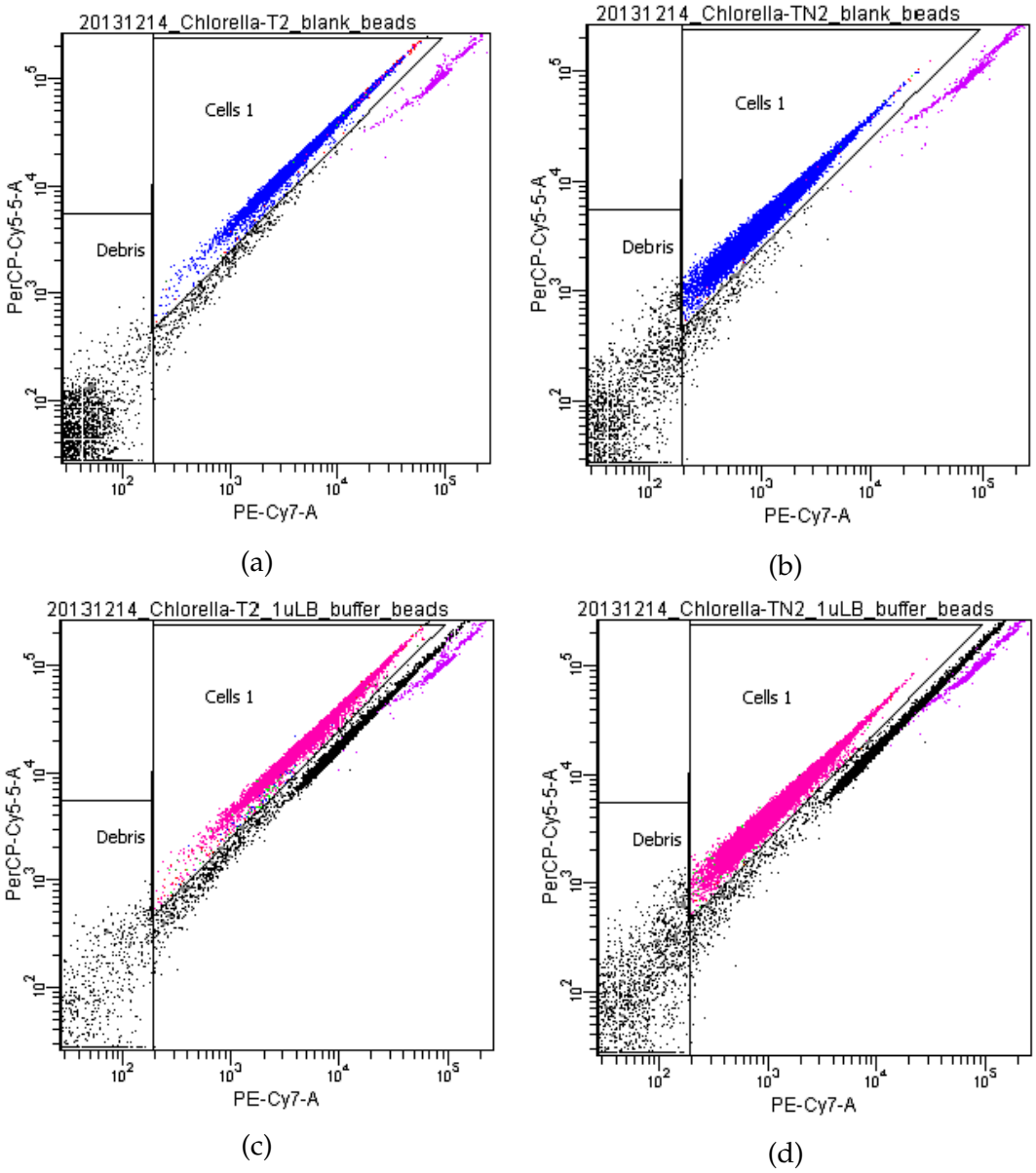

Figure 3.6: Sample cytograms used for cell gating as described in the Materials and Methods section of the main article, with cell events within the triangular gate in each PE-Cy7-A vs. PerCP-Cy5.5-A cytogram. Cell aggregates were excluded from these cell events by plotting cytograms of FSC-A vs. FSC-W for all cell events and rejecting events with FSC-W $>$ 80. Counting bead events, shown on these cytograms as purple events, were gated as events with Pacific Blue-A $>$ 2000 FIU and AmCyan-A $>$ 200 FIU, as algae cells exhibited minimal fluorescence at these wavelengths.

Table 3.3: Calculations for initial cell concentrations and TAG concentrations. Initial cell concentration was calculated using the number of counting bead events. Each flow cytometry sample included $50\ \mu\mathrm{L}$ of counting bead solution, containing approximately 54,000 counting beads. We could then use the number of counting beads and total sample volume ($991\ \mu\mathrm{L}$) to calculate the volume of sample analyzed in each measurement, which, along with the number of cell events measured, yielded the sample cell concentration and initial concentration of the cell culture. Average TAG concentrations per cell according to NMR measurements were calculated using the approach described in the Materials and Methods section of the main article.

Days after resuspension	3	3	4	4
Culture medium	Replete	N-limited	Replete	N-limited
Cell events	41124	36419	83502	72457
Bead events	2142	2828	3285	6939
Sample volume characterized (μL)	39.3	51.9	60.3	127.3
Sample cell concentration (cells/μL)	1046	702	1385	569
Initial cell concentration (10^6 cells/mL)	104 ± 6	70 ± 4	137 ± 7	56 ± 3
NMR insert used	A	B	B	A
Effective TMSP-d4 proton concentration (mM)	10.59 ± 0.02	10.81 ± 0.01	10.81 ± 0.01	10.59 ± 0.02
Precision of NMR measurement (μM protons)	301	174	174	301
Normalized integral over lipid region	0.368	0.896	0.264	1.085
Sample TAG proton concentration (mM)	3.9 ± 0.3	9.7 ± 0.2	2.9 ± 0.2	11.5 ± 0.3
Sample TAG concentration (μg/mL sample)	39 ± 3	97 ± 2	28 ± 2	115 ± 3
Sample concentration factor	1.97	1.98	1.97	1.98
Culture TAG concentration (μg/mL culture)	20 ± 2	49 ± 1	15 ± 1	58 ± 2
TAGs per cell (fg/cell)	190 ± 20	700 ± 40	110 ± 10	1020 ± 60

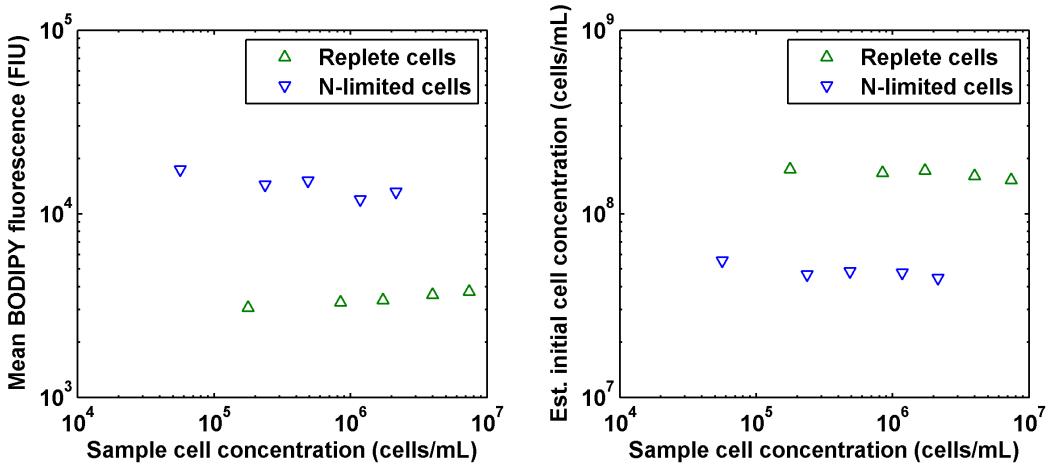

(a) (b)

Figure 3.7: Measured variation in (a) BODIPY fluorescence and (b) estimated initial cell concentration for a range of sample cell concentrations, varied by adding different amounts of an individual cell culture to flow cytometry samples as described in the Materials and Methods section. If we consider sample cell concentrations between 10^5 and 10^7 cells/mL, then the coefficients of variation for BODIPY fluorescence are 7.9% for the replete culture and 10.3% for the nitrogen-limited culture, whereas the coefficients of variation for estimated initial cell concentration are 5.4% for the replete culture and 3.6% for the nitrogen-limited culture. We take the larger measured coefficient of variation for each parameter, 10.3% for BODIPY fluorescence and 5.4% for estimated initial cell concentration, as the relative uncertainty for that parameter when measured for sample cell concentrations from 10^5 to 10^7 cells/mL. If we include sample cell concentrations less than 10^5 cells/mL then the coefficient of variation for the nitrogen-limited culture increases to 14.5% for BODIPY fluorescence and 8.6% for estimated initial cell concentration, so we do not claim that the flow cytometry protocol described here can be used for sample cell concentrations less than 10^5 cells/mL.

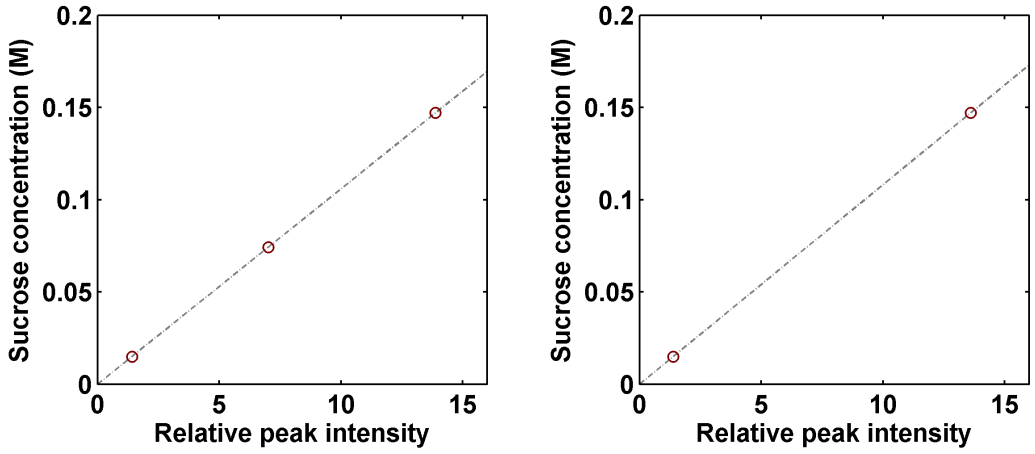

(a) (b)

Figure 3.8: Calibration curves for the TMSP-d4 reference coaxial inserts used for the ^{1}H NMR measurements, denoted as (a) Insert A and (b) Insert B. As described in the Materials and Methods section, inserts were calibrated by measuring the peak intensity of the anomeric proton of sucrose ($\delta = 5.4$ ppm) normalized by the TMSP-d4 reference peak for sucrose in D_2O at concentrations from 5 to 50 mg/mL. We calculated the effective TMSP-d4 proton concentration for each insert as the slope of a linear regression with no constant term for sucrose concentration as a function of normalized intensity of the sucrose anomeric proton peak. For insert A the calculated effective TMSP-d4 proton concentration was 10.59 mM, with a standard error of the effective proton concentration of 19 μM and a standard error of the estimate of 301 μM. For insert B the calculated effective TMSP-d4 proton concentration was 10.81 mM, with a standard error of the effective proton concentration of 13 μM and a standard error of the estimate of 174 μM. We used the calculated effective TMSP-d4 proton concentrations to calculate the concentrations of TAG protons in algae samples containing these inserts, with absolute uncertainties equal to the standard error of the estimate from these calibration curves.

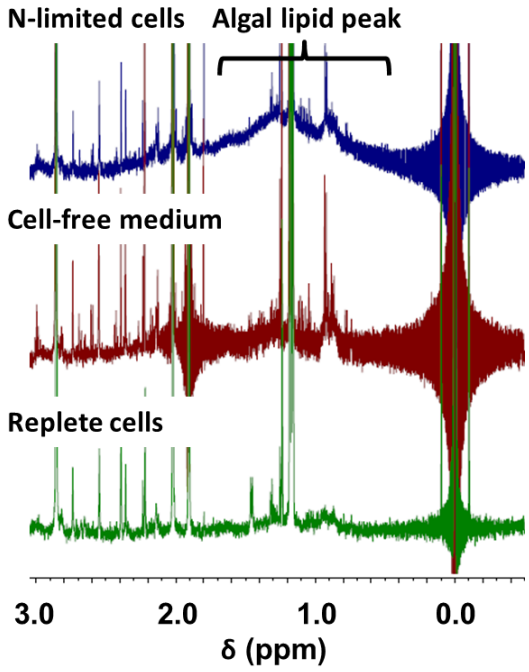

Figure 3.9: Measured NMR spectra for suspensions of *Chlamydomonas reinhardtii* CC-125 cells characterized in their native growth media. Nitrogen-limited and replete cells were cultured as described in Bono Jr. et al. (2013), with N-limited cells characterized 3 days after resuspension and replete cells characterized 1 day after resuspension. Cell-free medium is the supernatant for the N-limited cells. Spectra are an average of 512 scans. All other experimental details as described for *C. vulgaris* samples.

CHAPTER 4

DETECTION OF LIPID ACCUMULATION IN *CHLORELLA VULGARIS* CELLS VIA SINGLE-CELL IMPEDANCE CYTOMETRY

4.1 Abstract

In this work, we present single-cell impedance cytometry measurements for *Chlorella vulgaris* cells with a range of lipid contents. We show that ensemble-averaged single-cell impedance spectra for *Chlorella vulgaris* can be fitted to a double-shell model, yielding fitted parameters suggesting that lipid accumulation due to nutrient limitation results in a measurable decrease in cytoplasmic conductivity. We also demonstrate simultaneous single-cell measurement of fluorescence due to chlorophyll and BODIPY 505/515 as well as impedance at four frequencies, allowing lipid content to be correlated to impedance at the single-cell level. We show that nitrogen limitation significantly alters single-cell impedance spectra and relate single-cell impedance and lipid content via multilinear regression and principal component analysis. These results demonstrate the potential of dielectric spectroscopy for algal lipid monitoring during production of biodiesel feedstocks.

4.2 Introduction

Dielectric spectroscopy is a promising method for measuring algal lipid content. Basic capacitance measurements, i.e. single-frequency dielectric measurements,

The contents of this chapter are in preparation for submission to *Analytical Chemistry* for publication as "Detection of lipid accumulation in *Chlorella vulgaris* cells via single-cell impedance cytometry" (Bono Jr. et al., Manuscript in preparation)

are already used for basic biomass measurement (Kell et al., 1990) and have been extended to demonstrate sensitivity to lipid content in yeast cells (Maskow et al., 2008). Dielectric spectroscopy has been used to measure changes in cell cytoplasmic properties. Higashiyama et al. (1999) used bulk dielectric spectroscopy to relate fitted dielectric properties of the cytoplasm to lipid content in fungi cells. More recently, Haandbæk et al. (2014) used high-frequency single-cell impedance spectroscopy to detect differences in dielectric properties between yeast strains with different-sized vacuoles, demonstrating that single-cell impedance cytometry is capable of measuring cells' cytoplasmic properties.

Dielectric characterization methods have also been successfully used to characterize algae. Wu et al. (2005) showed that autotrophic and heterotrophic *Chlorella protothecoides* cells had different membrane and wall dielectric properties as measured via electrorotation, and Müller et al. (1998) and Zhao et al. (2006) fitted measured algae dielectric properties to a multishell model. In addition, we demonstrated the use of single-cell impedance cytometry to differentiate between phytoplankton species (Benazzi et al., 2007). More recently, there has been interest in using dielectric characterization to measure algal lipid content. Deng et al. (2013), Michael et al. (2014), and Hadady et al. (2014) showed that algae cells subjected to nitrogen starvation in order to induce lipid accumulation had different dielectrophoretic responses; however, these investigations only measured the sign of the dielectrophoretic response at different frequencies in order to sort algae cells with different lipid contents. We used bulk dielectric spectroscopy to detect lipid accumulation in *Chlamydomonas reinhardtii* and showed that the changes in dielectric properties were consistent with those predicted by a multishell model incorporating a decrease in cytoplasmic conductivity for cells with greater lipid accumulation (Bono Jr. et al., 2013), similar

to the effect observed by Higashiyama et al. (1999) for fungi cells. However, due to the mathematical complexity required to model the transmission line sample cell used we did not fit measured dielectric spectra to a multishell model. To date, measured dielectric properties of algae cells with different lipid contents has not been fitted to a multishell model in order to calculate changes in cytoplasm dielectric properties.

In the work described here, we used single-cell impedance cytometry to characterize *Chlorella vulgaris* cells with a range of lipid contents. We demonstrated that ensemble-averaged single-cell impedace spectra could be fitted to a multishell model in order to relate changes in lipid content to estimated changes in cytoplasmic conductivity. We found that impedance spectra for *Chlorella vulgaris* cells were adequately described by a double-shell model, with no improvement in fitting for a triple-shell model incorporating the trilaminar outer cell wall observed in many *Chlorella* species (Gerken et al., 2013; Griffiths and Griffiths, 1969). We also demonstrated combined impedance and lipid measurement for individual algae cells by simultaneously measuring single-cell impedance at four frequencies and fluorescence of cells labeled with the fluorescent lipid probe BODIPY 505/515. We showed that nitrogen limitation resulted in a significant change in single-cell impedance spectra, and investigated the relationship between impedance and lipid content for individual algae cells. This work demonstrates the potential of single-cell impedance cytometry for rapid, automated algal lipid measurement during production of algal biofuel feedstocks.

4.3 Theory

The effective permittivity of a dilute solution of particles with complex permittivity $\varepsilon_p^* = \varepsilon_p - j\sigma_p/\omega$ suspended in a medium with complex permittivity $\varepsilon_m^* = \varepsilon_m - j\sigma_{\mathrm{med}}/\omega$ at volume fraction φ is given by Maxwell's mixture equation (Kirby, 2010; Sun et al., 2009):

$$\frac{\varepsilon_{\mathrm{susp}}^*}{\varepsilon_m^*} = \frac{1 + 2\varphi f_{\mathrm{CM}}^*}{1 - \varphi f_{\mathrm{CM}}^*}, \qquad f_{\mathrm{CM}}^* = \frac{\varepsilon_p^* - \varepsilon_m^*}{\varepsilon_p^* + 2\varepsilon_m^*} \tag{4.1}$$

For spherically symmetric particles such as biological cells, the effective cell permittivity $\varepsilon_{\mathrm{p,eff}}^*$ is given by a similar relationship between the core, with radius $\mathrm{R_{core}}$ and complex permittivity $\varepsilon_{\mathrm{core}}^*$, and the shell, with radius $\mathrm{R_{shell}}$ and complex permittivity $\varepsilon_{\mathrm{shell}}^*$ (Kirby, 2010):

$$\varepsilon_{\mathrm{p,eff}}^* = \varepsilon_{\mathrm{shell}}^* \left[\frac{\frac{R_{\mathrm{shell}}^3}{R_{\mathrm{core}}^3} + 2f_{\mathrm{CM}}^*}{\frac{R_{\mathrm{shell}}^3}{R_{\mathrm{core}}^3} - f_{\mathrm{CM}}^*} \right], \qquad f_{\mathrm{CM}}^* = \frac{\varepsilon_{\mathrm{core}}^* - \varepsilon_{\mathrm{shell}}^*}{\varepsilon_{\mathrm{core}}^* + 2\varepsilon_{\mathrm{shell}}^*} \tag{4.2}$$

This relationship can be iterated multiple times for particles with multiple shells.

If we extend Maxwell's mixture equation to a polydisperse particle suspension where particle type i has volume fraction φ_i and Clausius-Mossotti factor $f_{\mathrm{CM},i}^*$, we can see that the suspension permittivity $\varepsilon_{\mathrm{susp}}^*$ is a nonlinear function of this distribution in properties:

$$\frac{\varepsilon_{\mathrm{susp}}^*}{\varepsilon_m^*} = \frac{1 + 2\sum_{i=1}^{n} \varphi_i f_{\mathrm{CM},i}^*}{1 - \sum_{i=1}^{n} \varphi_i f_{\mathrm{CM},i}^*}, \tag{4.3}$$

As a result, a distribution of cell properties such as size or lipid content results in a broadened bulk dielectric spectrum (Asami, 2002) that can complicate analysis for suspensions where the form of this distribution is unknown.

This complexity in characterizing polydisperse particles is avoided by characterizing individual cells via single-cell impedance spectroscopy (Holmes et al., 2009; Sun et al., 2009). When the impedance of an individual particle is measured as it passes between a pair of electrodes, the suspension consists of the cell and the immediately surrounding suspending medium. If we neglect impedance from the electrical double layers at the electrodes (valid for characterization at sufficiently high frequencies) and any parasitic impedances in the measurement system, then the resulting impedance $\mathrm{Z_{susp}}$ for an electrode geometry with geometric constant $\mathrm{G_f}$ is given by (Sun et al., 2009)

$$\mathrm{Z_{susp}} = \frac{1}{j\omega\varepsilon^*_{\mathrm{susp}}\mathrm{G_f}} \tag{4.4}$$

In practice parasitic impedance causes the measured $\mathrm{Z_{susp}}$ to differ from the above relationship. This can be controlled for by characterizing beads with known properties and normalizing the measured cell suspension impedance $\mathrm{Z_{susp,cell}}$ by the measured suspension impedance $\mathrm{Z_{susp,bead}}$ for beads with known dielectric properties. In this case the normalized impedance can be described by the relationship

$$\frac{\mathrm{Z_{susp,cell}}}{\mathrm{Z_{susp,bead}}} = \frac{\varepsilon^*_{\mathrm{susp,bead}}}{\varepsilon^*_{\mathrm{susp,cell}}} \tag{4.5}$$

and the unknown properties of cells can be estimated from this normalized impedance. Beads utilized for this purpose generally have negligible bulk conductivity; however, they can have significant conductivity arising from surface conductance $\mathrm{K_{surf,bead}}$. The resulting conductivity σ_{bead} can be calculated using the following relationship:

$$\sigma_{\mathrm{bead}} = 2\frac{\mathrm{K_{surf,bead}}}{\mathrm{R_{bead}}}. \tag{4.6}$$

The bead surface conductance is expected to vary with the medium conductivity σ_{med}. However, it is possible to fit it as a free parameter in a nonlinear

least-squares implementation of equation 4.5.

4.4 Materials and Methods

4.4.1 Algae culture

Chlorella vulgaris Beijerinck (CCAP 211/11b) was acquired from the Culture Collection of Algae and Protozoa (CCAP, SAMS Limited, Scottish Marine institute, Oban, Argyll, Scotland, UK) and maintained in liquid modified Bold Basal Medium with threefold Nitrogen and Vitamins (3N-BBM+V, CCAP). Replete and nitrogen-free TAP media for experimental cultures were prepared as described in Bono Jr. et al. (2013) based on earlier formulations (Deng et al., 2011; Gorman and Levine, 1965). Experimental cultures were prepared by inoculating 250 mL of TAP medium with 1.25 mL liquid primary culture and cultivating for 11 days at $25 \pm 1\,^{\circ}\mathrm{C}$, a photon flux density of $141 \pm 5\ \mu\mathrm{mol/m^2 s}$, continuous lighting, and no stirring or shaking. We varied lipid accumulation by resuspending the *Chlorella vulgaris* in fresh nitrogen-replete or nitrogen-limited TAP medium and cultivating resuspended cells in 50-mL cultures for an additional 4–9 days at the culture conditions described above, with 9 days corresponding to stagnation phase for cells resuspended in either medium. All other experimental details are as described in Bono Jr. et al. (2013).

4.4.2 Sample preparation

For high-frequency impedance cytometry, cells were resuspended in replete or nitrogen-limited TAP medium for 9 days, corresponding to stagnation phase, and diluted in phosphate-buffered saline (PBS, $\sigma = 1390$ mS/m) by adding 10 μL cell culture and 3.6 μL 10 vol% solution 7-μm polystyrene beads to PBS. For combined impedance and fluorescence cytometry, samples were prepared using an adaptation of the protocol developed by Cirulis et al. (2012) to label algae cells with the fluorescent lipid probe BODIPY 505/514 (4,4-Difluoro-1,3,5,7-Tetramethyl-4-Bora-3a,4a-Diaza-s-Indacene, Life Technologies, Grand Island, NY, USA). We combined 930 μL sodium phosphate buffer (40 mM, pH = 5.14), 10 μL cell culture, and 1 μL BODIPY 505/515 stock solution (1 mg/mL in HPLC-grade dimethyl sulfoxide, stored frozen in 10-μL aliquots), and incubated samples for at least 35 min. We then washed samples 1–2 times by centrifuging for 14 min at 3000 g, pipetting out 930 μL supernatant, and replacing the supernatant with 930 μL fresh sodium phosphate buffer. Samples characterized in 20% PBS (cells resuspended in replete TAP medium for 4 days) were then prepared by adding washed samples to 3 mL milli-Q water along with 1 mL PBS ($\sigma = 1390$ mS/m) and 3.6 μL 10 vol% solution 7-μm latex beads (Bangs Laboratories, Fishers, IN, US), yielding a solution with medium conductivity $\sigma_{med} = 357$ mS/m. Samples characterized in 40% PBS (cells resuspended in nitrogen-limited TAP medium for 5 days) were prepared by adding washed samples to 5 mL milli-Q water along with 4 mL PBS ($\sigma = 1390$ mS/m) and $1.8 - 3.6$ μL of 10 vol% solution 7-μm latex beads for a solution with medium conductivity $\sigma_{med} = 612$ mS/m.

4.4.3 Data Acquisition

Cell impedances and fluorescences were measured using a microfluidic device, impedance measurement system, and optical measurement system (Figure 4.2) which we have described previously (Holmes et al., 2007, 2009; Spencer et al., 2014). Briefly, the cells flow through a microfluidic channel that narrows to 30 μm wide and 40 μm at the point of interrogation by pairs of platinum electrodes 30 μm wide patterned onto overlapping glass surfaces. Sample flow rate was varied from 10 to 20 μL/min. Electrical and fluid connections were maintained by clamping the microfluidic device to spring-loaded electrical contacts and miniature O-rings in a plastic holder fabricated using an UP! Mini 3D printer (Beijing Tiertime Technology, Beijing, PR China) as described previously (Holmes et al., 2009; Spencer et al., 2014).

Single-cell impedance was measured using a Zurich Instruments HF2IS impedance spectroscope (Zurich Intruments AG, Zurich, Switzerland), with electrical signals from the device amplified beforehand using a Zurich instruments HF2TA transimpedance amplifier (Spencer et al., 2014). Single-cell fluorescence was measured using a 488 nm laser (15 mW solid state) directed into the chip via an objective lens (Plan Fluor x20, NA = 0.7, Nikon), with emitted light collected by the objective lens, dichroic mirror and bandpass filters (Chroma Technologies, Rockingham, VT, USA), and photomultiplier tubes (H7710-13, Hamamatsu) controlled by a Hamamatsi C7169 power supply and amplified by Hamamatsu C7319 amplifiers (Holmes et al., 2009; Spencer et al., 2014). The wavelengths measured were denoted as PMT1 ($\lambda = 525 \pm 25$ nm, PMT voltage 0.45 V), PMT2 ($\lambda = 670 \pm 20$ nm, 0.40 V), and PMT3 ($\lambda = 670$nm LP, 0.50 V), with the fluorescence signals measured simultaneously with

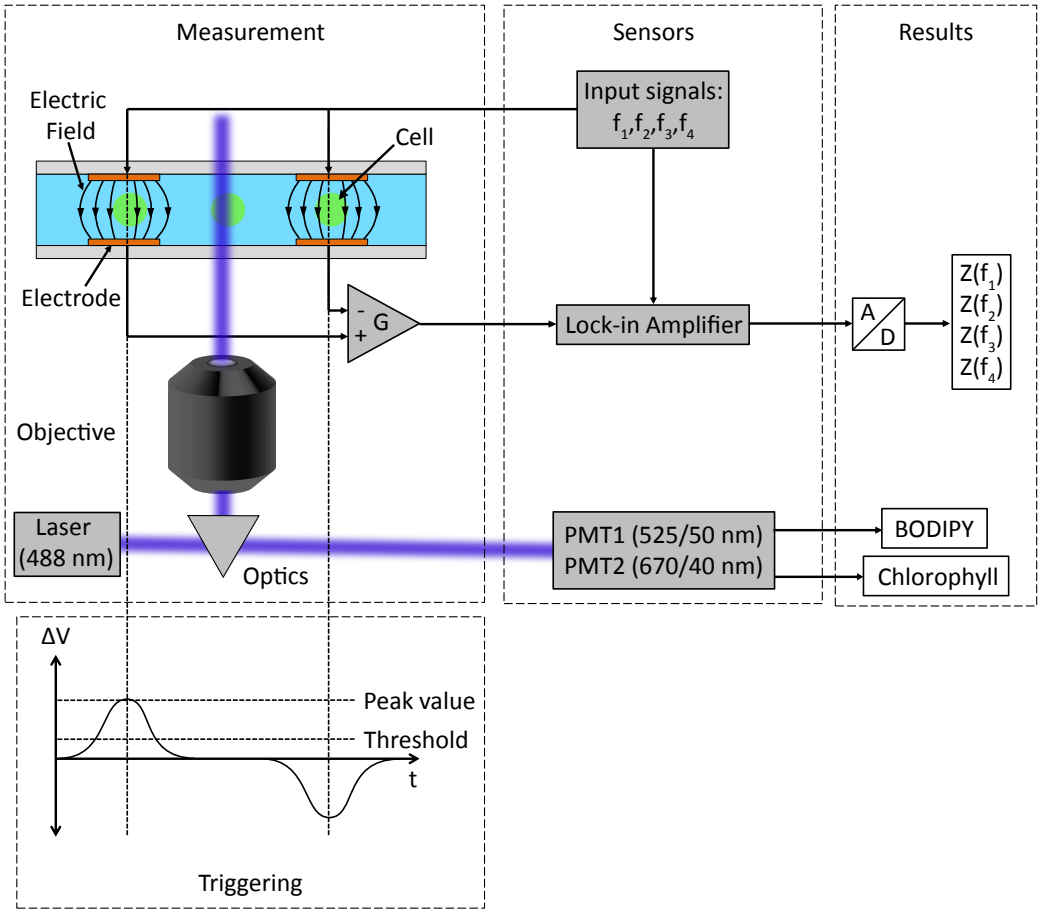

Figure 4.1: Schematic of combined impedance and fluorescence cytometry setup, including microfluidic device, sensors, outputs, and triggering method.

the impedance measurements by plugging the signal into the auxilary port of the impedance spectroscope.

In order to generate ensemble-averaged impedance spectra for fitting to a multishell model, we measured real and imaginary impedance for sinusoidal inputs of $4.0\ V_{pp}$ at two frequencies: 500 kHz and an upper frequency varied from 1 to 50 MHz. While the impedance spectrascope used can measure impedances at up to four frequencies simultaneously, measuring fewer frequencies allows for more voltage to be applied at each frequency without damaging the microfluidic device electrodes, increasing the signal-to-noise ratio of the resulting measure-

ments. In order to measure impedance spectra for individual cells, we measured real and imaginary impedance for sinusoidal inputs of $4.0\ V_{pp}$ at four frequencies: 500 kHz, 2 MHz, 12 MHz, and 20 MHz. Time-series data was recorded for all measured impedance signals, in addition to PMT1 and PMT2 for the combined impedance and fluorescence measurements, at a rate of 230 kS/s for two-frequency measurements and 115 kS/s for four-frequency measurements.

4.4.4 Gating and processing

Events were triggered when the real signal measured at 500 kHz passed a set threshold ($2.5 - 10 \times 10^{-5}$ V), selected for each experiment based on the noise level. Cells were gated from beads using size measured as impedance magnitude at 500 kHz $|\mathrm{Z}(500\mathrm{kHz})|$ (Figure 4.2), as low-frequency impedance is proportional to particle volume (Haandbæk et al., 2014; Spencer et al., 2014). In addition, for the combined impedance and fluorescence measurements cells were gated from cell debris using chlorophyll autofluorescence, measured as maximum voltage of PMT2 $(\mathrm{PMT2})_{\max}$ (excitation 488 nm, emission 670 ± 20 nm) for the event. For samples characterized in 20% PBS ($\sigma_{med} = 357$ mS/m), cell events were gated as $|\mathrm{Z}(500\mathrm{kHz})| < 3 \times 10^{-4}$ V and bead events were gated as $|\mathrm{Z}(500\mathrm{kHz})| \in [5.5 \times 10^{-4}, 8.5 \times 10^{-4}]$ V. For samples characterized in 40% PBS ($\sigma_{med} = 612$ mS/m), cell events were gated as $|\mathrm{Z}(500\mathrm{kHz})| < 5 \times 10^{-4}$ V and bead events were gated as $|\mathrm{Z}(500\mathrm{kHz})| \in [11 \times 10^{-4}, 19 \times 10^{-4}]$ V. For all samples where fluorescence was measured, cell events were also gated as $(\mathrm{PMT2})_{\max} > 0.02$ V.

In order to account for parasitic impedances of the microfluidic device and measurement system, measured cell impedances at each frequency were nor-

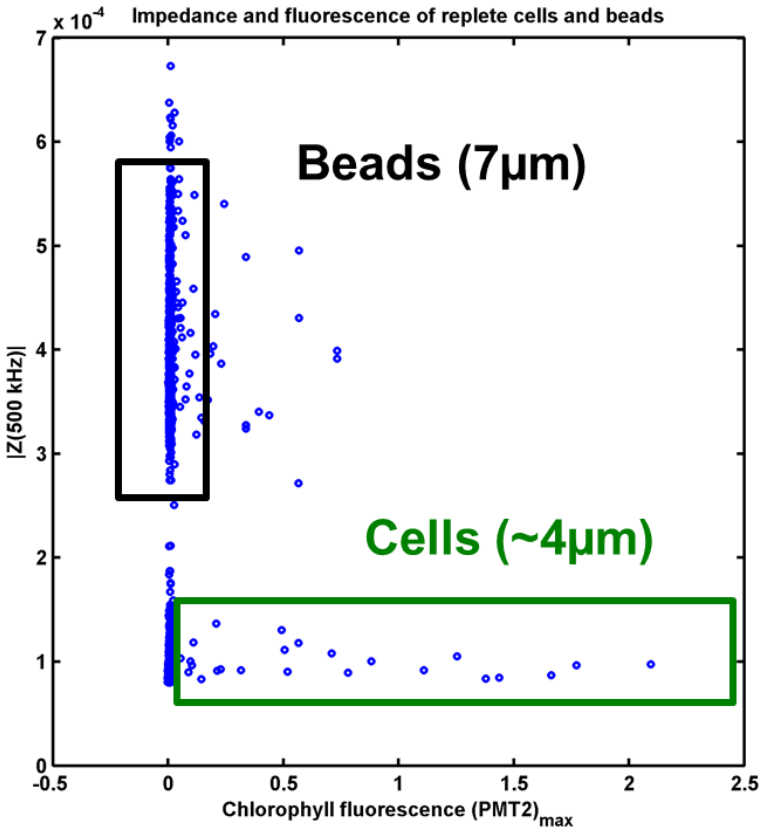

Figure 4.2: Gating of impedance cytometry events based on impedance magnitude at 500 kHz ($|\mathrm{Z}(500\mathrm{kHz})|$) and chlorophyll fluorescence $(\mathrm{PMT2})_{\mathrm{max}}$, both measured as voltage (V).

malized by the mean impedance at that frequency for the 7-μm latex beads flowed through the device along with the cells. Cell complex impedances were normalized by the complex impedance of the beads; whereas cell impedance magnitudes were normalized by the impedance magnitudes of the beads. When considering ensemble-averaged impedances, mean and standard deviations of the cells were calculated before normalizing by the bead impedances.

4.4.5 Safety

Proper laser selection and apparatus setup is important to minimize the risk of eye injury. Select the lowest-powered laser capable of accomplishing the desired fluorescence measurement. When possible, contain the entire laser beam so that the user is not exposed to it during ordinary experimental operation.

4.5 Results and Discussion

4.5.1 Multishell modeling

In order to investigate the suitability of the multishell model described in the Theory section, we measured ensemble-averaged impedance spectra for *Chlorella vulgaris* cells resuspended in nitrogen-replete and nitrogen-limited TAP medium and cultured an additional 9 days, at which point we expect both cultures to be at stagnation phase. In order to measure single-cell impedance at frequencies up to 50 MHz, we characterized the cells in PBS ($\sigma_{med} = 1390$ mS/m) so as to maximize electrical signal from the microfluidic device. As seen in Figures 4.3 and 4.4, this resulted in well defined ensemble-averaged impedance spectra from 500 kHz to 50 MHz. The measured normalized complex impedance spectra (Figure 4.4) were fitted to equation 4.5 using nonlinear least-squares analysis in MATLAB in an adaptation of the method used by Hawkins et al. (2011). In order to fit complex measurements, the real and imaginary complex impedance spectra were separated, concatenated into a single data vector, and simultaneously fitted using nonlinear least-squares analysis.

Moreover, we simultaneously fitted the spectra for nitrogen-replete and nitrogen-limited cells in PBS with the following parameters set as equal for both spectra: effective sample volume $\mathrm{V_{eff}}$, which should be uniform for all spectra measured on each physical microfluidic device; bead conductance $\mathrm{K_{surf,bead}}$, which should be uniform for all samples with the same medium conductivity σ_{med}; and wall conductivity and permittivity $\varepsilon_{\mathrm{wall}}$ and σ_{wall}, which we hypothesize should be the same for two stagnation-phase cultures characterized in a medium with the same conductivity. We fitted the measured spectra to both a double-shell model, with shells corresponding to the membrane and cell wall, and a triple-shell model, with an additional shell corresponding to the outer trilaminar cell wall observed in many *Chlorella* species (Gerken et al., 2013; Griffiths and Griffiths, 1969). This outer wall has been observed to contain the aliphatic polymer algaenan (Gerken et al., 2013), so we treated it as a low-permittivity layer. As with the inner cell wall, the outer cell wall permittivity $\varepsilon_{\mathrm{outer\ wall}}$ and conductivity $\sigma_{\mathrm{outer\ wall}}$ were hypothesized to be the same for two stagnation-phase cultures characterized in a medium with the same conductivity. However, we did allow cell wall thicknesses δ_{wall} and $\delta_{\mathrm{outer\ wall}}$ to differ for nitrogen-replete and nitrogen-limited cells, as cell wall thickness has been observed to vary with growth rate (Němcová and Kalina, 2000) and environmental conditions (Budd et al., 1969).

Fits of the measured complex impedance spectra to double-shell (Figure 4.4a) and triple-shell (Figure 4.4b) both were able to adequately describe the measured spectra, resulting in the fitted parameters listed in Table 4.1. However, the addition of an outer wall in the triple-shell model did not improve the fit to the measured data, with a root mean squared error that was slightly larger than that of the double-shell model 9.2×10^{-4} vs. 7.8×10^{-4}). Because

there was no improvement in fit to justify the incorporation of additional model complexity, we selected the double-shell model to compare fitted parameters for different measured spectra.

As Higashiyama et al. (1999) found that cellular lipid content correlated with a decrease in fitted cytoplasmic conductivity σ_{cyt} in fungi cells, we hypothesized that algae cells with higher lipid content would similarly have lower fitted σ_{cyt} values. The impedance spectra measured for *Chlorella vulgaris* cells cultured in nitrogen-replete and nitrogen-limited TAP medium for 9 days had similar fitted values of σ_{cyt}(751 and 785 mS/m). While we did not measure lipid content as fluorescence for these cells, this similarity is expected because 9 days after resuspension the nutrients in both media will be depleted, resulting in stress and presumably lipid accumulation in both cultures. In order to investigate algae cells with varied lipid content, we measured ensemble-average impedance spectra for cells resuspended in replete medium for 5 days (Figure 4.5a) and cells resuspended in nitrogen-limited medium for 4 days (Figure 4.5b). As seen in Table 4.1, the fitted cytoplasmic conductivity σ_{cyt} for cells cultured in replete medium was 1200 mS/m, the the upper bound of acceptable values selected based on results by Higashiyama et al. (1999). The fitted cytoplasmic conductivity was somewhat lower, 1090 mS/m, for cells cultured in nitrogen-limited medium, consistent with the trend noted by Higashiyama et al. (1999). This was true despite the fact that the replete cells were characterized in a sample medium with a lower conductivity (σ_{med} = 357 vs. 612 mS/m), suggesting that the decrease in cytoplasmic conductivity due to lipid deposits within the cytoplasm is greater than any increase that occurs due to the cell accumulating salt in order to maintain osmotic equilibrium with the surrounding medium.

While the number of free parameters means that not all parameters are an accurate measure of actual cell properties, the other fitted values in Table 4.1 can be compared to expected changes in the cell during nutritional stress. The fitted cell size $\mathrm{R_{cell}}$ was fairly consistent over all fitted double-shell values, decreasing slightly from 3.3 μm for replete cells 5 days after resuspension to 2.7 μm for nitrogen-limited cells 9 days after resuspension. This is consisted with the flow cytometry results presented in the previous chapter. The fitted cell wall thickness δ_{wall} was lowest for nitrogen-limited cells 9 days after resuspension (31 nm), slightly thicker for replete cells 9 days after resuspension (87 nm), and equal to the upper bound of acceptable values (200 nm) for both replete cells 5 days after resuspension and nitrogen-limited cells 4 days after resuspension.

As *Chlorella* cell walls have been found to thicken during slow growth (Němcová and Kalina, 2000) and environmental stress (Budd et al., 1969), we would expect to measure thinner cell walls for the cells resuspended for only 4–5 days. This may point to an inadequacy in the fit, or correspond to degradation of the cell walls after a sufficient period of nutrient limitation. Further investigation of *Chlorella vulgaris* cell wall thickness for the cultivation conditions used in this study are necessary in order to determine how accurately these fitted values correspond to actual cell wall thickness. The fitted parameters show that fitted cell wall conductivity σ_{wall} increases with medium conductivity σ_{med}, consistent with a cell wall consisting of a network of polysaccaride microfibrils (Gerken et al., 2013; Němcová and Kalina, 2000), which the suspending medium may permeate into.

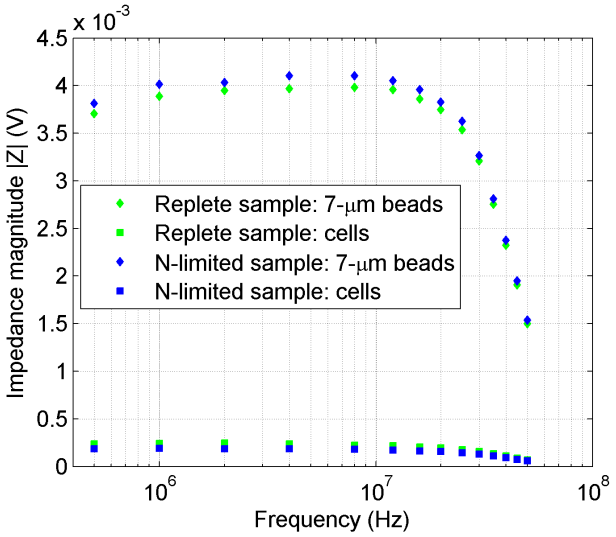

Figure 4.3: Measured impedance magnitude spectra for *Chlorella vulgaris* cells resuspended in replete (green) or nitrogen-limited (blue) TAP medium for 9 days and then characterized in PBS ($\sigma_{med} = 1390$ mS/m), plotted on the same axes as the measured impedance magnitude spectra for 7-μm latex beads flowed through the microfluidic device at the same time as the cells. Cells were gated by size, measured as impedance magnitude at 500 kHz ($|\mathrm{Z}(500\mathrm{kHz})|$). Each point is the ensemble-averaged value for at least 4400 cell events.

4.5.2 Combined impedance and fluorescence measurement

Previously, we have demonstrated use of this system to simultaneously measure the impedance and fluorescence of individual particles without the need for sheath flow (Holmes et al., 2007, 2009; Spencer et al., 2014). However, as fluorescence protocols developed for conventional flow cytometry are intended for a system with sheath flow and different optics, it is sometimes necessary to modify existing flow cytometry protocols for use in this combined impedance and fluorescence cytometry system. The fluorescence protocol used here is based on a protocol developed by Cirulis et al. (2012), who showed that the fluorescence of cells labeled with BODIPY 505/515 using the described protocol could be calibrated to lipid content measured via extraction and titration with a correlation coefficient of $r^2 = 0.95$. When used with sheath flow in a standard flow

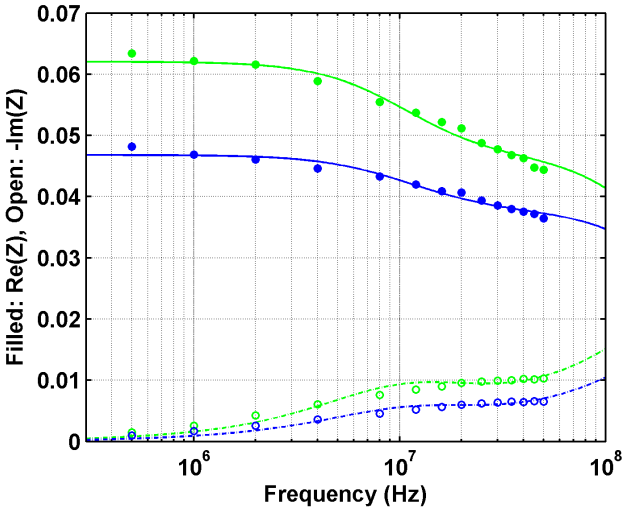

(a)

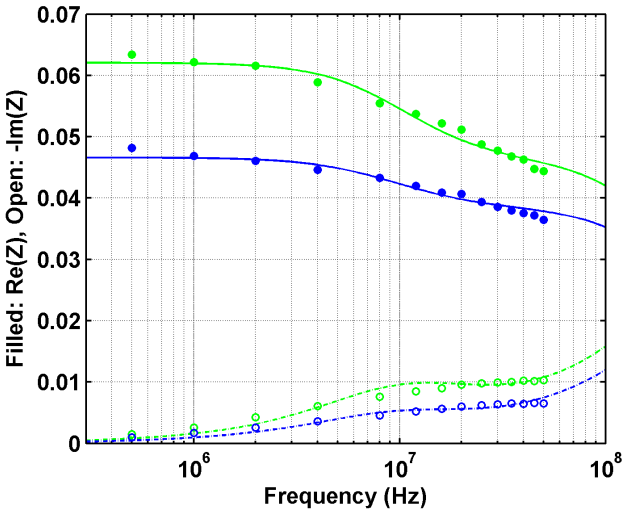

(b)

Figure 4.4: Measured normalized complex impedance spectra for *Chlorella vulgaris* cells resuspended in replete (green) or nitrogen-limited (blue) TAP medium for 9 days and then characterized in PBS ($\sigma_{med} = 1390$ mS/m), normalized by the impedance of 7-μm latex beads in PBS and plotted as real (filled symbols) and imaginary (open symbols) impedance components. Also shown are fits for (a) double-shell and (b) triple-shell models with the fit parameters listed in Table 4.1. Cells were gated by size, measured as impedance magnitude at 500 kHz ($|\mathrm{Z}(500\mathrm{kHz})|$). Each point is the ensemble-averaged value for at least 4400 cell events.

Table 4.1: Multivariable nonlinear fit coefficients for the complex impedance spectra measured for *Chlorella vulgaris* cells resuspended in replete or nitrogen-limited TAP medium for 4–9 days and then characterized in sample medium with conductivity σ_{med}, normalized by the impedance of 7-μm latex beads characterized in the same sample medium. Parameter values merged across multiple fits correspond to values set as uniform for two spectra fitted simultaneously. Starred values (*) were fits equal to the lower bound of acceptable values; double-starred values (**) were fits equal to the upper bound of acceptable values.

Model	Double-shell		Triple-shell model		Double-shell	
Culture medium	Replete	N-limited	Replete	N-limited	Replete	N-limited
Resuspension time (days)	9		9		5	4
Fluorescence gating	no		no		yes	yes
			Fixed			
R_{bead} (μm)	3.5		3.5		3.5	3.5
ε_{bead}	2.5		2.5		2.5	2.5
ε_{med}	80		80		80	80
σ_{med} (mS/m)	1390		1390		357	612
δ_{mem} (nm)	8		8		8	8
ε_{mem}					2.3	2.3
σ_{mem} (μS/m)	10		10		10	10
			Free			
R_{cell} (μm)	3.0	2.7	2.8	2.5	3.3	3.2
ε_{cyt}	80**	49	77	42	40*	41
σ_{cyt} (mS/m)	751	785	1185	1197	1200**	1090
ε_{mem}	2.0	2.4	3.4	4.6		
δ_{wall} (nm)	87	31	89	105	200**	200**
ε_{wall}	80**		79		80**	80**
σ_{wall} (mS/m)	1271		1450		96	201
$\delta_{outer\ wall}$ (nm)	–	–	38	39	–	–
$\varepsilon_{outer\ wall}$	–		2*		–	–
$\sigma_{outer\ wall}$ (mS/m)	–		12.1		–	–
$K_{surf,bead}$ (nS)	117		143		40.1	46.3
V_{eff} (μm^3)	172		171		166	171
			Statistics			
R^2	0.9994		0.9992		0.9730	0.9952
RMSE	7.8×10^{-4}		9.2×10^{-4}		0.0093	0.0025

cytometer, no wash step is necessary for this protocol due to the high oil/water partition coefficient of BODIPY 505/515 (Cooper et al., 2010). However, when used in a system without sheath flow, we found that two wash steps were necessary in order to measure BODIPY fluorescence using PMT1. Moreover, in order to maximize sensitivity of PMT1 to BODIPY we found that it was necessary to use a lower flow rate through the device (10 μL/min) compared to the higher flow rates that could be used for measurements of impedance alone (up to 40 μL/min). The chlorophyll autofluorescence measurement via PMT2 was far less sensitive to flow rate, and cells could be gated using chlorophyll fluorescence at a flow rate of 20 μL/min.

4.5.3 Single-cell impedance spectra

The fitting of measured ensemble-averaged impedance spectra to cell parameters in a multishell model demonstrates that subjecting *Chlorella vulgaris* cells to environmental stress as nitrogen limitation alters the cells' dielectric properties in a manner consistent with cytoplasmic lipid accumulation. However, relating single-cell impedance to lipid accumulation would allow for measurement of the distribution of lipid accumulation within a population and deconvolution of lipid accumulation from other physiological changes resulting from nutrient limitation. Algae cells in suspension exhibit a distribution of lipid contents for the same environmental conditions (Davis et al., 2012; Wang et al., 2014). Moreover, lipid accumulation during environmental stress may be accompanied by other changes in the properties of the cell wall or membrane (Budd et al., 1969; Gerken et al., 2013; van Donk et al., 1997; Wu et al., 2005). It is likely that these other changes also occur as a distribution in the cell population that is not fully

correlated with lipid accumulation, necessitating impedance measurement of individual cells in order to completely separate lipid accumulation from other physiological changes.

When we measured impedance spectra for individual cells at four frequencies — 500 kHz, 2 MHz, 12 MHz, and 20 MHz — we found that nitrogen limitation resulted in a significant change in single-cell impedance. As seen in Figure 4.6, cells resuspended in nitrogen-limited medium for 6 days and then characterized in 20% PBS exhibited higher impedance magnitudes than cells resuspended in nitrogen-replete medium, with statistically significant differences between the two populations at 2, 12, and 20 MHz for populations of only 26 cell events. When we consider impedance and lipid content for individual cells within each population, we see a general trend of cells with higher lipid content having higher impedance magnitudes when characterized in 20% PBS (Figure 4.7). We labeled these cells with BODIPY 505/515 and measured their fluorescence using the protocol that we found resulted in measurable BODIPY fluorescence (see sections on Sample Preparation, Data Acquisition, and Combined impedance and fluorescence measurement). In order to control for cell size and position within the laser beam, we quantified lipid content as the BODIPY/Chlorophyll fluorescence ratio $\mathrm{F} = (\mathrm{PMT1}/\mathrm{PMT2})_{\mathrm{max}}$.

As an initial attempt to relate single-cell impedance to lipid content, we fit the natural logorithm of the BODIPY/Chlorophyll fluorescence ratio ($\ln \mathrm{F} = \ln(\mathrm{PMT1}/\mathrm{PMT2})_{\mathrm{max}}$) as a function of measured polar impedance coordinates using a simple multilinear regression, plotted in Figure 4.8 as estimated $\ln \mathrm{F}$ (from the multilinear regression) with respect to actual measured $\ln \mathrm{F}$. While the actual expected relationship between lipid content and impedance

components is nonlinear as described in the Theory section, this simple linear estimate still shows a moderate correlation for individual cell events ($r^2 = 0.433$, $p = 1.04 \times 10^{-3}$).

In order to gain further insight into the relationship between measured fluorescence and impedance for individual cell events, we conducted principal component analysis on $\ln \mathrm{F}$ and the polar impedance compontents. As seen in Figure 4.9a, the first two principal components show that $\ln \mathrm{F}$ for individual cell events is correlated with impedance magnitude and to a lesser extent impedance angle. When we consider the third principal component as well (Figure 4.9b), we can see that in the third principal component $\ln \mathrm{F}$ is correlated with impedance angle at higher frequencies ($\angle \mathrm{Z}(12\mathrm{MHz})$, $\angle \mathrm{Z}(20\mathrm{MHz})$), but anti-correlated with impedance angle at lower frequencies ($\angle \mathrm{Z}(500\mathrm{kHz})$, $\angle \mathrm{Z}(2\mathrm{MHz})$). These results show that with further correlation of single-cell impedance with lipid content, possibly using more sophisticated statistical modeling techniques such as Gaussian process regression (Chen et al., 2007) or regression trees (Loh, 2011), it may be possible to relate measured impedance to lipid content with single-cell resolution.

Further correlation would also benefit from measuring additional properties for individual cells. Low-frequency impedance is proportional to particle volume (Haandbæk et al., 2014; Spencer et al., 2014). However, our multishell model fits to *Chlorella vulgaris* cells in low-conductivity media (Figure 4.5) show that for the medium conductivity used in our single-cell impedance spectra ($\sigma_{\mathrm{med}} = 357$ mS/m), the lowest impedance relaxation begins at a lower frequency than 500 kHz. Additional characterization will facilitate improved frequency selection and calibration of low-frequency impedance to *Chlorella vul-*

garis cell size. Moreover, our results and previous characterization (Budd et al., 1969; Němcová and Kalina, 2000) suggest that cell wall thickness varies as a function of cell growth rate and environmental stress. Successful deconvolution of cytoplasmic conductivity (which we expect to decrease with lipid accumulation) from cell wall thickness requires measurement of cell wall thickness in individual cells simultaneously with single-cell measurements of lipid content and impedance. It may be possible to develop a fluorescence protocol to simultaneously measure single-cell algal lipid content and cell wall thickness in order to separate the effects of lipid content and cell wall thickness on impedance.

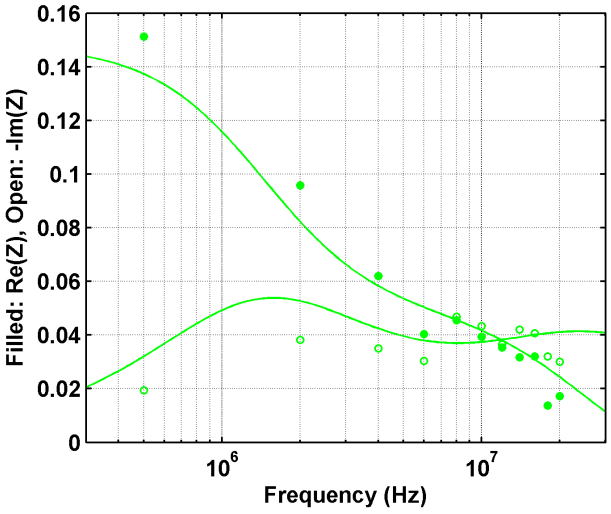

(a)

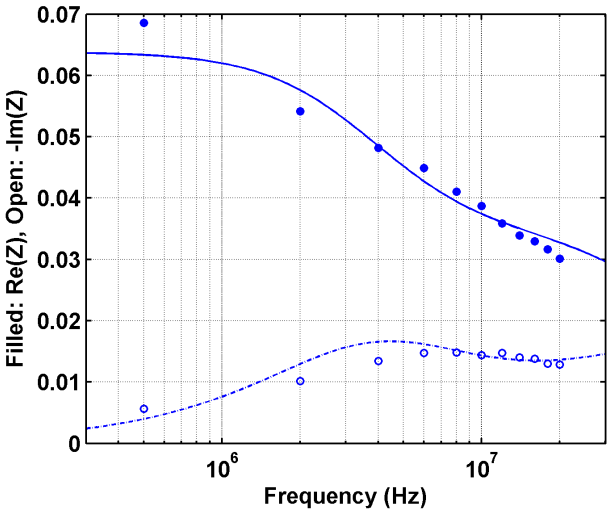

(b)

Figure 4.5: Measured complex impedance spectra for *Chlorella vulgaris* cells and fits with parameters listed in Table 4.1. Impedances are normalized by the impedance of 7-μm latex beads in the same medium and plotted as real (filled symbols) and imaginary (open symbols) impedance components. Cells were gated by both size, measured as impedance magnitude at 500 kHz ($|\mathrm{Z}(500\mathrm{kHz})|$), and chlorophyll fluorescence as shown in Figure 4.2.(a) Cells resuspended in replete TAP medium for 5 days and then characterized in 20% PBS, $\sigma_{med} = 357\mathrm{mS/m}$. Each point is the ensemble-averaged value for at least 100 cell events, with the exception of values at 2 MHz (19 cell events) and 4 MHz (30 cell events). (b) Cells resuspended in nitrogen-limited TAP medium for 4 days and then characterized in 40% PBS, $\sigma_{med} = 612\mathrm{mS/m}$. Each point is the ensemble-averaged value for at least 1300 cell events.

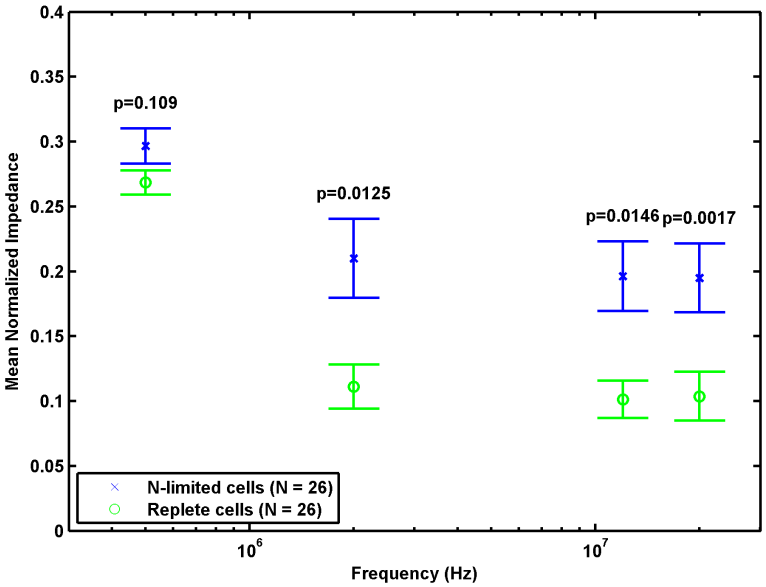

Figure 4.6: Measured mean single-cell impedance magnitude spectra for *Chlorella vulgaris* cells resupended in replete or nitrogen-limited TAP medium for 6 days (N = 26 for each population) and then characterized in 20% PBS, $\sigma_{cyt} = 357\mathrm{mS/m}$, normalized by the impedance of 7-μm latex beads in the same medium. Error bars are standard error of the mean, p-values are from a Wilcoxon rank-sum test on cell magnitudes. Cells were gated by both size, measured as impedance magnitude at 500 kHz ($|\mathrm{Z}(500\mathrm{kHz})|$), and chlorophyll fluorescence as shown in Figure 4.2.

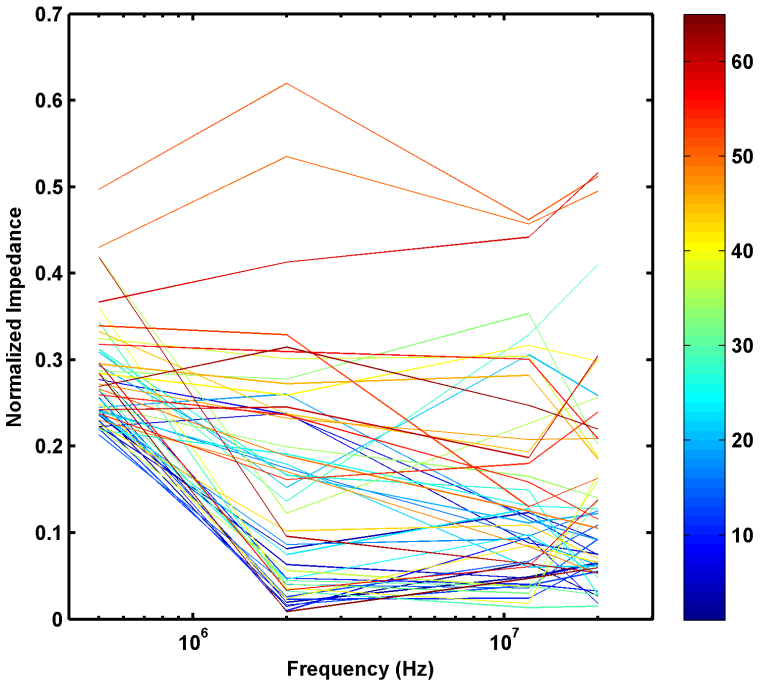

Figure 4.7: Measured single-cell impedance magnitude spectra for individual *Chlorella vulgaris* cells resupended in replete or nitrogen-limited TAP medium for 6 days and then characterized in 20% PBS, $\sigma_{cyt} = 357\mathrm{mS/m}$, normalized by the impedance of 7-μm latex beads in the same medium. Cells were gated by both size, measured as impedance magnitude at 500 kHz ($|\mathrm{Z}(500\mathrm{kHz})|$), and chlorophyll fluorescence as shown in Figure 4.2. Spectra for individual cells are colored by lipid content, measured as BODIPY/Chlorophyll fluorescence ratio $\mathrm{F} = (\mathrm{PMT1/PMT2})_{\mathrm{max}}$ and colored by fluorescence ratio rank according to the color map to the right of the spectra.

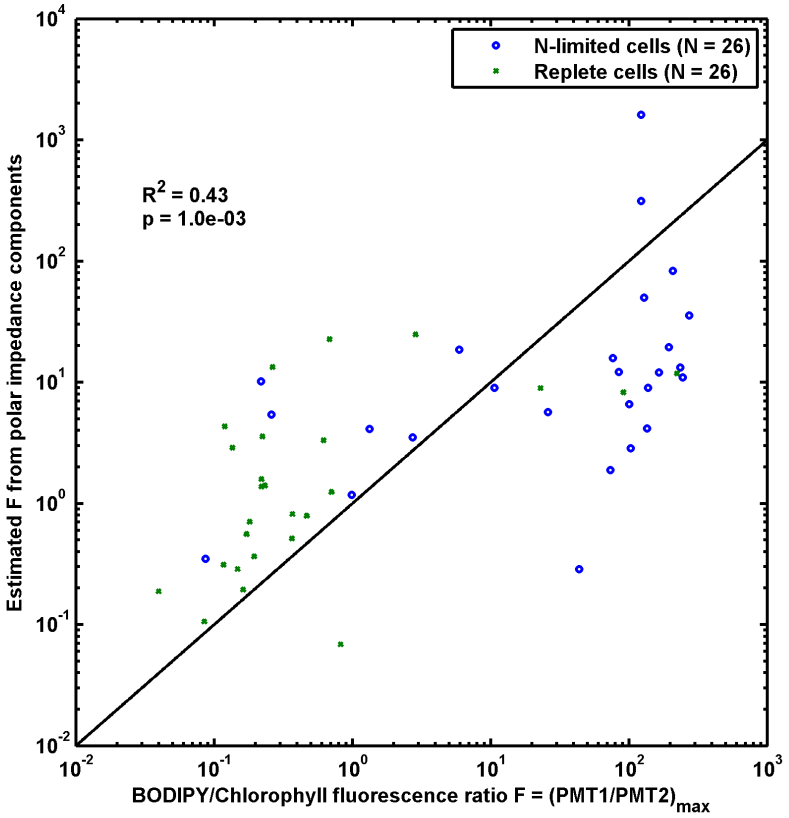

Figure 4.8: Single-cell *Chlorella vulgaris* lipid content, measured as BODIPY/Chlorophyll fluorescence ratio $\mathrm{F} = (\mathrm{PMT1}/\mathrm{PMT2})_{\max}$, plotted as estimated $\ln \mathrm{F}$ from a multilinear regression of measured polar impedance coordinates with respect to measured $\ln \mathrm{F}$ for each cell event. Multilinear regression is $\ln \mathrm{F} = -2.32 + 8.70|\mathrm{Z}_1| - 0.44\angle \mathrm{Z}_1 + 9.12|\mathrm{Z}_2| - 0.42\angle \mathrm{Z}_2 - 5.82|\mathrm{Z}_3| - 0.12\angle \mathrm{Z}_3 + 4.53|\mathrm{Z}_4| + 0.82\angle \mathrm{Z}_4$ ($r^2 = 0.433$, $p = 1.04 \times 10^{-3}$), where $\mathrm{Z}_1 = \mathrm{Z}(500\mathrm{kHz})$, $\mathrm{Z}_2 = \mathrm{Z}(2\mathrm{MHz})$, $\mathrm{Z}_3 = \mathrm{Z}(12\mathrm{MHz})$, and $\mathrm{Z}_4 = \mathrm{Z}(20\mathrm{MHz})$. Measured single-cell impedances and fluorescences are for *Chlorella vulgaris* cells resuspended in replete or nitrogen-limited TAP medium for 6 days and then characterized in 20% PBS, $\sigma_{cyt} = 357\mathrm{mS/m}$, normalized by the impedance of 7-μm latex beads in the same medium. Cells were gated by both size, measured as impedance magnitude at 500 kHz ($|\mathrm{Z}(500\mathrm{kHz})|$), and chlorophyll fluorescence as shown in Figure 4.2.

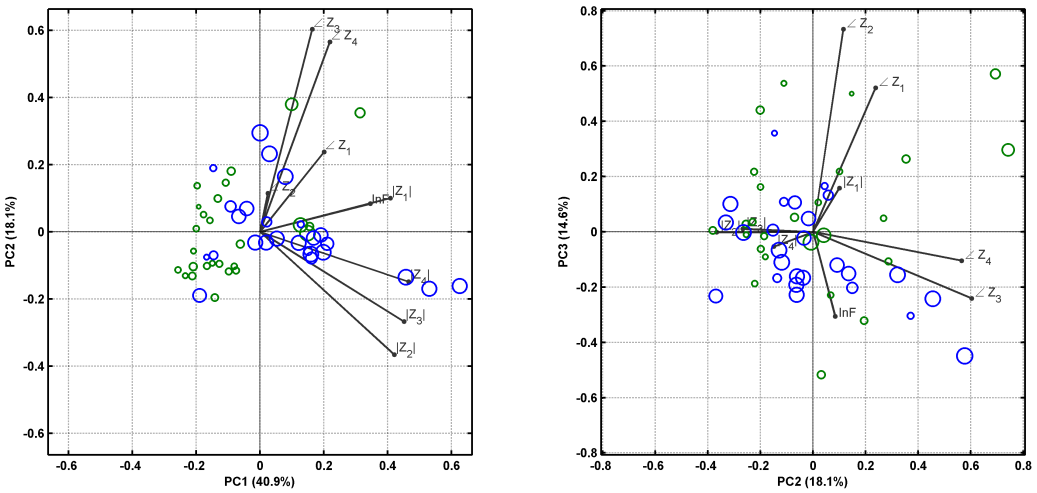

(a) (b)

Figure 4.9: Principal component analysis for measured polar impedance components and BODIPY/Chlorophyll fluorescence ratio $\mathrm{F} = (\mathrm{PMT1}/\mathrm{PMT2})_{\max}$ of *Chlorella vulgaris* cells resuspended in replete or nitrogen-limited TAP medium for 6 days and then characterized in 20% PBS, $\sigma_{cyt} = 357\mathrm{mS/m}$, normalized by the impedance of 7-μm latex beads in the same medium. Cells were gated by both size, measured as impedance magnitude at 500 kHz ($|\mathrm{Z}(500\mathrm{kHz})|$), and chlorophyll fluorescence as shown in Figure 4.2. Measured polar impedance components and fluorescence ratios for each cell event were scaled by converting to the Z-score for each variable over all cell events. Principal components are plotted as (a) PCA2 (18.1% total variation) vs. PCA1 (40.9% total variation) and (b) PCA3 (14.6% total variation) vs. PCA2 (18.1% total variation), with vectors for each variable superimposed over cell events colored as replete (green) or nitrogen-limited (blue) with point size equal to $\ln 1000\mathrm{F}$.

4.6 Conclusions

Measured ensemble-averaged single-cell impedance spectra of *Chlorella vulgaris* cells are consistent with a double-shell model, yielding fitted parameters indicating that cytoplasmic conductivity decreases with increasing nutrient limitation, consistent with environmental stress as nutrient limitation causing lipid accumulation which decreases cytoplasmic conductivity. Combined single-cell impedance and fluorescence measurements allow for correlation of impedance and lipid content at the single-cell level. Single-cell impedance spectra are significantly altered by nitrogen limitation, and single-cell impedance can be correlated with lipid content using a simple multilinear regression or principal component analysis. These results demonstrate the potential of single-cell impedance cytometry for algal lipid measurement, making it a promising technique for monitoring of industrial algal biofuel feedstocks.

4.7 Acknowledgements

The authors thank Katie Chamberlain (University of Southampton) for device fabrication; Maria-Nefeli Tsaloglou and Isaac Jones (both University of Southampton) for assistance with algae culture and media preparation; Beth Ahner, Dylan Sri-Jayantha, and Ravi Garcia (all Cornell University) for advice regarding algae culture; Jane Cooke (University of Southampton), James Smith (Cornell Universiry), and Veronica Pillar (Cornell University) for assistance with the logistics of this international collaboration; and Susanna Kahn (Cornell University) and members of the Center for Hybrid Biodevices (University of Southampton) for technical assistance and helpful discussions. MSB

was supported by the US National Institutes of Health (NIH) via the Physical Sciences-Oncology Center at Cornell University.

CHAPTER 5
CONCLUSIONS

In this dissertation, I demonstrated the potential of dielectric spectroscopy to measure the lipid content of algae cells for implementation in industrial biodiesel production. As an initial proof of concept, in Chapter 2 I showed that the dielectric properties of algae cell suspensions were altered by lipid accumulation. In Chapter 3, I developed an NMR-traceable flow cytometry protocol for improved calibration of dielectric measurement techniques and fundamental investigation of algal lipid accumulation. In Chapter 4, I characterized algae cells via single-cell impedance cytometry, which offers improved accuracy and decreased sample preparation compared to bulk dielectric spectroscopy.

This work has suggested several exciting areas for future study. In Chapter 2 I used a transmission line sample cell to measure bulk dielectric spectra of algae cell suspensions. I showed that the measured changes in transmission coefficient were consistent with those predicted by a model, but it would be highly beneficial to develop an algorithm for fitting measured transmission coefficient spectra to a multishell model in order to generate initial estimates of cell parameters from transmission line measurements.

In Chapter 3, I showed that liquid-state ^{1}H NMR measurements of algal tracylglyceride (TAG) content were highly correlated with single-cell fluorescence of algae cells labeled with BODIPY 505/515, with some additional BODIPY fluorescence presumably arising from BODIPY accumulated in non-TAG lipids. As I discuss in Chapter 3, the use of semisolid NMR techniques such as high-resolution magic-angle spinning (HR-MAS) NMR would facilitate quantitation of these ordered non-TAG lipids for correlation with BODIPY fluores-

cence. Moreover, my flow cytometry measurements suggest that during nitrogen limitation, only a subset of *Chlorella vulgaris* cells accumulate additional lipids. It is uncertain whether this variation in lipid content is due to variability in light and nutrients at different microenvironments within the unstirres algae culture, or is an example of phenotypic heterogeneity as part of a coordinated stress reponse. Cultivation of *Chlorella vulgaris* under more controlled conditions and transcriptomic analysis would facilitate investigation of this observed phenomenon.

In Chapter 4, I showed that nitrogen limitation significantly altered the impedance spectra of individual *Chlorella vulgaris* cells. As discussed in that chapter, application of statistical techniques such as Gaussian processes or regression trees would facilitate more sophisticated correlation of single-cell impedance spectra and lipid content. Moreover, as nutrient limitation may cause changes in the cell wall in addition to lipid accumulation, it would be beneficial to develop a double-stain protocol for labeling algal lipid deposits with BODIPY 505/515 and cell walls with calcofluor white (CFW). Aach et al. (1978) used Calcofluor white (CFW) to fluorescently label *Chlorella sacchrophilia* cell walls (Aach et al., 1978), and Pouneva (1997) observed that CFW fluorescence intensity varied with algal cell wall thickness. It may be possible to develop a double-stain protocol to simultaneously measure single-cell algal lipid content and cell wall thickness (via BODIPY and CFW fluorescence, respectively) in order to separate the effects of lipid content and cell wall thickness on impedance. Such a stain would also benefit development of algae strains with high lipid content and thinner cell walls for easier extraction of algal lipids during biodiesel production (Gerken et al., 2013). This would allow for deconvolution of lipid content from cell wall changes, and also provide researchers devel-

oping algae strains with the ability to fluorescently determine at the single-cell level both how much lipid a strain has and how thick the cell wall is that would need to be ruptured in order to extract the lipid for conversion to biodiesel.

The work described in this dissertation, as well as the potential future projects described above, will facilitate improved measurement of algal lipid content for both industrial monitoring and development of improved strains and cultivation protocols.

BIBLIOGRAPHY

Aach, H., S. Bartsch, and V. Feyen. 1978. Studies on *Chlorella* protoplasts. Planta 139:257–260.

Anderson, A. M., M. K. Carroll, E. C. Green, J. T. Melville, and M. S. Bono Jr. 2010. Hydrophobic silica aerogels prepared via rapid supercritical extraction. Journal of Sol-Gel Science and Technology 53:199–207.

Asami, K. 2002. Characterization of heterogeneous systems by dielectric spectroscopy. Progress in Polymer Science 27:1617–1659.

Axelsson, M., and F. Gentili. 2014. A Single-Step Method for Rapid Extraction of Total Lipids from Green Microalgae. PLoS ONE 9:e89643.

Beal, C. M., M. E. Webber, R. S. Ruoff, and R. E. Hebner. 2010. Lipid Analysis of *Neochloris oleoabundans* by Liquid State NMR. Biotechnology and Bioengineering 106:573–583.

Beal, C. M., A. S. Stillwell, C. W. King, S. M. Cohen, H. Berberoglu, R. P. Bhattarai, R. L. Connelly, M. E. Webber, and R. E. Hebner. 2012. Energy Return on Investment for Algal Biofuel Production Coupled with Wastewater Treatment. Water Environment Research 84:692–710.

Bearden, D. W. 2012. Environmental metabolomics. In R. K. Harris, and R. Wasylishen, eds., Encyclopedia of Magnetic Resonance,. John Wiley.

Benazzi, G., D. Holmes, T. Sun, M. C. Mowlem, and H. Morgan. 2007. Discrimination and analysis of phytoplankton using a microfluidic cytometer. IET Nanobiotechnology 1:94–101.

Berberoglu, H., L. Pilon, and A. Melis. 2008. Radiation characteristics of Chlamydomonas reinhardtii CC125 and its truncated chlorophyll antenna transformants tla1, tlaX and tla1-CWD. International Journal of Hydrogen Energy 33:6467–6483.

Bittar, T. B., Y. Lin, L. R. Sassano, B. J. Wheeler, S. L. Brown, W. P. Cochlan, and Z. I. Johnson. 2013. Carbon allocation under light and nitrogen resource gradients in two model marine phytoplankton. Journal of Phycology 124:217–226.

Bligh, E., and W. Dyer. 1959. A rapid method of total lipid extraction and purification. Canadian Journal of Biochemistry and Physiology 37:911–917.

Bondu, S., N. Kervarec, E. Deslandes, and R. Pichon. 2008. The use of HRMAS NMR spectroscopy to study the in vivo intra–cellular carbon/nitrogen ratio of *Solieria chordalis* (Rhodophyta). Journal of Applied Phycology 20:673–679.

Bono Jr., M. S., A. M. Anderson, and M. K. Carroll. 2010. Alumina aerogels prepared via rapid supercritical extraction. Journal of Sol-Gel Science and Technology 53:216–226.

Bono Jr., M. S., B. A. Ahner, and B. J. Kirby. 2013. Detection of algal lipid accumulation due to nitrogen limitation via dielectric spectroscopy of *Chlamydomonas reinhardtii* suspensions in a coaxial transmission line sample cell. Bioresource Technology 143:623–631.

Bono Jr., M. S., R. D. Garcia, D. V. Sri-Jayantha, B. A. Ahner, and B. J. Kirby. Manuscript in preparation. Measurement of lipid accumulation in *Chlorella vulgaris* via flow cytometry and ^{1}H NMR for development of an NMR-traceable flow cytometry protocol .

Bono Jr., M. S., D. C. Spencer, A. La Gioia, H. Morgan, and B. J. Kirby. Manuscript in preparation. Detection of lipid accumulation in *Chlorella vulgaris* cells via single-cell impedance cytometry .

Budd, T. W., J. L. Tjostem, and M. E. Duysen. 1969. Ultrastructure of *Chlorella pyrenedoisa* as affected by environmental changes. American Journal of Botany 56:540–545.

Cai, H., Y. Chen, X. Cui, S. Cai, and Z. Chen. 2014. High-Resolution ^{1}H NMR Spectroscopy of Fish Muscle, Eggs and Small Whole Fish via Hadamard-Encoded Intermolecular Multiple-Quantum Coherence. PLoS ONE 9:e86422.

Cakmak, T., P. Angun, Y. E. Demiray, A. D. Ozkan, Z. Elibol, and T. Tekinay. 2012. Differential Effects of Nitrogen and Sulfur Deprivation on Growth and Biodiesel Feedstock Production of *Chlamydomonas reinhardtii*. Biotechnology and Bioengineering 109:1947–1957.

Chandler, G. T., and D. C. Volz. 2004. Semiquantitative Confocal Laser Scanning Microscopy Applied to Marine Invertebrate Ecotoxicology. Marine Biotechnology 6:128–137.

Chauton, M. S., T. R. Størseth, and G. Johnsen. 2003. High-resolution magic angle spinning ^{1}H NMR analysis of whole cells of *Thalassiosira pseudonana* (Bacillariophyceae): Broad range analysis of metabolic composition and nutritional value. Journal of Applied Phycology 15:533–542.

Chen, T., J. Morris, and E. Martin. 2007. Gaussian process regression for multivariate spectroscopic calibration. Chemometrics and Intelligent Laboratory Systems 87:59–71.

Chen, W., C. Zhang, L. Song, M. Sommerfeld, and Q. Hu. 2009. A high throughput Nile red method for quantitative measurement of neutral lipids in microalgae. Journal of Microbiological Methods 77:41–47.

Chia, M. A., A. T. Lombardi, M. Da Graça Gama Melão, and C. C. Parrish. 2013. Effects of cadmium and nitrogen on lipid composition of *Chlorella vulgaris* (Trebouxiophyceae, Chlorophyta). European Journal of Phycology 48:1–11.

Cirulis, J. T., B. C. Strasser, J. A. Scott, and G. M. Ross. 2012. Optimization of Staining Conditions for Microalgae with Three Lipophilic Dyes to Reduce Precipitation and Fluorescence Variability. Cytometry Part A 81A:618–626.

Cooper, M. S., W. R. Hardin, T. W. Petersen, and R. A. Cattolico. 2010. Visualizing "green oil" in live algal cells. Journal of Bioscience and Bioengineering 109:198–201.

Davey, P. T., W. C. Hiscox, B. F. Lucker, J. V. O'Fallon, S. Chen, and G. L. Helms. 2012. Rapid triacylglyceride detection and quantification in live micro-algal cultures via liquid state ^{1}H NMR. Algal Research 1:166–175.

Davis, R. W., J. V. Volponi, H. D. T. Jones, B. J. Carvalho, H. Wu, and S. Singh. 2012. Multiplex Fluorometric Assessment of Nutrient Limitation as a Strategy for Enhanced Lipid Enrichment and Harvesting of *Neochloris oleoabundans*. Biotechnology and Bioengineering 109:2503–2512.

de la Jara, A., H. Mendoza, A. Martel, C. Molina, L. Nordström, V. de la Rosa, and R. Díaz. 2003. Flow cytometric determination of lipid content in a marine dinoflagellate, *Crypthecodinium cohnii*. Journal of Applied Phycology 15:433–438.

Dean, A. P., D. C. Sigee, B. Estrada, and J. K. Pittman. 2010. Using FTIR spectroscopy for rapid determination of lipid accumulation in response to nitrogen limitation in freshwater microalgae. Bioresource Technology 101:4499–4507.

Deng, X., X. Fei, and Y. Li. 2011. The effects of nutritional restriction on neutral lipid accumulation in *Chlamydomonas* and *Chlorella*. African Journal of Microbiology Research 5:260–270.

Deng, Y.-L., J.-S. Chang, and Y.-J. Juang. 2013. Separation of microalgae with different lipid contents by dielectrophoresis. Bioresource Technology 135:137–141. doi:10.1016/j.biortech.2012.11.046.

Deng, Y.-L., M.-Y. Kuo, and Y.-J. Juang. 2014. Development of flow through dielectrophoresis microfluidic chips for biofuel production: Sorting and detection of microalgae with different lipid contents. Biomicrofluidics 8:064120.

Gao, C., W. Xiong, Y. Zhang, W. Yuan, and Q. Wu. 2008. Rapid quantitation of lipid in microalgae by time-domain nuclear magnetic resonance. Journal of Microbiological Methods 75:437–440.

Gardner, W. S., W. A. Frez, E. A. Cichocki, and C. C. Parrish. 1985. Micromethod for Lipids in Aquatic Invertebrates. Limnology and Oceanography 30:1099–1105.

Gerken, H. G., B. Donohoe, and E. P. Knoshaug. 2013. Enzymatic cell wall degradation of *Chlorella vulgaris* and other microalgae for biofuels production. Planta 237:239–253.

Gimpel, J. A., E. A. Sprecht, D. R. Georgianna, and S. P. Mayfield. 2013. Ad-

vances in microalgae engineering and synthetic biology applications for biofuel production. Current Opinion in Chemical Biology 17:489–495.

Goodenough, U. W., and J. E. Heuser. 1985. The *Chlamydomonas* Cell Wall and Its Constitutent Glycoproteins Analyzed by the Quick-Freeze, Deep-Etch Technique. The Journal of Cell Biology 101:1550–1568.

Gorman, D. S., and R. Levine. 1965. Cytochrome f and plastocyanin: their sequence in the photosynthetic electron transport chain of *Chlamydomonas reinhardi*. Proceedings of the National Academy of Sciences of the United States of America 54:1665–1669.

Govender, T., L. Ramanna, I. Rawat, and F. Bux. 2012. BODIPY staining, an alternative to the Nile Red fluorescence method for the evaluation of intracellular lipids in microalgae. Bioresource Technology 114:507–511.

Griffiths, D., and D. Griffiths. 1969. The fine structure of autotrophic and heterotrophic cells of *Chlorella vulgaris* (Emerson strain). Plant and Cell Physiology 10:11–19.

Haandbæk, N., S. C. Bürgel, F. Heer, and A. Hierlemann. 2014. Characterization of subcellular morphology of single yeast cells using high frequency microfluidic impedance cytometer. Lab on a Chip 14:369–377.

Hadady, H., J. J. Wong, S. R. Hiibel, D. Redelman, and E. J. Geiger. 2014. High frequency dielectrophoretic response of microalgae over time. Electrophoresis doi:10.1002/elps.201400306.

Hannon, M., J. Gimpel, M. Tran, B. Rasala, and S. Mayfield. 2010. Biofuels from algae: challenges and potential. Biofuels 1:763–784.

Hawkins, B. G., C. Huang, S. Arasanipalai, and B. J. Kirby. 2011. Automated Dielectrophoretic Characterization of Mycobacterium smegmatis. Analytical Chemistry 83:3507–3515.

Henderson, T. J. 2002. Quantitative NMR Spectroscopy Using Coaxial Inserts Containing a Reference Standard: Purity Determinations for Military Nerve Agents. Analytical Chemistry 74:191–198.

Higashiyama, K., T. Sugimoto, T. Yonezawa, S. Fujikawa, and K. Asami3. 1999. Dielectric Analysis for Estimation of Oil Content in the Mycelia of Mortierella alpina. Biotechnology and Bioengineering 65:537–541.

Hoffmann, M., K. Marxen, R. Schulz, and K. H. Vanselow. 2010. TFA and EPA Productivities of Nannochloropsis salina Influenced by Temperature and Nitrate Stimuli in Turbidostatic Controlled Experiments. Marine Drugs 8:2526–2545.

Holland, S. L., T. Reader, P. S. Dyer, and S. V. Avery. 2014. Phenotypic heterogeneity is a selected trait in natural yeast populations subject to environmental stress. Environmental Microbiology 16:1729–1740.

Holmes, D., J. K. She, P. L. Roach, and H. Morgan. 2007. Bead-based immunoassays using a micro-chip flow cytometer. Lab on a chip 7:1048–1056.

Holmes, D., D. Pettigrew, C. H. Reccius, J. D. Gwyer, C. van Berkel, J. Holloway, D. E. Davies, and H. Morgan. 2009. Leukocyte analysis and differentiation using high speed microfluidic single cell impedance cytometry. Lab on a chip 9:2881–2889.

Hu, Q., M. Sommerfeld, E. Jarvis, M. Ghirardi, M. Posewitz, M. Seibert, and

A. Darzins. 2008. Microalgal triacylglycerols as feedstocks for biofuel production: perspectives and advances. The Plant Journal 54:621–639.

Huang, G., F. Chen, D. Wei, X. Zhang, and G. Chen. 2010. Biodiesel production by microalgal biotechnology. Applied Energy 87:38–46.

Hyka, P., S. Lickova, P. Přibyl, K. Melzoch, and K. Kovar. 2013. Flow cytometry for the development of biotechnological processes with microalgae. Biotechnology Advances 31:2–16.

James, G. O., C. H. Hocart, W. Hillier, H. Chen, F. Kordbacheh, G. D. Price, and M. A. Djordjevic. 2011. Fatty acid profiling of Chlamydomonas reinhardtii under nitrogen deprivation. Bioresource Technology 102:3343–3351.

Jones, C. S., and S. P. Mayfield. 2012. Algae biofuels: versatility for the future of bioenergy. Current Opinion in Biotechnology 23:346–351.

Kell, D. B., G. H. Markx, C. L. Davey, and R. W. Todd. 1990. Real-time monitoring of cellular biomass: methods and applications. Trends in Analytical Chemistry, 9:190–194.

Kirby, B. 2010. Micro- and Nanoscale Fluid Mechanics: Transport in Microfluidic Devices. Cambridge University Press.

Lee, D.-H., C. Y. Bae, J.-I. Han, and J.-K. Park. 2013a. In Situ Analysis of Heterogeneity in the Lipid Content of Single Green Microalgae in Alginate Hydrogel Microcapsules. Analytical Chemistry 85:8749–8756.

Lee, J.-Y., C. Yoo, S.-Y. Jun, C.-Y. Ahn, and H.-M. Oh. 2010. Comparison of several methods for effective lipid extraction from microalgae. Bioresource Technology 101:S75–S77.

Lee, T.-H., J.-S. Chang, and H.-Y. Wang. 2013b. Current developments in high-throughput analysis for microalgae cellular components. Biotechnology Journal 8:1301–1314.

Levy, S. F., N. Ziv, and M. L. Siegal. 2008. Bet Hedging in Yeast by Heterogeneous, Age-Correlated Expression of a Stress Protectant. PLoS Biology 10:e1001325.

Loh, W.-Y. 2011. Classification and regression trees. WIREs Data Mining Knowledge Discovery 1:14–23.

Maskow, T., A. Röllich, I. Fetzer, J.-U. Ackermann, and H. Harms. 2008. On-line monitoring of lipid storage in yeasts using impedance spectroscopy. Journal of Biotechnology 135:64–70.

Mata, T. M., A. A. Martins, and N. S. Caetano. 2010. Microalgae for biodiesel production and other applications: A review. Renewable and Sustainable Energy Reviews 14:217–232.

Maxwell, E. N. 2007. Ultra-Wideband Electronics, Design Methods, Algorithms, and Systems for Dielectric Spectroscopy of Isolated B16 Tumor Cells in Liquid Medium. Ph.D. thesis, University of South Florida, Department of Electrical Engineering.

Merkley, N., and R. T. Syvitski. 2012. Profiling whole microalgal cells by high-resolution magic angle spinning (HR-MAS) magnetic resonance spectroscopy. Journal of Applied Phycology 24:535–540.

Michael, K. A., S. R. Hiibel, and E. J. Geiger. 2014. Dependence of the dielectrophoretic upper crossover frequency on the lipid content of microalgal cells. Algal Research 6:17–21.

Millis, K. K., W. E. Maas, D. G. Cory, and S. Singer. 1997. Gradient, High-Resolution, Magic-Angle Spinning Nuclear Magnetic Resonance Spectroscopy of Human Adipocyte Tissue. Magnetic Resonance in Medicine 38:399–403.

Montero, M. F., M. Aristizábal, and G. G. Reina. 2011. Isolation of high-lipid content strains of the marine microalga *Tetraselmis suecica* for biodiesel production by flow cytometry and single-cell sorting. Journal of Applied Phycology 23:1053–1057.

Mourant, J. R., Y. R. Yamada, S. Carpenter, L. R. Dominique, and J. P. Freyer. 2003. FTIR Spectroscopy Demonstrates Biochemical Differences in Mammalian Cell Cultures at Different Growth Stages. Biophysical Journal 85:1938–1947.

Müller, T., T. Schnelle, and G. Fuhr. 1998. Dielectric single cell spectra in snow algae. Polar Biology 20:303–310.

Na, J.-G., H. S. Lee, Y.-K. Oh, J.-Y. Park, C. H. Ko, S.-H. Lee, K. B. Yi, S. H. Chung, and S. G. Jeon. 2011. Rapid estimation of triacylglycerol content of *Chlorella* sp. by thermogravimetric analysis. Biotechnology Letters 33:957–960.

Němcová, Y., and T. Kalina. 2000. Cell wall development, microfibril and pyrenoid structure in type strains of *Chlorella vulgaris, C. kessleri, C. sorokiniana* compared with *C. luteoviridis* (Trebouxiophyceae, Chlorophyta). Algological Studies 100:95–105.

O'Rourke, E. J., A. A. Soukas, C. E. Carr, and G. Ruvkun. 2009. *C. elegans* Major Fats Are Stored in Vesicles Distinct from Lysosome-Related Organelles. Cell Metabolism 10:430–435.

Pal, D., I. Khozin-Goldberg, Z. Cohen, and S. Boussiba. 2011. The effect of light, salinity, and nitrogen availability on lipid production by Nannochloropsis sp. Applied Microbiology and Biotechnology 90:1429–1441.

Pouneva, I. 1997. Evaluation of Algal Culture Viability and Physiological state by Fluorescent Microscopic Methods. Bulgarian Journal of Plant Physiology 23:67–76.

Pozar, D. M. 2012. Microwave Engineering. 4 edition. John Wiley & Sons.

Pruvost, J., G. V. Vooren, G. Cogne, and J. Legrand. 2009. Investigation of biomass and lipids production with Neochloris oleoabundans in photobioreactor. Bioresource Technology 100:5988–5995.

Rodolfi, L., G. C. Zittelli, N. Bassi, G. Padovani, N. Biondi, G. Bonini, and M. R. Tredici. 2008. Microalgae for Oil: Strain Selection, Induction of Lipid Synthesis and Outdoor Mass Cultivation in a Low-Cost Photobioreactor. Biotechnology and Bioengineering 102:100–112.

Schmollinger, S., T. Mühlhaus, N. R. Boyle, I. K. Blaby, D. Casero, T. Mettler, J. L. Moseley, J. Kropat, F. Sommer, D. Strenkert, D. Hemme, M. Pellegrini, A. R. Grossman, M. Stitt, M. Schoda, and S. S. Merchant. 2014. Nitrogen-Sparing Mechanisms in *Chlamydomonas* Affect the Transcriptome, the Proteome, and Photosynthetic Metabolism. The Plant Cell 26:1410–1435.

Siaut, M., S. Cuiné, C. Cagnon, B. Fessler, M. Nguyen, P. Carrier, A. Beyly, F. Beisson, C. Triantaphylidès, Y. Li-Beisson, and G. Peltier. 2011. Oil accumulation in the model green alga *Chlamydomonas reinhardtii*: characterization, variability between common laboratory strains and relationship with starch reserves. BMC Biotechnology 11:7.

Sills, D. L., V. Paramita, M. J. Franke, M. C. Johnson, T. M. Akabas, C. H. Greene, and J. W. Tester. 2013. Quantitative Uncertainty Analysis of Life Cycle Assessment for Algal Biofuel Production. Environmental Science & Technology 47:687–694.

Spencer, D. C., G. Elliott, and H. Morgan. 2014. A sheath-less combined optical and impedance micro-cytometer. Lab on a Chip 14:3064–3073.

Stephenson, A. L., E. Kazamia, J. S. Dennis, C. J. Howe, S. A. Scott, and A. G. Smith. 2010. Life-Cycle Assessment of Potential Algal Biodiesel Production in the United Kingdom: A Comparison of Raceways and Air-Lift Tubular Bioreactors. Energy Fuels 24:4062–4077.

Sturm, B. S. M., and S. L. Lamer. 2011. An energy evaluation of coupling nutrient removal from wastewater with algal biomass production. Applied Energy 88:3499–3506.

Sun, T., S. Gawad, C. Bernabini, N. G. Green, and H. Morgan. 2007. Broadband single cell impedance spectroscopy using maximum length sequences: theoretical analysis and practical considerations. Measurement Science and Technology 18:2859–2868.

Sun, T., C. Bernabini, and H. Morgan. 2009. Single-Colloidal Particle Impedance Spectroscopy: Complete Equivalent Circuit Analysis of Polyelectrolyte Microcapsules. Langmuir 26:3821–3828.

Szczpaniak, L. S., E. E. Babcock, F. Schick, R. L. Dobbins, A. Garg, D. K. Burns, J. D. McGarry, and D. T. Stein. 1999. Measurement of intracellular triglyceride stores by ^{1}H spectroscopy: validation in vivo. American Journal of Physiology - Endocrinology and Metabolism 276:E977–E989.

van Donk, E., M. Lurling, and D. O. Hessen. 1997. Altered Cell Wall Morphology in Nutrient-Deficient Phytoplankton and Its Impact on Grazers. Limnology and Oceanography 42:357–364.

Velmurugan, N., M. Sung, S. S. Yim, M. S. Park, J. W. Yang, and K. J. Jeong. 2013. Evaluation of intracellular lipid bodies in Chlamydomonas reinhardtii strains by flow cytometry. Bioresource Technology 138:30–37. doi: 10.1016/j.biortech.2013.03.078.

Vigeolas, H., F. Duby, E. Kaymak, G. Niessen, and P. Motte. 2012. Isolation and partial characterization of mutants with elevated lipid content in *Chlorella sorokiniana* and *Scenedesmus obliquus*. Journal of Biotechnology 162:3–12.

Wang, T., Y. Ji, Y. Wang, J. Jia, J. Li, S. Huang, D. Han, Q. Hu, W. E. Huang, and J. Xu. 2014. Quantitative dynamics of triacylglycerol accumulation in microalgae populations at single-cell resolution revealed by Raman microspectroscopy. Biotechnology for Biofuels 7:58.

Weyer, K. M., D. R. Bush, A. Darzins, and B. D. Willson. 2010. Theoretical maximum algal oil production. BioEnergy Research 3:204–213.

Wu, Y., C. Huang, L. Wang, X. Miao, W. Xing, and J. Cheng. 2005. Electrokinetic system to determine differences of electrorotation and traveling-wave electrophoresis between autotrophic and heterotrophic algal cells. Colloids and Surfaces A: Physicochemical Engineering Aspects 262:57–64.

Zhao, K., W. Bai, and H. Mi. 2006. Dielectric spectroscopy of *Anabaena 7120* protoplast suspensions. Bioelectrochemistry 69:49–57.